Design of Smart Biomaterials Using Functionalized Gold Nanorods in Combination with Near-Infrared Light

Qinghui Shou
Doctoral Program in Materials Science and Engineering

Submitted to the Graduate School of
Pure and Applied Sciences
in Partial Fulfillment of the Requirements
for the Degree of Doctor of Philosophy in
Engineering

at the
University of Tsukuba

Contents

List of abbreviations

AuNR(s)	Gold nanorod(s)
CMC	Critical micelle concentration
CTAB	Cytltrimethane ammonium bromide
DLS	Dynamic Light Scattering
DMEM	Dulbecco's Modified Eagle's Medium
DMF	Dimethylformamide
DMPA	2,2-dimethoxy-2-phenylacetophenone
DMSO	Dimethyl sulfoxide
DSC	Differential scanning calorimetry
EBL	Electronbeam lithography
FWHM	Full width at half maximum
LSPR	Longitudinal surface plasmon resonance
11-MUD	11-mercapto-1-undecanol
NIR light	Near-infrared light
PCL	Poly(ε-caprolactone)
PEG	Polyethyleneglycol
PEG-SH	SH- terminated polyethyleneglycol
PNIPAAm	Poly(N-isopropylacrylamide)
RI-ROP	Surface initiated ring opening polymerization
SMPs	Shape-memory polymer(s)
TGA	Thermogravimetric analysis
TEM	Transmission electron microscopy
THF	Tetrahydrofuran
TSPR	Transverse surface plasmon resonance
XPS	X-ray photoelectron spectroscopy

Chapter 1 Background and Objective

1.1. A short history of gold nanomaterials

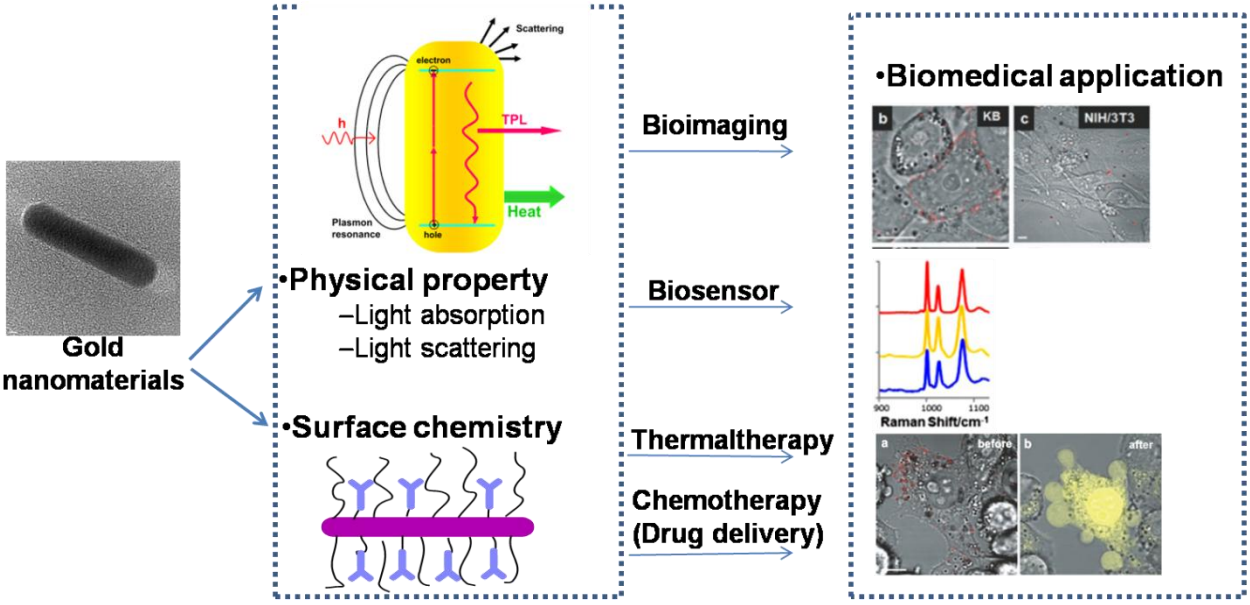

Fig. 1.1. Physical property, surface chemistry and biological application of gold nanomaterials.

Recent years, there is a boom of development of nanotechnology. Due to the quantum effect, large surface area, materials that at least with one dimensional under 100 nm is generally has high surface activity than their bulk counterpart. Such materials are called nanomaterials.[1] Nanomaterials with various morphologies, for example, one dimensional nanomaterials (nanosheet, nanotubes, two dimentional nanomaterials (nanoparticles, nanostars, et al.) were discovered. The synthesis method and applications were highly developed these years. Here, works on gold nanomaterials were focused.

The theory to synthesize nanoparticles with various sizes and dispersity was developed more than 60 years ago[2]. The control of shape has attracted much attention in the last 15 years. The main strategy is through capping agent, including surfactant[3,4]. As for gold nanomateials, there are several exiting points in gold nanoparticles. The strategy to hydrophilic and hydrophobic gold nanoparticles was done in 1953[5] and 1994[6], respectively. After that, there have been numerous reports introducing various shaped particles, nanoshells, nanosheet, nanocages, nanowire, et al.

As shown in **Fig. 1.1.**, basic chemistry and physical knowledge was used to make full use of nanoparticles, and such application largely depends on the morphology of nanoparticles and also functional groups[7]. Therefore, many efforts have been taken to modify or directly synthesize nanoparticles with functional group. One of the important applications is in the biological field, including cell uptake and imaging, hyperthermia, sensor or diagnosis, gene or drug delivery[8,9].

1.2. Gold nanorod and its surface chemistry.

1.2.1. Seed-mediated synthesis

Although several methods were developed these year, the method to synthesize AuNRs with high yield is the so called "seed mediated method"[10]. The procedure is shown in **Fig. 1.2**. It is included by two steps:

Step 1: Synthesis of seeds with diameter about 1.5-3.5 nm.

Generally cationic surfactant cytltrimethane ammonium bromide (for short CTAB) acts as capping agent, and the control of small size was realized by using one strong reductant sodium borohydride ($NaBH_4$).

Step 2: Preparation of the growth solution.

Mixing of CTAB with gold ions, which forms complexes. Concentration of CTAB is much higher than its critical micelle concentration (CMC). The complexes structure is shown as follows:

Au ion + CTAB micelle ⇄ complex of Au ion and CTAB micelle.[11]

A small portion of Silver nitrate was then added. The role of silver is not clear, but it is crucial to synthesize single crystalline structure AuNRs.[10]

After that, a weak reductant ascorbic acid was used to reduce Au^{3+} to Au^0.

Finally, the seed solutions were added to the growth solution. And Au nanorods were further developed on the surface of spherical seeds.

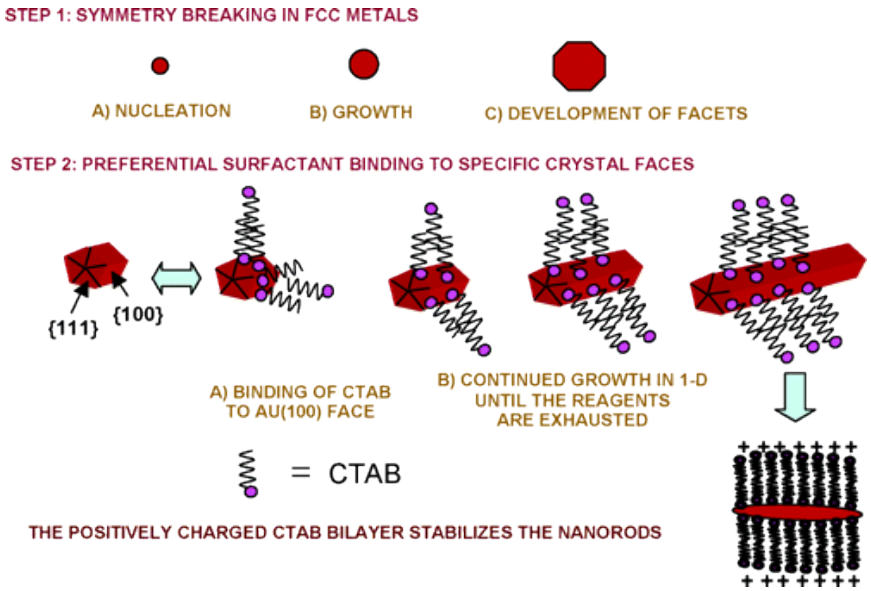

Fig. 1.2. Seed mediated synthesis of gold nanrods through bottom-up approach and molecular self-assembly.[12]

As for the mechanism to synthesize AuNRs, it is supposed that several factors are crucial to form anisotropic-structure nanorods: a CTAB concentration that CTAB forms cylinder-like structure, a "zipper" mechanism that CTAB has a strong affinity with specific facets of gold.[12] (**Fig. 1.3**)

1.2.2 Surface modification and functionalization of AuNRs

CTAB forms bilayer structure on AuNRs surface, which was first discovered by Ei-sayed et al. in 2001 and further investigated by CJ, Murphy et al.[13]. By FT-IR and thermogravimetric analysis (TGA), there are two layers with different desorption energy and the ammonium headgroups was bound to the AuNRs surface.

Further, Gómez-Graña et al.[14] revealed the thickness and compactness of bilayer structure using small angle x-ray (SAXS) and neutron (SANS) scattering and concluded that CTAB bilayer is interdigitated with each other. The CTAB capped AuNRs manifest a positive surfaced charge, the value of which depending on the CTAB concentration. Therefore, the change of surface charge is usually performed as on evidence for the surface coating by cationic molecules and anionic molecules[15,16].

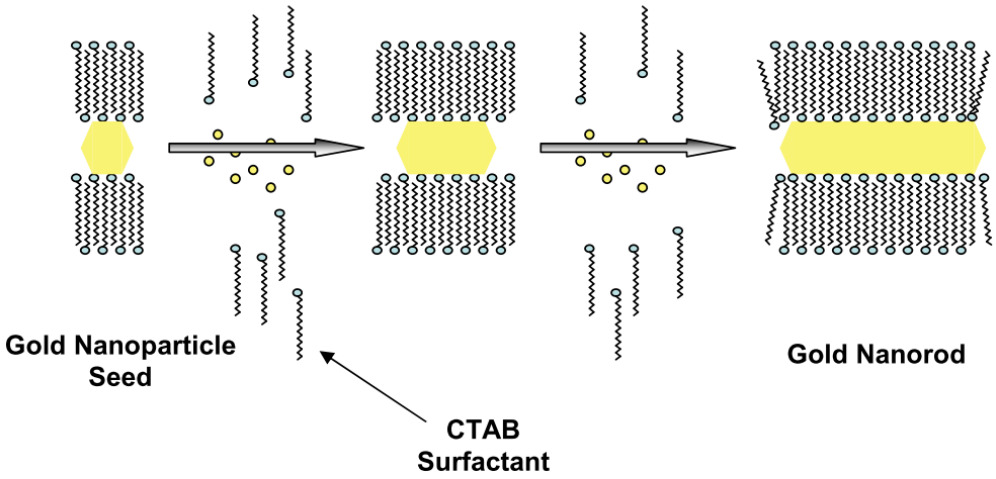

Fig. 1.3. "Zipper" mechanism to form bilayer structures.[12]

The main method for modification follows into 4 methods below:

1.2.2.1. Encapsulation by polymers

The surface charge of AuNRs is about +40 ev by zeta-potential analysis. Therefore, AuNRs could be modified directly by hydrophobic cationic polymers. Further, through layer by layer technique, AuNRs could be modified by many types of polymers, giving both positive and negative charge on AuNRs surfaces.[16]

1.2.2.2. Thiol with hydrophilic ligand

To make full use of AuNRs in biological field, the dispersity, colloidal stability, and easy-to-functional are important. For gold nanoparticles, the mostly developed case for such system is using gold-thiol chemistry.

For example, for the ligand-exchange of CTAB with hydrophilic ligands with thiols, many thiols, such as 3-mercaptopropionic acid, 11-mercaptoundecanoic acid, or glutathione are used[17,18]. However, due to the specific bilayer structure of CTAB, the direct exposure of CTAB- capped AuNRs to alkanethiol agents usually results in incomplete removal and uncontrollable aggregation of AuNRs.

1.2.2.3. Modification with "grafting to" method

The PEGylation method a remarkable modification method was reported in 2006[15]. When mixing the SH-terminated poly ethyleneglycol (PEG, MW 5000) with AuNRs, and dialysis against water, the PEG-modified AuNRs could be well stable in water without aggregation. The problem, however, is CTAB could not be exchanged thoroughly by SH- terminated PEG (PEG-SH).

To improve the exchange efficiency of CTAB, C. Kinnear et al. mended the PEGlytion method by using two-step method. (**Fig. 1.4**)[19]. Briefly, first step, the partially exchanged AuNRs was mixed with ethanol with different volume ratios. The relationship of volume fraction of ethanol with concentration of PEG was studied and the phase diagram of AuNRs was drawn, as shown in **Fig.1.5**.

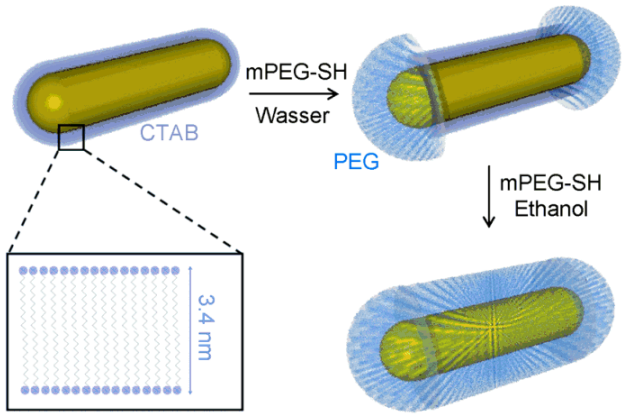

Fig. 1.4. A 'two-step" method to modify AuNRs[19]. The first step is to modify AuNRs using PEGylation method introduced in 2006[15], and the remaining CTAB on PEG- modified AuNRs could be further detached by mixing with a certain amount of ethanol[19].

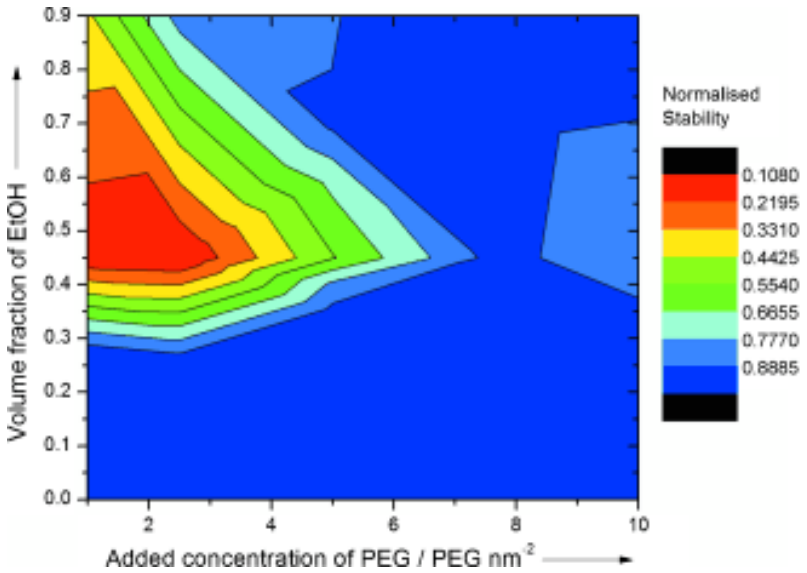

Fig. 1.5. Phase diagram of the GNRs. The normalized stability is the ratio of intensity of the LSPR peak after five days relative to the initial value. PEGylation reaction for 24 h, C_{CTAB}=1 mM[19].

1.2.2.4. Modification using "grafting from" method"

To perform surface grafting on AuNRs surface, the general idea is introducing initiators with SH- end group to exchange the robust CTAB bilayer structure, and then polymerization could be performed. Many polymers that can responsive to environment pH, temperature, electric field, et al can be expected. And the common polymerization process, e.g. atom transfer radical polymerization, ring opening polymerization are available.

For example, disulfide initiator $[BrC(CH_3)_2COO(CH)_{11}S]_2$ in dimethylformamide (DMF) solution was introduced onto the surface of AuNRs, after adding monomer N,N,N',N',N''-pentamethyldiethylenetriamine, degassing, and catalyst $Cu^{I}Br$, the surface initiated polymerization was carried out[20]. The resultant poly(N-isopropylacrylamide (PNIPAAm) modified AuNRs is report to well disperse in pure water. And the hydrophobic drug loading/release process was realized through the hydrophobic-hydrophilic transition (**Fig. 1.6**).

Another example is by using a large amount of 4-mercapophenol, the ligand exchange process could be well controlled And with carboxybiphenyl-terminated polystyrene (Mw=5000 g mol^{-1}) could be covalently coupled through esterification method[21] (**Fig. 1.7**).

Up to now, there is still limited work on modification with "grafting from" methods comparing with the wide options of polymerization strategies.

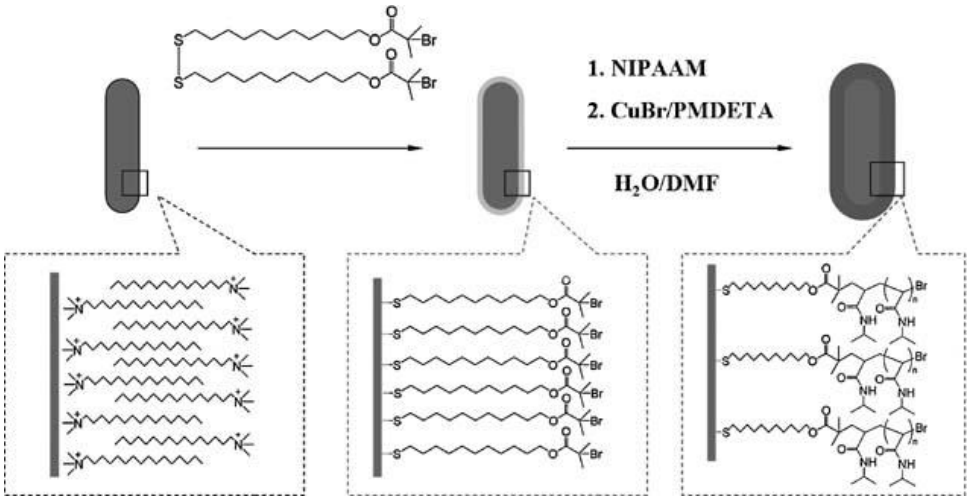

Fig. 1.6. Preparation of PNIPAAm modified AuNRs through SI-ATRP reaction[20].

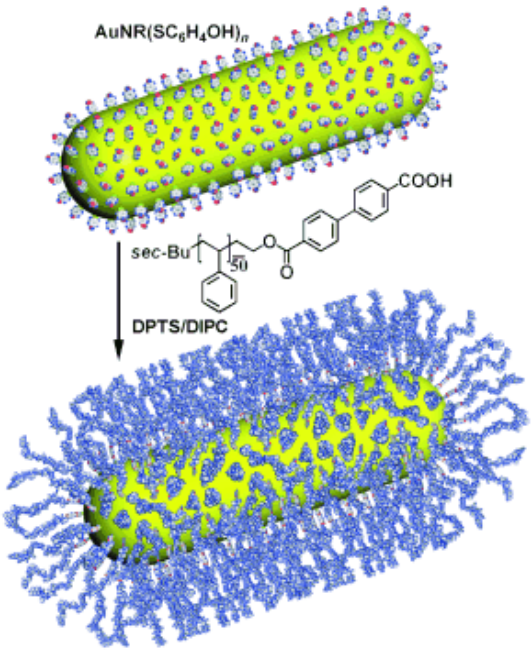

Fig. 1.7. Schematic of the reaction of 4-mercaptophenol-coated AuNRs with carboxyl-terminated polystyrene[21].

1.2.3. The optical property photothermal effect of gold nanorods

If gold nanorods was regarded as nano-scale molecule, a extinction coefficient could be calculated according to the Beer-Lambert law. Several factors can be obtained as follows: the size of nanoparticles (by

TEM), a.u. (by UV-Vis), concentration (by inductively coupled plasma atomic emission spectroscopy, ICP-AES).

Generally, an extinction coefficient in the order of 10^9 $M^{-1}cm^{-1}$ was obtained[22], which is one order and 4 orders larger that of spherical gold nanoparticles and traditional organic chromophores (boron dipyrromethene 1.1* 10^5 $M^{-1}cm^{-1}$).

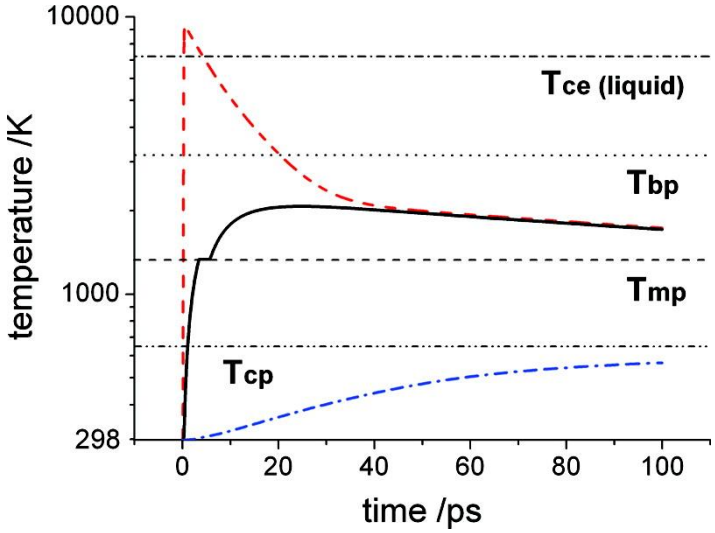

Fig. 1.8. Simulated temporal evolution of electron temperature.[23]

When a gold nanoparticles interacts with a femtosecond laser pulse, the photothermal process is as follows [23,24] (**Fig. 1.8**):

(a) laser-light absorption through electron-electron scattering. A thermal equilibrium is reached within a few 100 fs.

(b) Transferring of the electron energy to the lattice via electron-phonon coupling with a few ps.

(c) Transferring of the lattice energy to the surrounding medium through phonon-medium interaction. It takes several tens to several hundreds of ps. which depends on the particle morphology, thermal properties (thermal conductivity), and laser intensity.

1.3. **Shape memory polymers**

If using gold nanomaterials on biomedical field, a matrix is need to load them. One of the candidates is stimulus responsive polymers. By selection of momomer, chain length, branched number, many polymers with the hydrophobic to hydrophilic transition, the crytalline to amorphous transition have been developed into smart biomaterials. And one type of stimulus responsive polymer, shape memory polymers were focused.

Shape-memory polymers (SMPs), which have the ability to return from a deformed state to their original shape induced by an external stimulus, have drawn much attention from fundamental research to practical applications.[25] SMPs possess several advantages compared with shape-memory alloys (SMAs) due to the large deformation ability, low cost, environmentally friendly processing, and potential biocompatibility and

biodegradability. These advantages are especially significant for biomedical applications such as minimally invasive implants[25,26].

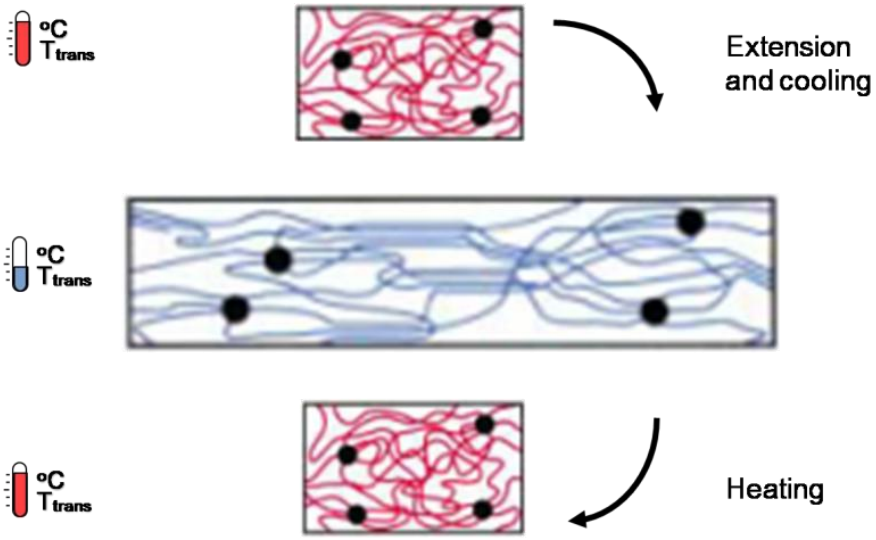

Fig. 1.9. Mechanism of shape memory effect covalent crosslinking with $T_{trans}=T_m$[25].

Among the SMPs, thermally induced SMPs are the most extensively investigated group of SMPs[27] . They are thermoplastic elastomers or thermosets that are programmed by mechanically deforming the shape of a polymer at temperatures which exceed its glass transition temperature (T_g) or melting temperature (T_m). This deformed shape (or temporary shape) can be fixed when the material is cooled below the T_g or T_m. If the polymer chains are chemically or physically crosslinked, thematerial returns to its original shape (or permanent shape) by heating it again to above the T_g or T_m. During this process, an increase of entropy serves as a driving force for the material to recover its initial shape. Therefore, the use of T_m as the triggering switch is more favorable because the enthalpy change of the solid-liquid phase transition is much larger than that of a glass-rubber transition.

Aoyagi *et. al* have been developing the thermally induced SMP switch the T_m near the biologically relevant temperature using crosslinked poly(ε-caprolactone) (PCL)[28]. PCL is an important class of biocompatible and biodegradable synthetic polymers which has been approved for biomedical applications by the US Food and Drug Administration[29]. Lendlein *et al.* have developed shape-memory biodegradable sutures by using oligomeric PCL[30]. Rodriguez *et al.* have reported on miscible blends comprised of linear-PCL and chemically cross-linked PCL networks. The blends demonstrate unique shape-memory-assisted self-healing, which is the material's ability to close local microscopic cracks and heal those cracks by bonding the crack surfaces[31]. Neuss *et al.* have developed shape-memory tissue engineering scaffolds by using crosslinked PCL dimethacrylate network[32]. On the other hand, we have recently demonstrated PCL cell culture surfaces with shape-memory nanopatterns[28]. The direction of aligned cells on nanopatterns can be tuned to a perpendicular direction by shape-memory activation of nanopatterns that transition from a memorized temporal pattern to the original permanent pattern by heating at 37 ^oC[33]. We have also envisioned application of this surface

shape memory phenomenon in the areas of microfluidic control systems that actuate near the biologically relevant temperature, such as pumps and valves[34].

1.4. **The aim and objective of this study**

Aim 1: Study of the absorption/detachment of CTAB from the surface of gold nanorods.

As mentioned above, gold nanorods should be modified with thiol to make use in biological field. Such ligand exchange reaction was carried out in the mixture of water and organic solvent. Generally, hydrophilic polymers or small hydrophobic molecules was used for ligand exchange. However, for hydrophobic polymers, it was difficult to do ligand exchange. The main reason is, fundamentally, the dynamic absorption/detachment of CTAB fron AuNRs surface is still not clarified.

As shown in **Fig. 1.5**, the stability of AuNRs with volume ratios of organic solvent and concentration of PEG was drawn. With varying volume ratio of organic solvent, the concentration of CTAB also play a role, which has never been investigated.

Aim 2: Synthesis of polymer modified gold nanorods using grafting from method, and fabricated composite films.

PCL- modified AuNRs were synthesized with two methods. Further, considering the semi-crystalline structure of PCL, it was used as shape-memory polymers. If cultured cell on the matrix with temporary pattern, as the temperature increased, the pattern will disappeared. And the cell lost its orientation. However, for such work, the increase of temperature is a must to induce the shape-memory effect.

Therefore, it is easy to expect that by combining stimulus polymers with nanomaterials, the crystalline to amouphrous transition will be controlled with near-infrared light. It is a must to graft polymers on nanoparticles, it won't influence the phase behaviour of shape memory polymers. Therefore, the main task it do surface grafting on AuNRs surface and incorporate into polymer films.

Aim 3: Using shape-memory film with surface pattern, the cell orientation was controlled using near-infrared light.

Mechano-biology has been well developed by using many types of polymers. However, there is still a lack of work to controlling the cell function using remote vehicle, such as light. In this work, the controlling of cell orientation was realized by using NIR-actuated shape memory films.

Chapter 2. Procedure for the Removal of CTAB Surfactant on the Surface of AuNRs Using Water/DMSO Mixture

2.1. Introduction

In this study, we propose one strategy for the complete removal of CTAB and further modification of the surfaces of AuNRs by control of experimental parameters, because there are still question regarding the detachment mechanisms of CTAB from the surface of AuNRs. Specifically, we used a mixture of dimethyl sulfoxide (DMSO)/water as a cosolvent to control the partitioning of CTAB between the gold surface and the solution phase. The rationale behind the selections of DMSO/water ratio or CTAB concentration is discussed in detail regarding the detachment mechanisms of CTAB from the surface of AuNRs, which has not been discussed previously.

After the removal of CTAB, hydroxyl (OH-) terminated alkanethiols was added additionally for the stabilization and further potential functionalization of AuNRs to make useful for various applications. To our best knowledge, there is only one report by E.R. Zubarev's group, in which AuNRs can be decorated with 4-mercaptophenol through mixing AuNRs aqueous solution with 4-mercaptophenol in tetrahydrofuran[21]. And further, the surface OH- group was used to initiate ring opening polymerization of ε-caprolactone by our group, and the obtained polycaprolactone- modified AuNRs fillers could be well dispersed in PCL bulk materials[35]. However, some challenges still exist. i.e., there is a large amount of CTAB left on the surface of AuNRs. The possible reason is that arenethiol with benzene ring is a rigid structure, and it would generate higher hindrance force when conjugated with gold comparing with alkanethiol, and therefore is not easy to exchange all of the CTAB [36,37]. A three-step was followed to realize of ligand-exchange and phase-transfer reaction; (i) removal of free CTAB by centrifugation, (ii) ligand-exchange of CTAB capped AuNRs, and (iii) phase transfer from water to aprotic solvent. A series of OH- terminated alkanethiols were utilized to modify AuNRs, such as 2-mercaptoethanol (2-ME), 6-mercapto-1-hexanol (6-MH), 9-mercapto-1-nonanol (9-MN), and 11-mercapto-1-undecanol (11-MUD). A complete removal of CTAB should provide chemical functionality for conjugation chemistry, good water solubility, and colloidal stability during modification and purification steps.

2.2. Experimental

2.2.1. Reagents and Materials.

Gold (III) chloride trihydrate, cetyltrimethyl ammonium bromide (CTAB), sodium borohydride ($NaBH_4$), silver nitrate, L-ascorbic acid, 2-mercaptoethanol (2-ME), 6-mercapto-1-hexanol (6-MH), 9-mercapto-1-nonanol (9-MN), and 11-mercapto-1-undecanol (11-MUD) were purchased from Aldrich. Dimethyl sulfoxide (DMSO) and dichloromethane were purchased from Wako Pure Chemical Industries. Milli-Q water was used in the whole experiment. Without specific description, all of the chemicals were used as received.

2.2.2. Synthesis of gold nanorods

AuNRs are synthesized using a seed-mediated method[38]. For the preparation of Au seeds, 0.25 mL of an aqueous solution of $HAuCl_4 \cdot 3H_2O$ (0.01 M) was added to 7.5 mL of a CTAB solution (0.10 M). After gently mixed by hand, 0.6 mL of an aqueous ice-cold $NaBH_4$ solution (0.01 M) was added all at once, followed by rapid inversion mixing for 2 min. Then the test tube was kept in a water bath maintained at 28 ℃ for at least 2 h before further use.

Solutions of 0.2 mL of $HAuCl_4 \cdot 3H_2O$ and 4.75 mL of CTAB were mixed to develop a deep yellow color, and then 30 uL of $AgNO_3$ solutions (0.01 M) were added, followed by gentle mixing by inversion. Then 32 uL of 0.10 M ascorbic acid was added. Finally, 10 uL of seed solution was added, and was gently mixed for 10 s and left undisturbed for at least 3 h.

Freshly prepared AuNRs aqueous solutions were centrifuged in the speed of 10000 rpm for 15 min. The supernatant was decanted, and centrifuged again after diluting it with Milli-Q water as the same volume of original solution. After centrifugation twice, a series solution of CTAB was added to adjust the concentration of CTAB to 15 uM. The free CTAB was removed without observable precipitation.

2.2.3. The stability of AuNRs after mixing with DMSO.

The AuNRs were centrifuged twice, in order to reduce the free CTAB and impurities (free gold ions, $AgNO_3$, ascorbic acid, etc.) as much as possible while AuNRs can keep stable against precipitation. And then, a series of CTAB aqueous solutions was added to make a AuNRs aqueous solution with different concentrations of CTAB.

After that, AuNRs in aqueous solution were mixed with DMSO with varied volume ratio from 0.1 to 0.9. The volume ratio was defined to be V_{AuNR}:V_{DMSO}. It should be mentioned that subscript of "AuNRs" means AuNRs aqueous solution. The colloidal stability of AuNRs soon after mixing with varying volume of DMSO was investigated by following changes of two characteristic absorptions of AuNRs using UV/Vis/NIR spectrophotometer. Hydrodynamic diameter was obtained using dynamic light scattering (DLS).

Meanwhile, to study the influence of volume ratio of water and DMSO with a constant amount of AuNRs, the DMSO/water volume ratio was adjusted by addition of MilliQ water. To discriminate this mixture from that simply mixing AuNRs aqueous solution with DMSO, such ratio was defined as V_{water}:V_{AuNR}:V_{DMSO}.

The procedure to prepare samples to draw phase diagram of AuNRs is as follows: the twice-purified AuNRs pellets were diluted with a certain volume of CTAB aqueous solution with different concentrations, after which Milli-Q water was added to adjust the total volume of water. The resultant AuNRs aqueous solutions were left undisturbed in a water bath maintained at 28 ℃ for at least 24 h. Finally, the above samples were mixed with DMSO with varying volume ratios.The total volume of mixture solvent was calculated using the apparent molar volumes of DMSO/water mixtures at 25 ^oC[39], which was listed in **Table 2.1**. Because of the widely distributed concentration of CTAB from about 1 μM to 10 mM investigated in this work, the change of volume with mixing ratio has been ignored. Therefore, through this procedure, the final concentrations of both AuNRs and CTAB after mixing with DMSO with different fractions are constant.

Table 2.1. Calculation of the total volume of mixture solvent using the apparent molar volumes of DMSO/water mixtures at 25 ^{o}C

V_{DMSO} (%)	0	10	20	30	40	50	60	70	80	90
Actual volume	1	0.996	0.994	0.992	0.987	0.982	0.981	0.977	0.979	0.984

2.2.4. Ligand exchange and phase transfer of AuNRs

A series of ω-derivative alkanethiols were dissolved in DMSO, and the freshly prepared DMSO solution was injected into the AuNRs solution. After mixed by vortex mixer, the solution was stirred for 24 h using magnetic stirrer. X-ray photoelectron spectroscopy (XPS, Theta Probe by Thermo Electron) was performed to analyze the surface composition. 10 μL of AuNRs solution was dipped onto the surface of silica substrate, and evaporate the liquid before measurement. An Axial inductively coupled plasma atomic emission spectrometer (ICP-AES) was used to determine the concentration of gold in the solutions.

The mole ratio of gold ions and thiols was fixed at 1 to 100, in which condition, thiol is abundant to capped all the gold clusters[40]. The detailed calculation process was added in the supplementary data.

The phase transfer experiment was carried out by the following method below. After centrifugation at the speed of 5000 rpm, the supernatant were aspirated using micro-pipette carefully, and then 1 mL Milli-Q water was added. Finally, 0.5 mL dichloromethane was added and slightly swirled.

2.2.5. Characterization

Morphologies of the gold nanoparticles were observed with a scanning electron microscope (SEM, Hitachi S-4800), and number-average diameters were obtained by measuring the diameters of more than 200 particles using SmileView software (JEOL Corp., Japan). Hydrodynamic diameter was obtained using dynamic light scattering (DLS) (DLS-8000, Otsuka Electronics Co., Osaka Japan) at 25 ° C with a Ne-He laser (λ=632.8 nm). UV-Vis-NIR was performed using UV/Vis/NIR spectrophotometer (V-7200 Jasco Inc.). When UV-Vis-NIR spectroscopy was carried out, the reference solution was made using mixture of DMSO and water with the same volume ratio of the corresponding sample. X-ray photoelectron spectroscopy (XPS, Theta Probe by Thermo Electron) was performed to analyze the surface composition. 10 μL of AuNRs solution was dipped onto the surface of silica substrate, and evaporate the liquid before measurement. An Axial inductively coupled plasma atomic emission spectrometer (ICP-AES) was used to determine the concentration of gold in the solutions.

2.3. Results and discussion

The ligand exchange and phase transfer protocol were illustrated in Fig. 2.1. To remove the CTAB capped on the surface of AuNRs, the centrifugation of AuNR was first carried out twice in order to remove the free CTAB as much as possible while keeping AuNRs stable against precipitation. Then the ligand exchange with OH- terminated alkanethiols was carried out by mixing AuNRs aqueous solution with thiol in DMSO

solution. After thorough exchanging for a certain time, dichloromethane was used as nonpolar solvent to dissolve the thiol modified AuNRs.

Fig. 2 characterizes the properties of CTAB-capped AuNRs after the purification by centrifugation. The concentrations of CTAB in the AuNRs solutions are decreased by 99.985% after the purification. (0.1 M and 15 uM before and after the purification, respectively). This value is regarded enough to sustain the colloidal stability of AuNRs for several days[41]. After the purification, the mean size and aspect ratio of AuNRs are 36±2*13±1 nm and 2.8, respectively (**Fig. 2.2a**). A transverse surface plasmon resonance (TSPR) absorption and a longitudinal surface plasmon resonance (LSPR) absorption were found to be around 536 nm 772 nm, respectively (**Fig. 2.2b**). The surface composition of CTAB-capped AuNRs was also characterized by XPS. It was reported that CTAB forms a bilayer structure on the surface of AuNRs, and Br-Au was interacted with each other on the surface of AuNRs. Thereby bromine is usually used to identify the capping effect [42,43]. **Fig. 2.3 a-b** show that bromine signal was detected on the AuNRs surface.

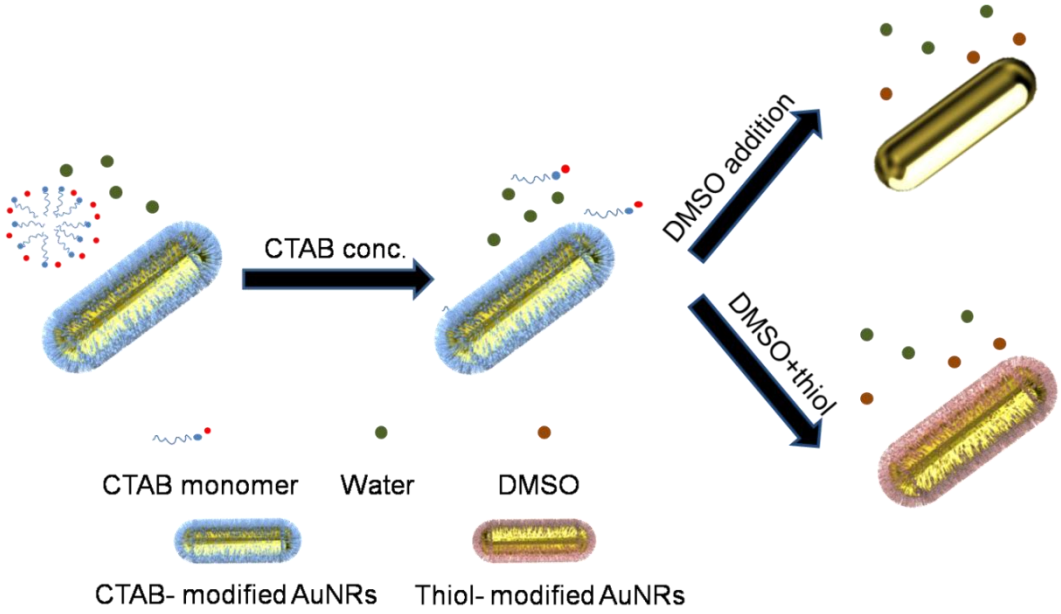

Fig. 2.1. Scheme for the detachment of CTAB from AuNRs surface and further modification with hydroxyl-terminated thiols. After centrifugation and adjusting the concentration of CTAB, AuNRs aqueous solution was mixed with DMSO with varying volume ratios. The condition that CTAB on AuNRs surface could be fully detached was discovered. Further, hydroxyl modified alkanethiols were added in this solution to perform ligand exchange reaction, and finally AuNRs could be well capped with thiols.

2.3.1. The stability of AuNRs after two-time centrifugation in DMSO/Water mixture solvent

The stability of AuNRs (C_{AuNRs}= 0.13 mM, C_{CTAB} ≅15 uM) with varying volume ratios of water and DMSO was studied by direct observation of color change, LSPR peak shift, and hydrodynamic diameter change. **Fig. 2.4a-b** show AuNRs solutions just after mixing and 2 h after mixing with DMSO, respectively. When V_{AuNR}:V_{DMSO} is either ≧0.8 or ≤0.4, AuNRs could keep stable without observable precipitation. On the other hand, color changed drastically and AuNRs precipitated within 2 hat V_{AuNR}:V_{DMSO}=0.5-0.7. **Fig. 2.5** shows LSPR peaks observed by UV-Vis spectroscopy. Red shift of the LSPR absorption peaks are clearly observed at V_{AuNRs}:V_{DMSO}≥0.9 and ≤0.4, while no regular LSPR absorption were observed at V_{AuNRs}:V_{DMSO}=0.5-0.8.

This can be explained by two possible reasons; end-to-end assembly and/or precipitation of AuNRs. It was reported that CTAB in the tail part of AuNRs are easy to be detached compared with that in the shoulder part, causing self-assembly into two dimensional structures[44]. But most likely, full width at half maximum (FWHM) of LSPR band increased and TSPR widened because AuNRs precipitated.

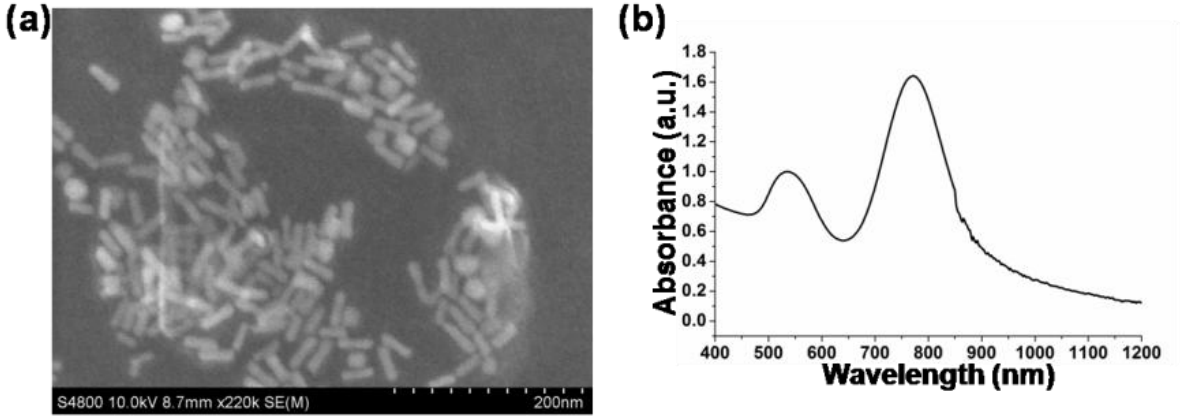

Fig. 2.2. Propertiesof gold nanorods (AuNRs) after two times' centrifugation. (a) SEM image of AuNRs. Scale bars: 200 nm. (b) UV-Vis spectroscopy of AuNRs.

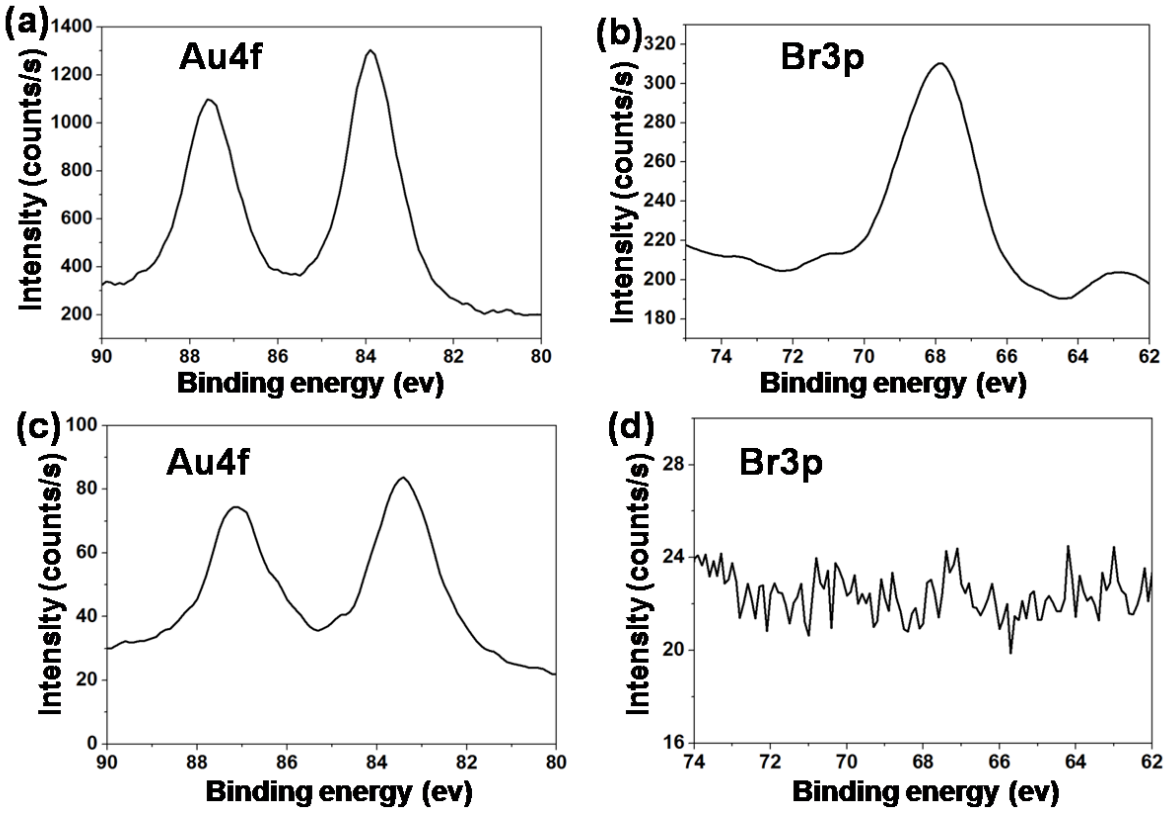

Fig. 2.3. Analysis of surface composition of AuNRs (a) and (b) AuNRs after two times' centrifugation, (c) and (d), with V_{AuNRs}/V_{DMSO} =0.5 (C_{AuNRs}= 0.13 mM, C_{CTAB} ≅15 uM).

Meanwhile, since the concentrations of AuNRs vary with volume ratios of DMSO/water, and to exclude the influence of different concentrations of AuNRs, the same experiment was done except that concentration of AuNR was fixed, and the result was shown in **Fig. 2.7**. When the volume ratio of total water and DMSO is0.9 (V_{water}:V_{AuNR}:V_{DMSO}=2.4:0.3:0.3) or in the range of 0.1-0.3 (V_{water}:V_{AuNR}:V_{DMSO} =0.6:0.3:2.4-0.0:0.3:2.7), there was a LSPR absorption, which also has a red shift with the increase of fraction of DMSO. On the other hand, when this ratio is in the range of 0.4-0.8 (V_{water}:V_{AuNR}:V_{DMSO}=0.9:0.3:1.8-2.1:0.3:0.6), there is no remarkable LSPR absorption. Therefore, the similar trends in Fig. 3 and Fig. S2 indicate that the varying solubility of AuNRs resulted from the difference of volume ratios of DMSO and water.

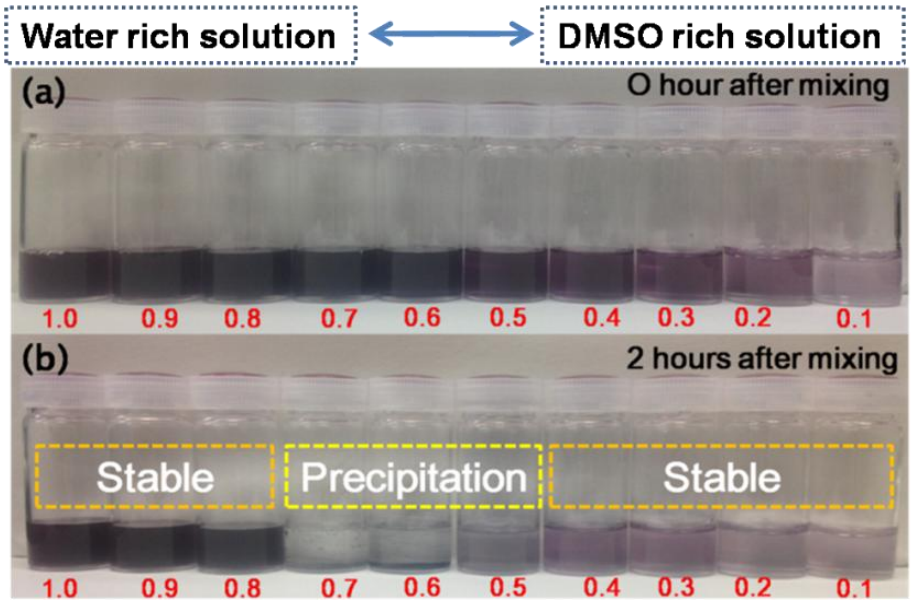

Fig. 2.4. Digital pictures of CTAB- capped AuNRs in the mixture of water and DMSO soon after mixing and two hours after mixing. C_{AuNRs}= 0.13 mM, C_{CTAB} ≅15 uM

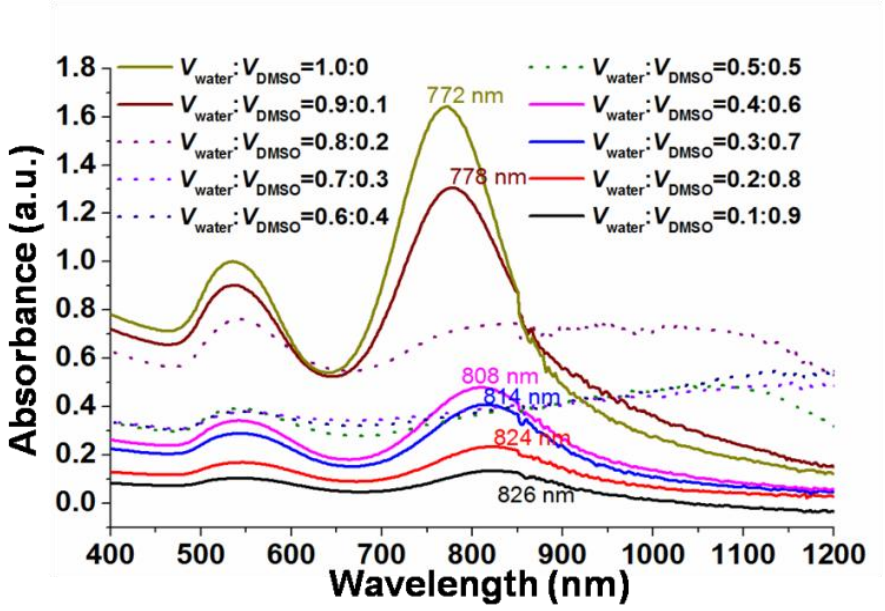

Fig. 2.5. UV-Vis spectroscopy of AuNRs water/DMSO mixture solutions with varying volume ratios of water/DMSO (C_{CTAB}≅15 uM, C_{AuNRs}= 0.13 mM).

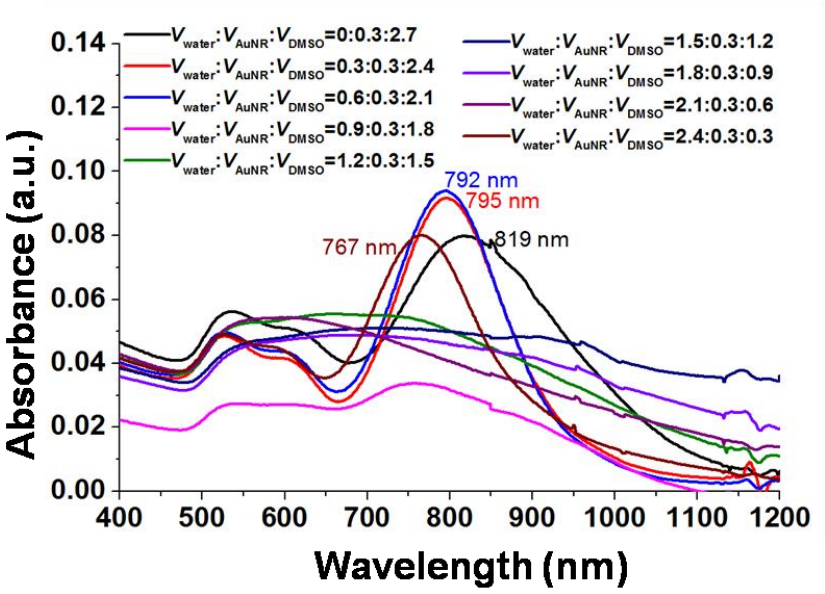

Fig. 2.6 UV-Vis-NIR spectroscopy of AuNRs samples mixing with DMSO. To keep the concentration of AuNRs constant, the volume ratio of water/DMSO was adjusted by water.

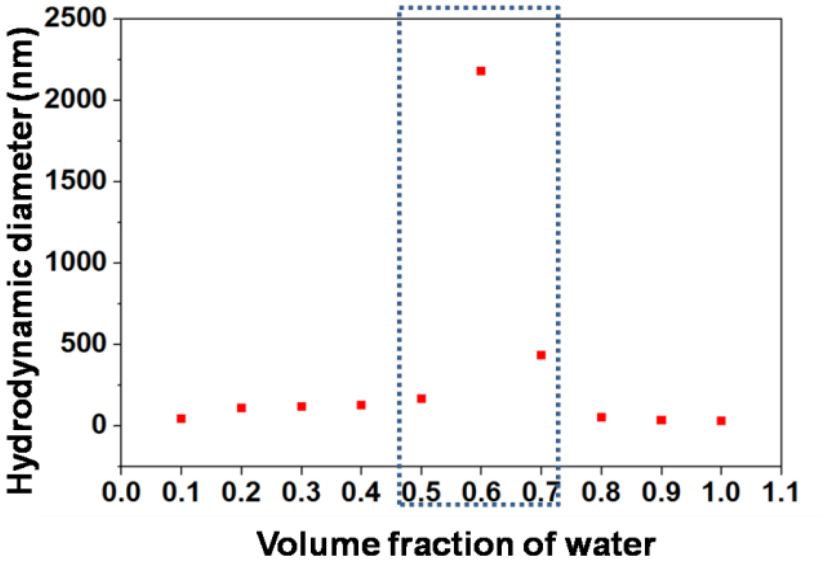

Fig. 2.7. Hydrodynamic diameter of AuNRs invarying volume ratios of water/DMSO. C_{AuNRs}= 0.13 mM, C_{CTAB} ≅15 uM.

Figure 2.7 shows the hydrodynamic diameter of AuNRs in water/DMSO mixture at different ratios measured by DLS. The AuNRs stably dispersed in both high volume ratio water and DMSO. The diameter increased from 30 nm to 50 nm as DMSO fraction increased, and eventually became large than 2,000 nm at V_{AuNRs}:V_{DMSO}=0.6 because of the aggregation and precipitation of AuNRs. With further increase of DMSO fraction, the diameter decreased to 41 nm again.

When the particles obtained through first mixing AuNRs aqueous solutions with V_{AuNRs}/V_{DMSO} =0.5, and centrifuged at 600 rpm to be separated from the supernatant were measured by XPS (**Fig. 2.8a and b**), the

signal of bromine is unobservable. Therefore, it was confirmed that on condition of V_{AuNRs}/V_{DMSO}=0.5, CTAB on the surface of AuNRs could be fully detached.

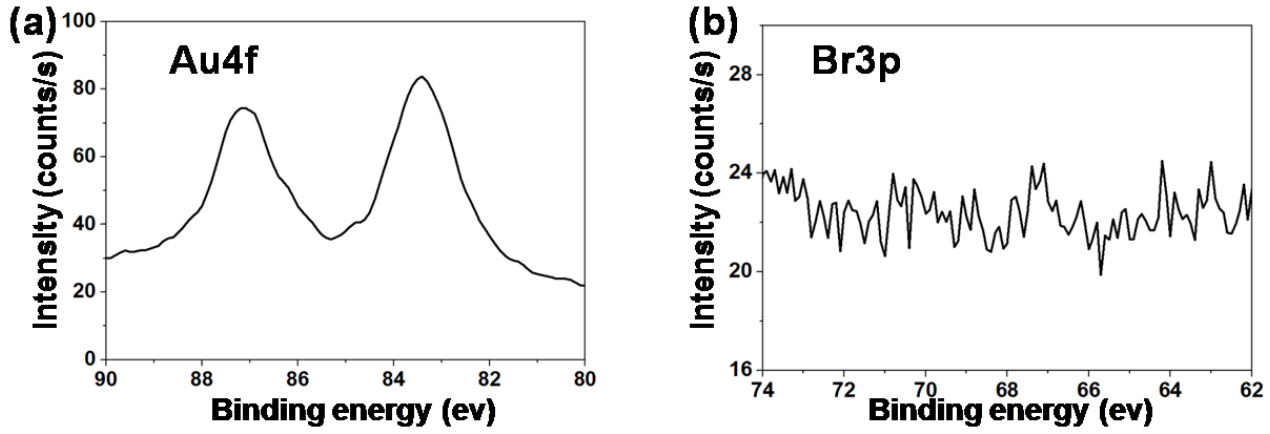

Fig. 2.8. Analysis of surface composition of AuNRs with V_{AuNRs}/V_{DMSO} =0.5 (C_{CTAB} ≅15 uM).

The partitioning of CTAB between the gold surface and the solution through solvent exchange processes has been reported using dimethyl formamide (DMF) or ethanol [19,45]. For example, when a small amount of DMF was added (weight fraction W_{DMF} < 0.3), cationic ammonium group in CTAB is soluble to form a bilayer structure. When large amount of DMF was used (W_{DMF} > 0.7), although the ammonium group become unstable, the alkyl chain in CTAB can confront with external environment to keep the colloidal solubility. With a certain portion of DMF (W_{DMF}=0.3-0.7), both ammonium group and alkyl chain can dissolve in the mixture solution and thus, CTAB was detached from the surface of AuNRs.[45] Similarly, this theory could be used to explain the efficiently removing of CTAB with the windows of V_{AuNRs}/V_{DMSO}=0.5-0.7 and the colloidal stability in other regions.

Table 2.2. Critical micelle concentration of pure CTAB with varying volume fractions of DMSO. Temp.=25 °C. (data from Ref. [46])

V_{DMSO} (%)	0	10	20	30	40	50	60	66	69
C_{CMC} (mM)	0.92	1.48	2.24	3.60	5.62	8.91	14.00	-	-

The self-assembly behavior and critical micelle concentration (CMC) of CTAB in water and DMSO was systematically studied by several decades[46]. Because an interaction of water and DMSO inhibits micelle formation, micelle cannot form with volume ratio of water/DMSO below ~0.34 (**Table 2.2**). On the other hand, when this value is below 0.31, pure CTAB could not dissolve in the mixture solvent. Therefore, the hypothesis that CTAB could form monolayer on AuNRs surface with high ratio of DMSO because CTAB forms reverse micelle in same mixture solvent is untenable. Actually, the attempt to solubilize AuNRs powders obtained by lyophilization in pure DMSO at 29 °C resulted in precipitation (data not shown). By comparing the data in **Table 2.2** and the solubility behavior of CTAB in varying ratio of DMSO and water, possibly the self-assembly and solubility of CTAB is not the only reasons for stability of AuNRs in mixture solvent.

2.3.2. The phase diagram of AuNRs related with the CTAB concentration and volume ratios of DMSO/Water

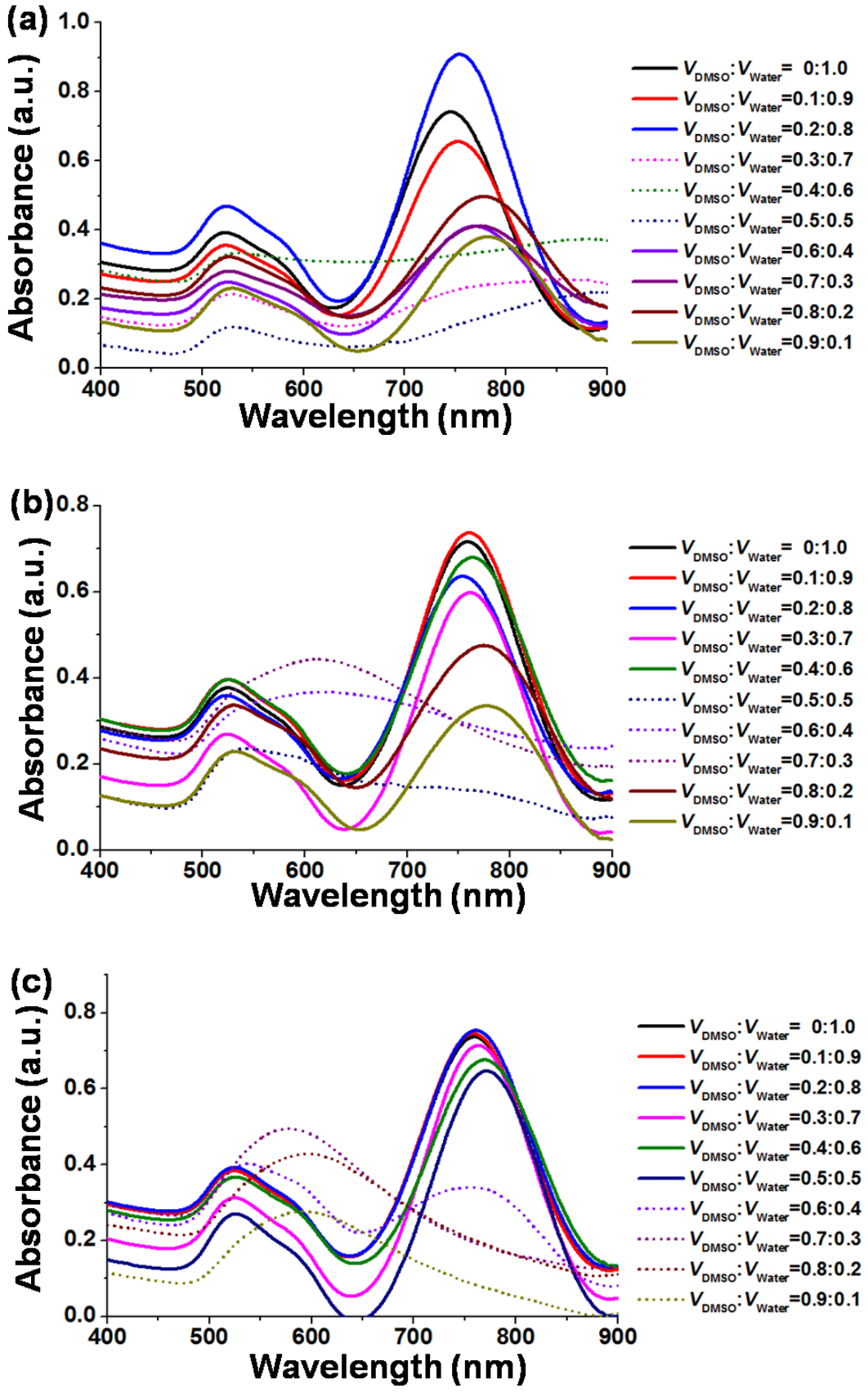

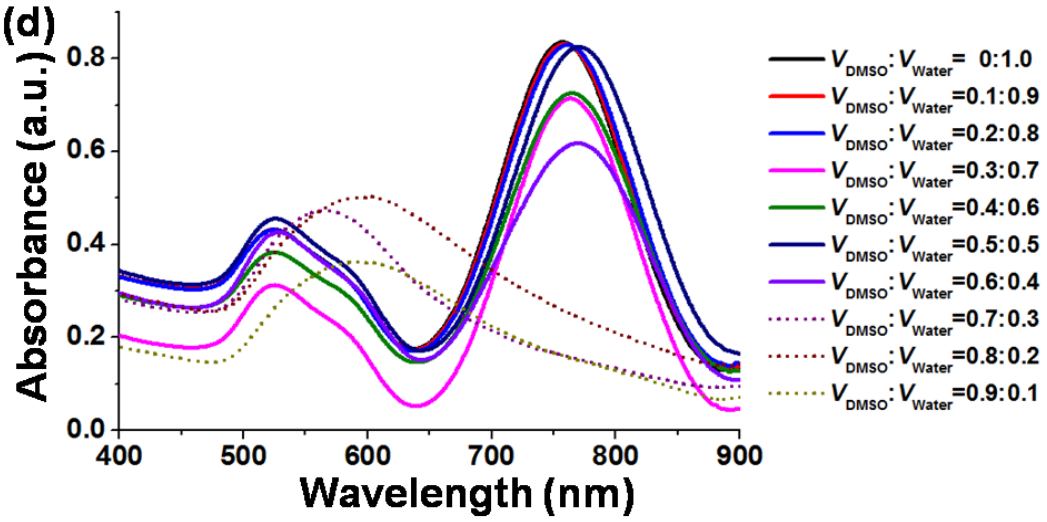

Fig. 2.9. UV-Vis spectroscopy of AuNRs water/DMSO mixture solutions with varying volume ratios of water/DMSO ($C_{[Au]}$ = 0.13 mM) with a final concentration of CTAB (a) C_{CTAB} = 100 uM, (b) C_{CTAB} = 1 mM, (c) C_{CTAB} = 5 mM, (d) C_{CTAB} = 10 mM.

As discussed above, the stability or disturbance of bilayer/monolayer structure of CTAB on the surface of AuNRs highly depends on the volume ratio of DMSO/Water. The same conclusion could be obtained from our experiments, i.e. the change of color, LSPR peak (by UV-Vis spectroscopy), and hydrodynamic diameter (by DLS). The dynamic equilibrium of absorption/detachment of CTAB between the surface of AuNRs and solution also seemed to be influenced by the concentration of CTAB. Because of its quick response, the change of LSPR peak was followed to study this effect on the stability of AuNRs in mixture solvent. Briefly, AuNRs with a series of concentrations of CTAB (from 15 μM to 100 mM) were prepared, and the UV-Vis spectroscopy was performed soon after mixing AuNRs aqueous solution with DMSO (**Fig. 2.9**). For all samples, a resultant red shift of LSPR band results from the increase of the dielectric constant as the fraction of DMSO increased[47]. Moreover, to evaluate the conditions that AuNRs are easy to aggregate and precipitate from solution, the band ratio of LSPR/TSPR is defined as R (with R_0 in aqueous solutions). With the change in concentration of CTAB, the SPR band ratios (LSPR/TSPR) with various volume fractions of DMSO were recorded in **Fig. 2.10**. For samples in aqueous solution with varying concentrations of CTAB, although positions of the peaks of LSPR and TSPR vary with concentration of CTAB, band ratios of (LSPR/TSPR) are almost the same (**Table 2.3**). The possible reason for this is that diffusing speed of CTAB from AuNR surface is relatively slow, so that there is no remarkable aggregation within a short time (for example, 1 day). With the mediate DMSO fraction, the change of R/R_0 is not regular, but with high DMSO fraction (V_{DMSO}>80%), R/R_0 is in the range of 0.8-1.0. The colloidal stability of gold nanoparticles was generally indicated by the change of the full width at half maximum (FWHM). Fox example, FWHM of LSPR peak against CTAB concentrations was recorded after staying for 5 days, and AuNRs with CTAB concentration above CMC was confirmed [19]. In this work, however, all the concentrations of CTAB were below CMC, and the colloidal study varying with DMSO fraction was investigated. In this article, as an empirical value, the threshold of aggregation is defined as R/R_0<0.7. Corresponding, a total of 140 samples with CTAB

concentration and DMSO fraction were tested and a phase diagram of AuNRs was drawn, and shown in **Fig. 2.11.** The x- axis is the volume ratio of DMSO, and the y- axis is the final concentration of CTAB in mixture solvents (in terms of logarithmic axis). Three regions were included, and indicated as Region I, Region II, and Region III. The critical points for the efficient removal of CTAB was plotted (Solid dot between Region I and Region II, open dot between Region II and Region III).

Table 2.3. The intensity of LSPR and TSPR of AuNRs sample in aqueous CTAB solution and the SPR band ratio between them.

Concentration of CTAB	100 uM	1 mM	5 mM	10 mM
LSPR	0.74	0.72	0.74	0.84
TSPR	0.39	0.38	0.38	0.43
LSPR/TSPR	1.89	1.90	1.92	1.93

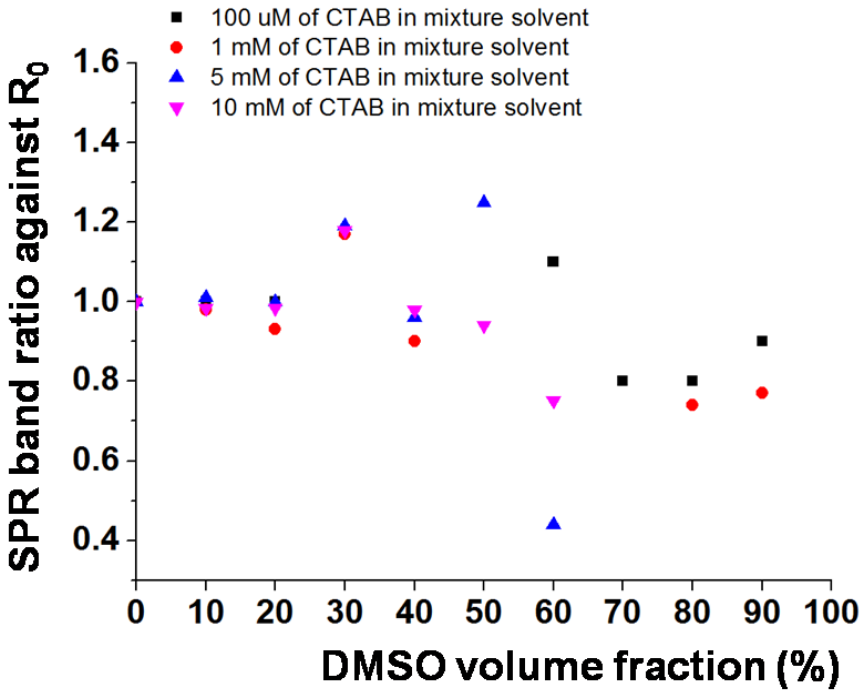

Fig. 2.10. the SPR band ratios varying with volume fractions of DMSO against R_0.

The CMC of CTAB is also drawn in Fig. 8 (black dot line) based on the data in **Table 2.1**. It is noteworthy that all the values of CMC are located in Region I. The critical volume fraction of DMSO (the boundary line between Region I and II) manifest an increase trend from 10% to about 70%, which means the CTAB-bilayer bound AuNRs can resist to the exchange of water with DMSO with the increase of CTAB concentration. Since all the concentrations are below the CMC in the respective volume ratio, the influence of micelle is considered to be negligible. In Regions II, AuNRs quickly loss their stability, and precipitate from solution. In Region III, AuNRs still attain colloidal stability even without free CTAB monomer or micelle in solution. The threshold of DMSO fraction (the boundary line between Region II and III) is

increased from 30% to about 90% with the increase of CTAB concentration. With high fraction of DMSO, the bilayer CTAB structure was disturbed and possibly one layer that is not stable was detached. The alkyl chain interacted with the external environment which maintained the colloidal solubility[19,45]. At the same time, due to the indissolubility of CTAB with weight fraction of DMSO above 0.31[46], the detachment of CTAB from the surface of AuNRs is inhibited. This is possibly the main reason for the inhibition of CTAB in solution to the solubility of AuNRs.

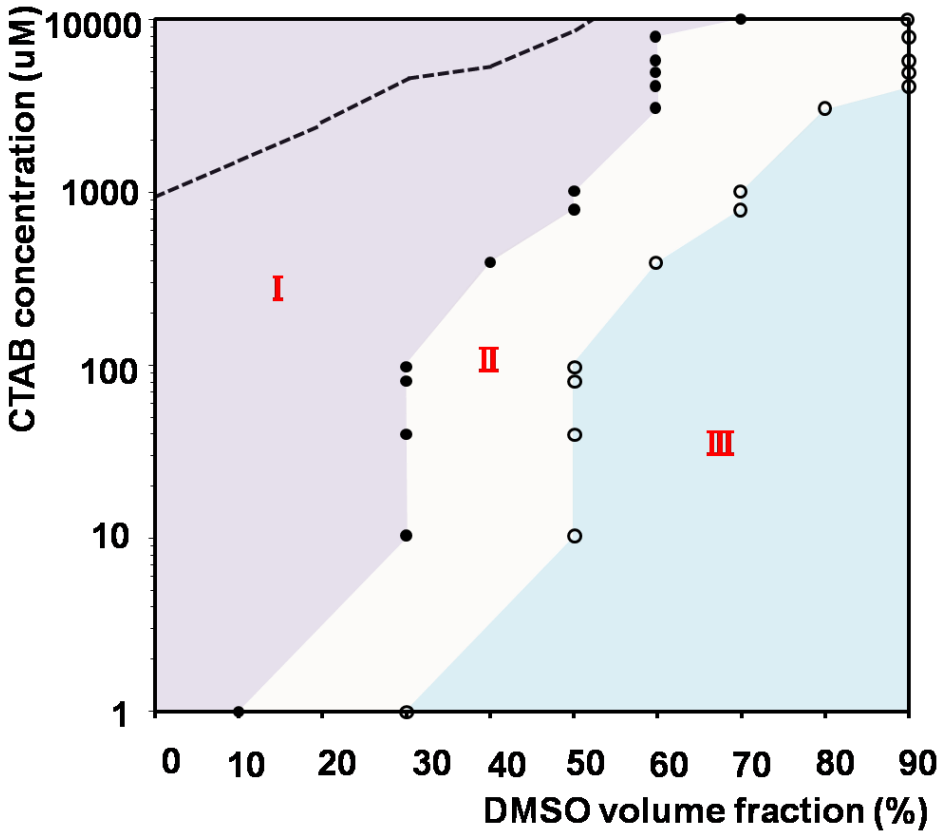

Fig. 2.11. Phase diagram of AuNRs with varying volume ratios of water/DMSO and concentrations of CTAB ($C_{[Au]}$ = 0.13 mM). All the data was recorded by UV-Vis spectroscopy soon after mixing AuNRs aqueous solution with DMSO. The threshold for the efficient removal of CTAB was determined by R/R_0<0.7 (Solid dot between Region I and Region II, open dot between Region II and Region III). The critical Black dot line is the critical micelle concentration in the respective volume fraction of DMSO. The X-axis denotes the value of DMSO volume fraction, and the Y-axis denotes the value of CTAB concentration in logarithm scale.

2.3.3. The ligand exchange reaction using hydroxyl- terminated thiols

Since CTAB on the surface of AuNRs could be completely removed with V_{AuNRs}/V_{DMSO}= 0.5, the ligand exchange experiment using a series of OH- terminated alkanethiols were carried out under this condition. Further the possibility of exact OH- terminated AuNRs into dichloromethane experiment was investigated.

First, 2-ME that is mixable with water was used. After mixing AuNRs with different amount of 2-ME, intensity of peaks of both LSPR and TSPR decreased with time (**Fig. 2.12a-c**), although with the increase of 2-ME, the two peaks could stay for a longer time, both of them decreased by more that 50% after 2 h. Correspondingly, the same color turned up as that simply mixing DMSO and water, and AuNRs could be

stable for a longer time than AuNRs in the same condition but without addition of thiol. Finally, within one day, all the AuNRs precipitated. Therefore, attempt to use 2-ME to sustain the stability of AuNRs was not successful.

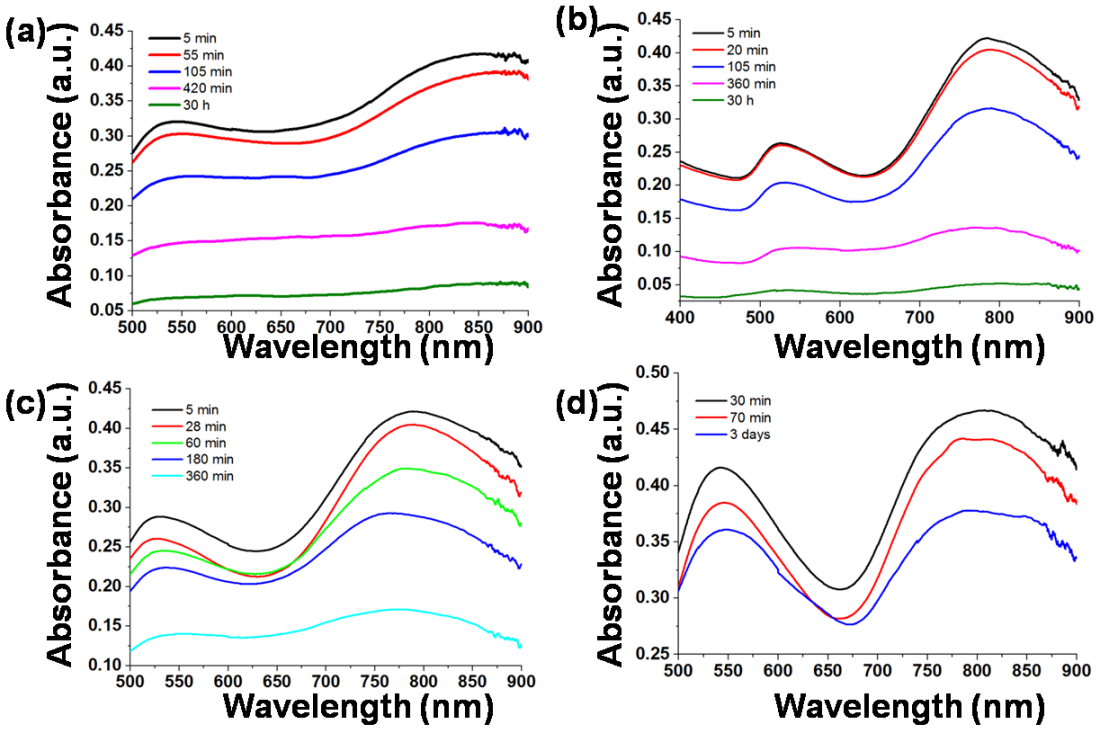

Fig. 2.12. UV-Vis spectroscopy of mixture of alkanethiol in DMSO and AuNRs in water (V_{AuNRs}/V_{DMSO} =0.5) (a) 2 uL mercapto-ethanol, (b) 5 uL mercapto-ethanol, (c) 10 uL mercapto-ethanol, (d) 5 uL 6-mercapto-1-hexanol.

In the case of 6-MH which is also dissolved in mixture of DMSO and water, color changed immediately after mixing without apparent opacity. In **Fig. 2.12d**, the intensity ratio of LSPR to TSPR decreased in the first few minutes, and kept constant after the following days. Concomitantly, there was no apparent precipitation observed by naked eyes. The color change without remarkable aggregation indicates that AuNRs has self-assembled. Wang et al. has studied the self-assembly of AuNRs after introduction of carboxylic acid[18]. Since the current work mainly focus on the ligand exchange, the self-assembly behavior of 6-MH modified AuNRs has not investigated further. After removing of solvent by centrifugation, the collected pellet could not be dispersed in dichloromethane. Therefore, the AuNRs capped by 6-MH were stable in DMSO/Water mixture solution, whereas insoluble in dichloromethane.

When 9-MN was used for three length scales of AuNRs, all the solution became turbid (data not shown). The opacity resulted from the limited solubility of 9-MN in mixture of DMSO and water. After centrifugation of the AuNRs mixed with 9-MN, we first tried to dissolve the pellet in dichloromethane directly, but it formed globule instantly after contacted with dichloromethane. Then the precipitate was first mixed with a certain amount of water to make a suspension of AuNRs, and then dichloromethane was dropped into it, but still AuNRs were located in the water phase.

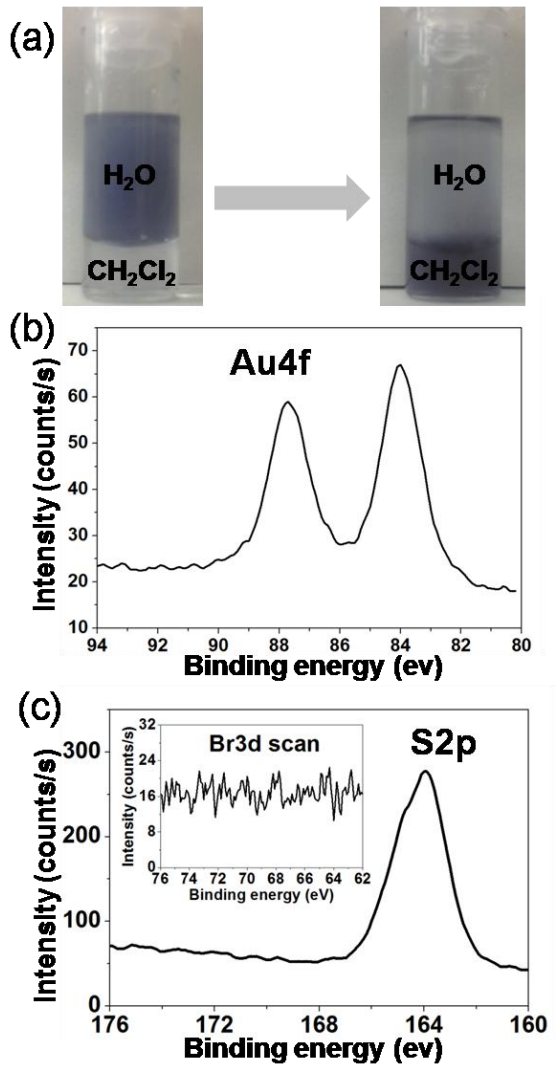

Fig. 2.13. Phase transfer after ligand exchange and addition of dichloromethane using 11-MUD. (a) After addition of dichloromatane and simple shaking, AuNRs would transfer from water to dichloromatane phase. XPS analysis of surface composition of AuNRs after mixed with DMSO and transferred into dichloromethane. Detection of (c) Au and (d) S on AuNRs surface measured by XPS. Inset of c is Br3d signal.

When 11-MUD was used, similarly, the pellet after centrifugation cannot be dissolved in dichloromethane directly. In comparison, when AuNRs were modified with 11-MUD, and transferred to dichloromethane, as shown in **Fig. 2.13a**, the color change transition from water to dichloromethane indicates that AuNRs are transferred from water to dichloromethane. Since CTAB is easy to be dissolved in dichloromethane, the CTAB protected AuNR cannot be dispersed in dichloromethane, so the phase change of AuNR can be one evidence that the AuNRs has been capped with 11-MUD.

Surface composition of AuNRs was also measured after the ligand-exchange reaction. CTAB forms a bilayer structure on the surface of AuNRs, and thereby bromine has been used to identify the capping effect[43]. Bromine signal was also detected on the AuNRs surface before ligand-exchange (**Fig. 2.3d**). In comparison, there were no residual bromine signals discerned in AuNRs capped by 11-MUD, as shown in **Fig. 2.13b-c**. Instead, the thiol signal was discerned, and peak separation of the $S_{3/2}$ level gives two peaks shown in **Fig.**

2.14, one in 163.8 eV, the other one in the range of 162.7 eV, which are in sequence classified into free mercapto and chemisorbed thiol (or thiolate)[48,49]. The covalently bound thiol was about 60% among all the thiols composition. Further attempts to remove free thiols by centrifugation would make AuNRs precipitate. The possible reason for the aggregation is that the attachment of thiol to gold is kinetically slow compared to the detachment of CTAB from AuNR surface[50]. In the mediate ratio of DMSO/Water, the quick color change and disappear of LSPR peak after mixing is one evidence for that. The kinetic control of absorption/detachment of AuNRs needs to be addressed, for example tuning the polarity by changing the solvent [21].

With the thoroughly removing of CTAB by the solvent mixture, the chain length of alkanethiols is very important to transfer AuNRs into dichloromethane. 2-ME, 6-MH, and 9-MN are not strong enough to sustain colloidal stability in dichloromethane. Among them, 11-MUD is the best candidate to have a successful phase transfer.

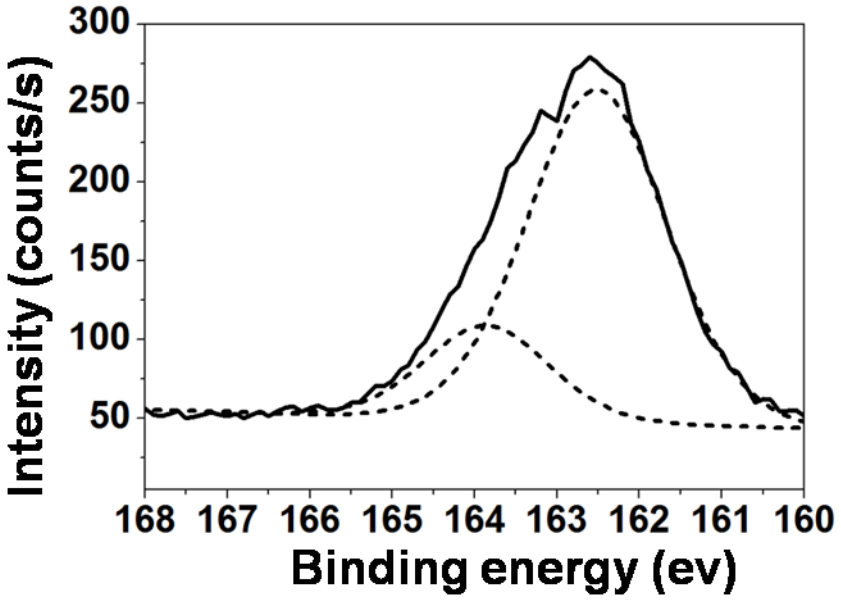

Fig. 2.14. Peak separation of the the $S_{3/2}$ level after AuNRs phase-tranfer from water into dichroromathane.

2.4 Conclusion

A method to remove CTAB efficiently from AuNRs surface for further functionalization is introduced in this work. The efficiency of detachment of CTAB is highly depends on the volume ratio of water and DMSO, and concentration of CTAB. Based on the characterization of color change, LSPR peak position, hydrodynamic diameter, the critical points that AuNRs will lose colloidal solubility are collected and the assembly-behavior diagram was drawn. Three regions, which stand for AuNRs stabilized by CTAB-bilayer, AuNRs easy to aggregation, and AuNRs stabilized by CTAB-monolayer, are included. Both the minimum and maximum thresholds of DMSO fraction for an efficient removal of bound CTAB are increased with the increase of DMSO fraction. Such diagram could be useful when dynamically controlling the ligand exchange reaction in mixture solvent of water and polar organic solvent. Further, under one condition (C_{AuNRs}= 0.13

mM, C_{CTAB} ≅15 uM, V_{AuNRs}:V_{DMSO}=0.5), CTAB could be fully removed from AuNRs surface confirmed with XPS analysis. The chain length of alkanethiols is pivotal for the successful phase transfer. A series of hydroxyl terminated alkanethiols were utilized to modify AuNRs. The thorough ligand exchange of CTAB into hydroxyl terminated alkanethiols and phase transfer to dichloromethane were realized when 11-mercapto-undercanol was used. The hydroxyl terminated AuNRs can be used as a matrix for surface initiated ring opening polymerization, or surface initiated atom transfer radical polymerization, then found use in the biological filed , such as for diagnostics [51].

Chapter 3. Near Infrared Light-Responsive Shape Memory Poly(ε-caprolactone) Films that Actuate in Physiological Temperature Range

3.1. Introduction

Researchers have been focusing on the photothermal effect of metal nanoparticles or photochromic dyes[52,53]. Photothermal effect is a phenomenon produced by the photo excitation of material, resulting in the production of thermal energy[54]. Among them, gold nanoparticles (AuNPs) have been widely employed in numerous biomedical applications including the hyperthermia therapy and biological sensing due to their biocompatibility[55,56]. Especially, gold nanorods (AuNRs) have received much attention due to their biocompatibility, optical property, and photothermal effects[57]. One of the advantages is that the surface Plasmon resonance (SPR) extinction in the near infrared (NIR) regions of AuNRs (650-900 nm) provides opportunities in NIR photoabsorption and scattering, in which there is very limited absorption in most biological tissue such as hemoglobin and water[58].

There have been several reports on remote-controllable SMPs using nanoparticles with absorption in NIR windows[59,60]. For example, Hribar *et al.* have recently reported on NIR light-induced temperature transitions in the shape-memory composites of biodegradable poly(amino ester)s and AuNRs[59]. However, in most of the cases, gold nanoparticles were modified by small molecules, such as thiols with long alkyl chains. The well dispersy of polymers with polymer modified fillers has been explored for many types of particles. It is still unknown whether such technich could be used to modify gold nanorods.

Polycaprolactone, both biocompatible and biodegradable. It was fabricated to nanofibles or thin films, have been widely used as a scaffold for tissue engineering. If we decorate gold nanorods with polycaprolactone, the cytocompatibility of the resultant gold nanorods can be greatly increased. Further, through the well developed conjugation chemistry, many biological targets such as RGD, enzyme, can be further conjugated on gold nanorods, which greatly facilitates the cell recognition. Up to now, there is no report to modify gold nanorods with polycaprolactone.

In the present work, the surface modification of AuNRs were completed. Two methods, “grafting from”, and “grafting to” were used. For the “grafting to” method, polycaprolactone with thiol terminal group was synthesized, and characterized. gold nanorods were directly exchanged with it. For the “grafting from”, first one gold nanorods are ligand exchanged with 4-mercaptophenol, and surface initiate polymerization using caprolactone.

After that, NIR-responsive shape-memory films were newly developed through photo-initiated polymerization of PCL macromonomers with acryloyl terminal groups. Due to the high yield of PCL-modified AuNRs obtained from “grafting from” method, it was used to incorporate in PCL films during cross-linking process. The shape-memory switching temperatures of PCL films were successfully adjusted to near body temperature while retaining a sharp transition in a narrow temperature range. Finally, the local and remote activation of shape memory effect has been demonstrated by irradiating NIR light in the limited area.

3.2. Experimental

3.2.1. Materials

Gold (III) chloride trihydrate, cetyltrimethyl ammonium bromide (CTAB), sodium borohydride ($NaBH_4$), silver nitrate, L-ascorbic acid, 2,2-dimethoxy-2-phenylacetophenone (DMPA) as a photo initiator, were purchased from Sigma-Aldrich (St. Louis, MO, USA). 4-Mercaptophenol was purchased from Tokyo Chemical Industry Co. Ltd. (Tokyo, Japan). ε-Caprolactone was purchased from Tokyo Chemical Industry Co. Ltd. (Tokyo, Japan) and purified by distillation over calcium hydride under reduced pressure. Tetrahydrofuran (THF), acetone, methanol and other organic solvents used in this work were purchased from Wako Pure Chemical Industries (Osaka, Japan). Milli-Q water (Merck, Millipore, MA, USA) was used for all experiment. Without specific description, all of the chemicals were used as received.

3.2.2. Synthesis of PCL- modified AuNRs through "grafting to" method

To synthesis PCL with mercapto terminal group, one method by other researched was followed[61]. Briefly, 2-mercapto-ethanol was used as initiator, and stannous (II) trifluoromethane su lfonate was used as catalyst. The polymerization was carried out at room temperature. By adjusting the molar ratio of 2-mercapto-ethanol to ϵ-caprolactone, PCL with terminal SH- group (defined as PCL-SH) with different molecular weight was synthesized. Two types of PCL-SH with two molecular-weight were synthesized and used for surface-modification.

After that, 5 mM of PCL-SH was dissolved in dimethyl formamide (DMF), and mixed with 1 mL of AuNRs after two-time centrifugation, after 2 h, the solution was dialyzed again water using dialysis membrane (1000 cut-off). The pellet was dried by vacuum pump. The obtained powder was dissolved with dichloromethane.

3.2.3. Synthesis of PCL- modified AuNRs via "grafting from" method

First, milligram-scale of gold nanorods were synthesized by a seed-mediated growth method[62]. Briefly, spherical gold nanoparticles were used as a seed, and CTAB was used as a capped agent to direct the anisotropic growth of gold clusters to form AuNRs.

Then, hydroxyl group was introduced to the surface of AuNRs using the reported method[21]. 4-mercaptophenol (2.5 g) in 30 mL of THF was dropped into the AuNRs aqueous solution. After 12 h, 4-mercaptophenol modified AuNRs were separated out by rinsing with THF and centrifugation several times.

4-mercaptophenol modified AuNRs (10 mg) were dissolved in round-bottom flask and dehydrated and removing oxygen under reduced pressure for 16 hours prior to polymerization. After that, 20 mL ε-caprolactone was added using syringe under flowing dry nitrogen, and after supersonic treatment for 1 hour, a catalytic amount of tin hexanoate were added to the flask under flowing dry nitrogen. The reaction was proceeded for 24 hours at 60 ^{o}C.

After the reaction for 24 h, a homogenous solution was obtained, and there was still some amount of black precipitate in the bottom of flask, which possibly because of limited solubility of AuNRs in ε-caprolactone. 50 mL of THF was added to the above solution. It was centrifuged at 3500 rpm for 15 minutes, the

precipitate was removed. The transparent and slightly red color supernatant was injected into a large amount of diethyl ether and hexane (volume ratio=1:1), in which PCL could precipitate. After vacuum drying, powders were obtained.

To calculate the molecular weight of AuNRs, it was dissolved in $CDCl_3$. and carried out using 1HNMR. The same experiment was done after dealing with AuNRs powders in $CDCl_3$ with iodine for 2 h, and separating the polymer from AuNRs precipitate by centrifugation at 15,000 rpm.

3.2.4. Preparation of AuNR-embedded PCL films

The gold nanorod-embedded shape-memory PCL films were prepared by crosslinking two- and four-branched PCL (2b- and 4b-PCL) with acrylate end-groups in the presence of AuNRs. Considering the possible influence of heat in thermal cross-linking which was generally performed at 80 oC but to avoid the effect of heating to the dispersion of AuNRs in PCL solution, photo- cross-linking was used instead of thermal cross- linking.

To synthesize PCL film, first four branched polycaprolactone PCL (4b10) and two branched polycaprolactone PCL (2b20) and the macromonomer (4b10m and 2b20m) with acryloyl as terminal group were synthesized based on our previous report[28].

2b20m (350 mg) and 4b10m (150 mg) were weighted containing DMPA (15 wt%) and PCL-modified AuNRs at varying concentrations. AuNRs, PCL mamcromonomer, photo-initiator were mixed together using vortex mixer, and supersonic treatment was performed for about 1 min. After repeating vortex and supersonic treatments for several rounds, a homogeneous solution can be obtained. The solution was place in 0.2 mm space between glass plates with Teflon® frame spacer and cured under the irradiation of UV light with 365 nm. The intensity of UV lamp was 2 mW/cm^2. After the thorough reaction for at least 3 hours, and the resultant films was immersed in a large amount of acetone to remove the unreacted compounds, and finally washed using methanol after which the film was dried using vacuum pump. The films obtained were defined as 50/50 PCL-low, 50/50 PCL-high, 70/30 PCL-low, 70/30 PCL-high, respectively.

3.2.5. Near infrared light-responsive shape recovery performance

Shape memory performance was evaluated along the order below. First, PCL film (3 mm by 1.2 cm) was heated to 40 ^oC (above T_m) and elongated to the predetermined strain of 100 %, and the temperature was then cooled to 4 ^oC (below crystallization temperature T_c) for 10 min to fix applied strain while keeping the tensile strain. The films were then irradiated with 805 nm NIR at varying power densities between 0.4 and 1 W cm^{-2} at a constant beam diameter of 5.6 mm. The surface temperature of film samples was measured using an infrared thermal imaging camera during irradiation of NIR light.

Shape memory performance was performed along the order below. First, PCL film (3 mm by 1.2 cm) was heated to 40 ^oC (above T_m) and elongated to the predetermined strain of 100 %, and the temperature was then cooled to 4 ^oC (below crystallization temperature T_c) for 10 min to fix applied strain while keeping the tensile strain. Shape recovery of the film was induced by near infrared light with power densities of 0.4-1 W cm^{-2} (Wavelength of 805 nm, spot size of 5.6 mm, ML620G40 Mitsubishi, Japan). The surface temperature of film samples was measured using an infrared thermal imaging camera during irradiation of NIR light.

3.2.6. Characterization

UV-Vis-NIR absorption experiment was performed using UV/Vis/NIR spectrophotometer (V-7200 Jasco, Tokyo, Japan). To measure the absorption of samples, reflectance mode was utilized and transformed to absorption mode. Transmission electron microscopy (TEM) images were obtained on a JEM-2100F (JEOL, Tokyo, Japan). Phosphotungstic acid hydrate was used as the negative staining agent. Particle size distributions were obtained by measuring more than 50 particles from the corresponding transmission electron micrographs using SmileView software (JEOL Corp., Japan). To prepare thin film for TEM observation, first a xylene solution of PCL and PCL modified gold nanorods was prepared by vortex mixing and ultrasonication, and kept for 2 h to make a homogenous solution. Separately, a TEM grid with thin carbon film coated was fixed on the sample holder of spin coating machine. After that, 5 uL of sample was dropped onto the TEM copper grid, and instantly spin-coating was done to disperse the liquid sample (speed: 8000 rpm; acceleration time: 1 s. spin time: 60 s).

^{1}HNMR (300 MHz, JEOL, Tokyo, Japan) was used for the characterization of polymers and nanorods. $CDCl_3$ was used as solvents. To avoid peak broadening phenomenon of thiol-protected gold nanoparticles, iodine was used to cleave the Au-S covalent bonding.[63] The melting temperature was measured by differential scanning calorimetry (DSC 6100, Seiko Instruments Inc., Chiba, Japan) at 5 ^{o}C min^{-1} of programming rate.

The degree of crystallinity was calculated based on the equation

$$\chi = \frac{\Delta H_m}{\Delta H_m^o} \times 100\%$$

ΔH_m is the melting enthalpy of the samples used in this work.

ΔH_m^o is the melting enthalpy of full crystalline PCL (139.5 Jg^{-1})[64].

The successful surface grafting of PCL on the AuNRs was evaluated via the weight loss as a function of temperature by thermogravimetric analysis (TGA, EXSTAR6000 TG/DTA, SII Nanotechnology, Tokyo, Japan). Surface temperature of the sample was measured using infrared camera (FLIR System Japan K.K., Tokyo, Japan).

3.3. Results and discussion

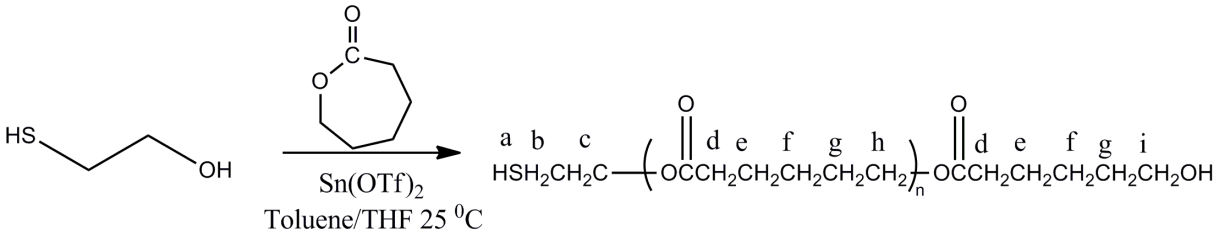

Fig. 3.1. Synthesis of thiol terminated polycaprolactone (PCL-SH) according to previously reported method[61]

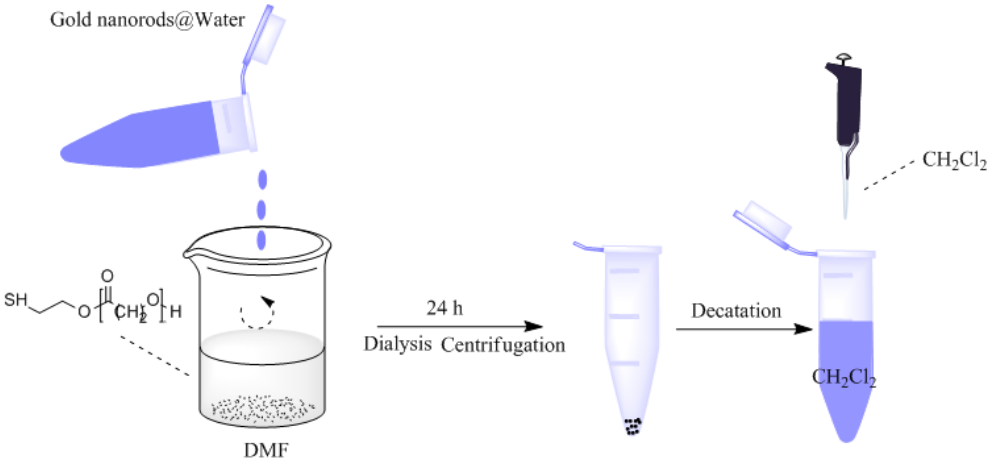

Fig. 3.2. Preparation of PCL-SH modified AuNRs through "grafting to method".

Table 3.1. Characterization of PCL-SH by GPC and ^{1}HNMR

	Mn (^{1}HNMR)	Mn (GPC)	Mw/Mn
PCL-SH (a)	1700	1700	1.08
PCL-SH (b)	3500	2500	1.25

The procedure to synthesize PCL-SH was shown in **Fig. 3.1** and characterized with ^{1}HNMR (**Fig. 3.3**) and GPC (**Fig. 3.4**). The molecular was obtained by calculation the integration area of the proton from the methylene proton close to the terminal OH- group (δ=3.64), and the proton close to ester bond (-$CH_2CH_2CH_2CH_2$*CH_2*O-, δ=4.05). The obtained data was shown in **Table 3.1**.

AuNRs were modified with PCL-SH with different MW and amount, the procedure of which is shown in **Fig. 3.2**, and the images of AuNRs that dissolved in dichloromethane was shown in **Fig. 3.5**. It is clear that with the increase of amount and molecular weight of PCL-SH, colloidar stability of AuNRs was increased.

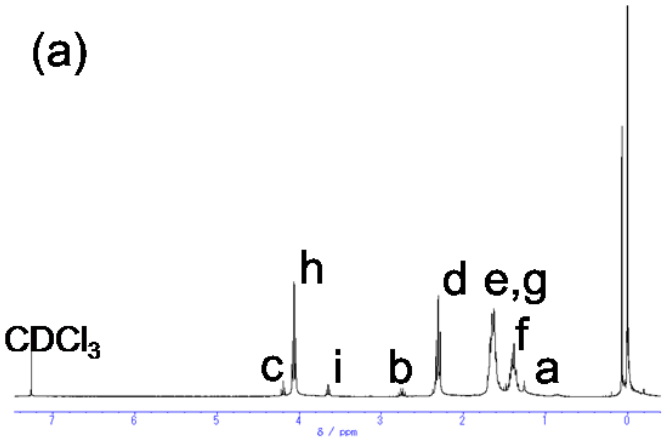

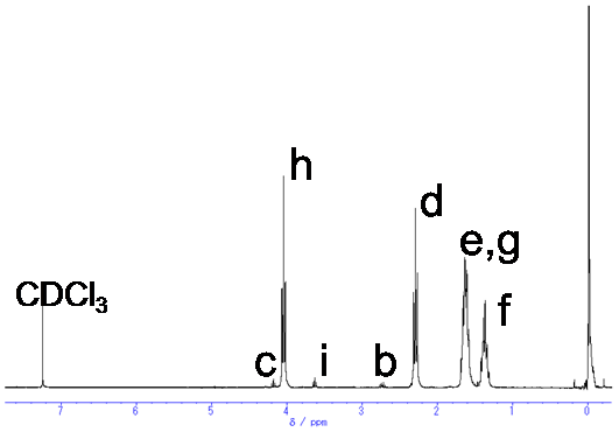

Fig. 3.3. Characterization of PCL-SH by ^{1}HNMR with different molar ratio of initiator to monomer.

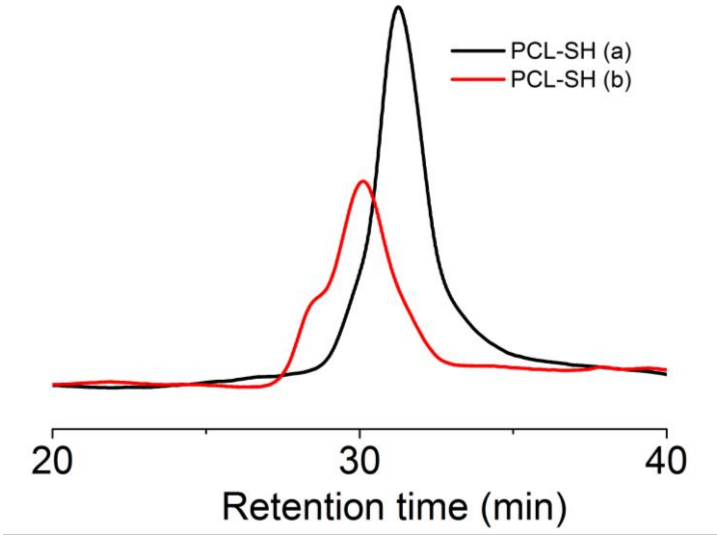

Fig. 3.4. Characterization of PCL-SH by GPC.

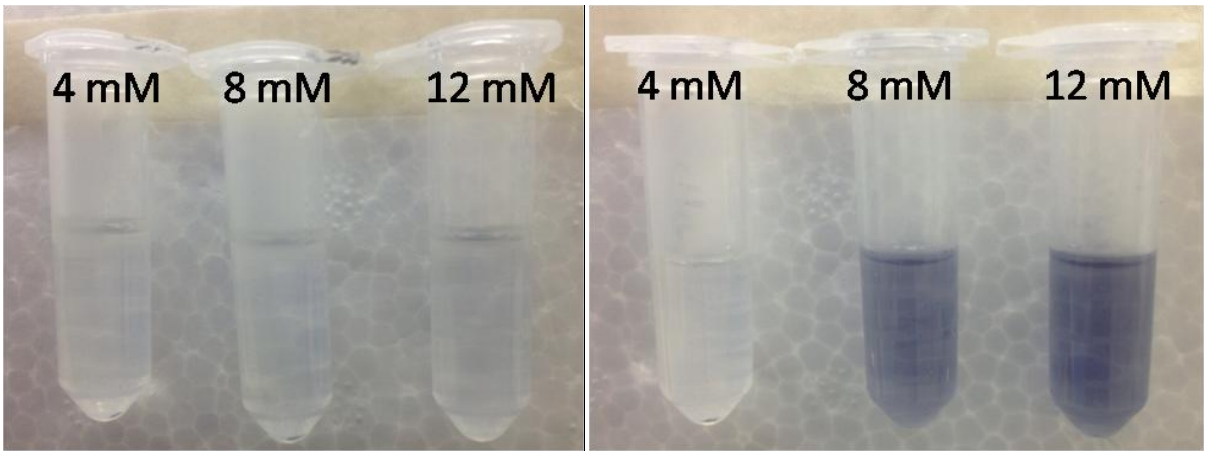

Fig. 3.5. Image of AuNRs in dichloromethane after surface modification with 4 mM, 8 mM, 12 mL of PCL-SH(1700) (left image) and PCL-SH(3500) (right image).

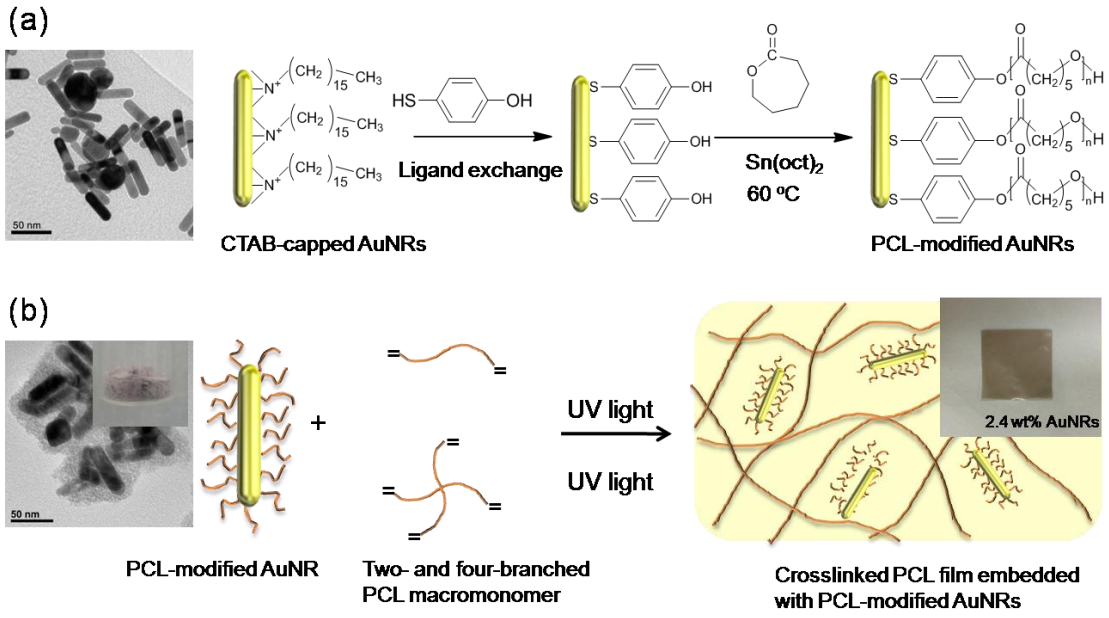

Fig. 3.6. (a) Synthesis of PCL-modified AuNRs by surface initiated ring opening polymerization. (b) Preparation of AuNR-embedded PCL film by crosslinking two-branch and four-branch PCL macromonomers in the presence of the PCL-modified AuNRs. The TEM/digital images of 4-mercaptophenol, PCL modified AuNRs and PCL-AuNRs composites films were given.

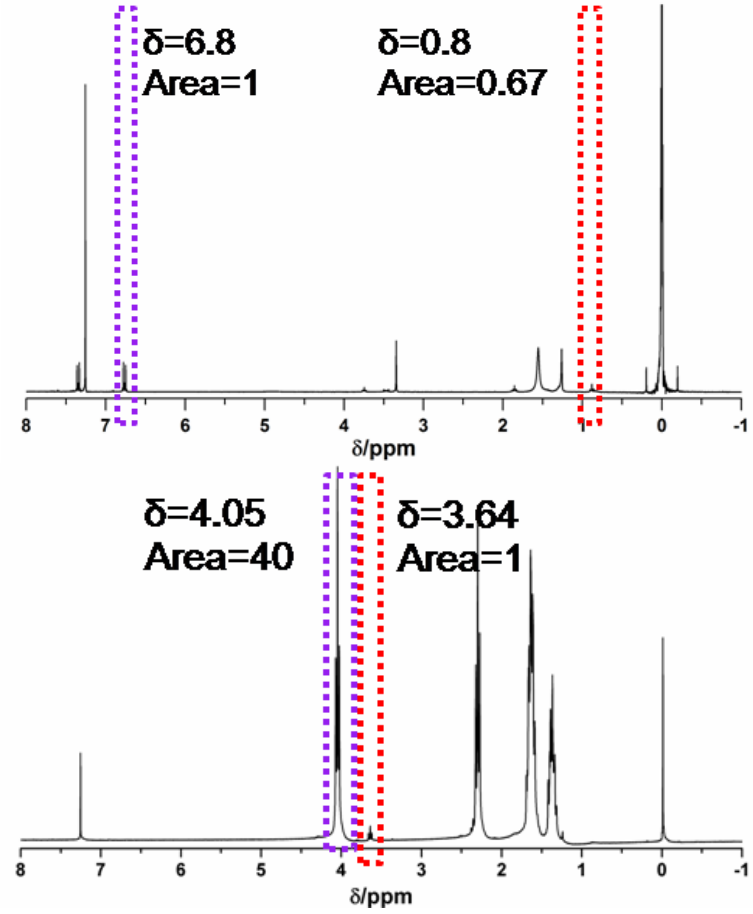

Figure 3.7. ^{1}HNMR spectra of AuNRs modified by (above) 4-mercaptophenol and (below) PCL.

The scheme to synthesize AuNRs-PCL film was shown in **Fig. 3.6.** The polymer matrix is synthesized based on our previous report. The transition temperature was tuned by adjust the initiators and monomer numbers[65]. Melting temperature and melting enthalpies (ΔH_m) obtained from DSC measurement was shown in table 1.

The surface was modified by PCL through introducing hydroxyl- group and surface initiated ring opening polymerization respectively. Then PCL was grown on the surface of AuNRs through SI-ROP reaction, the "grafting from" way. Considering the activated temperature of tin hexanoate is above 40 ^oC[66], and the covalent bond between gold and thiol will be generally unstable above 80 ^oC[67], the SI-ROP reaction was carried out at 60 ^oC.

To characterize the molecular weight of the polymer grafted on the surface of AuNRs, iodine was used to destroy the Au-S covalent bonding and the molecular weight was measured by comparing the integration area of the proton from the methylene proton adjacent to the terminal hydroxyl group (δ=3.64), and the proton close to ester bond (-$CH_2CH_2CH_2CH_2$*CH_2*O-, δ=4.05). A degree of polymerization of 41 was obtained. Meanwhile, it is know that the NMR line in small metal particles will broaden with respect to the bulk solution due to Knight shift oscillations near the surface[68]. According to **Fig. 3.7** of ^{1}HNMR spectra of AuNRs in chloroform-d, AuNRs decorated with 4-mercaptophenol, 67% CTAB were exchanged with 4-mercaptophenol by calculation the integral area of terminal methyl of alkyl chain (δ=0.88) and protons in benzene ring (δ=7.33, 7.36). The reason why CTAB has not be fully removed by 4-mercapophenol is possibly because that the rigid structure of benzene group is hard to react with all CTAB with high volume density on nanorods surface[36].

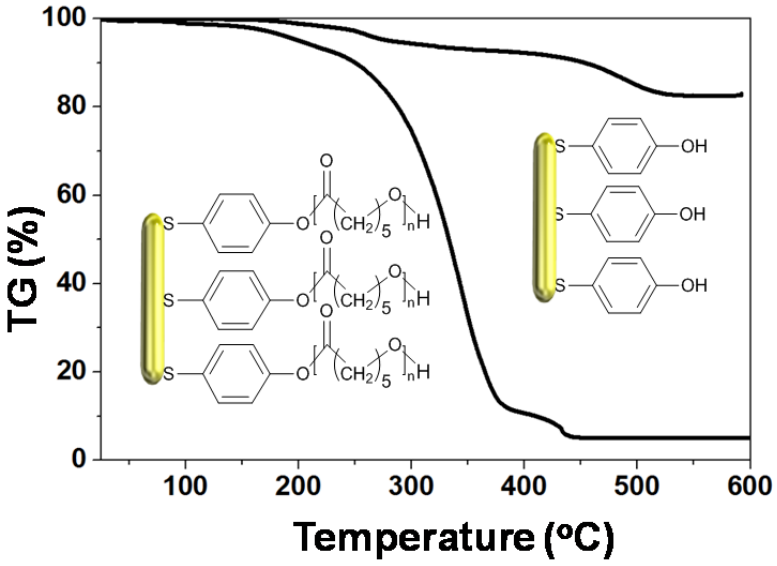

Fig. 3.8. The TG-DTA curves for AuNRs after ligand exchange reaction with 4-mercaptophenol and modification with PCL.

The CTAB capped, and PCL modified AuNRs and PCL-AuNRs nanocomposites films were also shown in **Fig. 3.6**. The average size of gold nanorods was 43.0±3.7 nm (length) and 11.0±1.0 nm (width). AuNRs

were surrounded by polymers with lighter contrast. The PCL-modified AuNRs shown inset of have a homogeneous weak pink color.

The successful modification of the PCL on the nanorod surfaces was also confirmed by TGA (**Fig. 3.8**). It was found that, below 200 ^{o}C, the weight loss of PCL modified AuNRs is 5%, while the weight loss of 4-mercaptophenol modified AuNRs was about 1%, indicating there is only limited water in both samples. Between 200 ^{o}C and 500 ^{o}C, the weight loss of PCL modified AuNRs is 90%, while the weight loss of 4-mercaptophenol modified AuNRs is 14%. Therefore, the successful surface modification of gold AuNRs by PCL was realized.

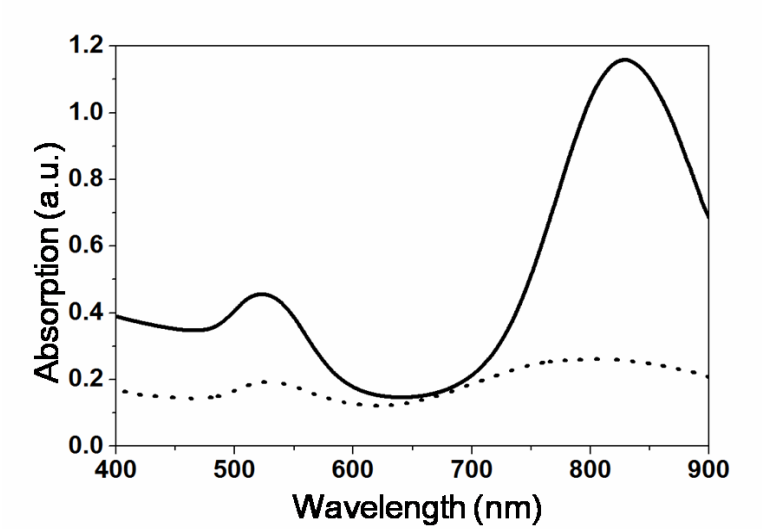

Fig. 3.9. UV-Vis-NIR spectra of CTAB-capped AuNRs in aqueous solution (solid) and PCL-modified AuNRs in THF (dotted).

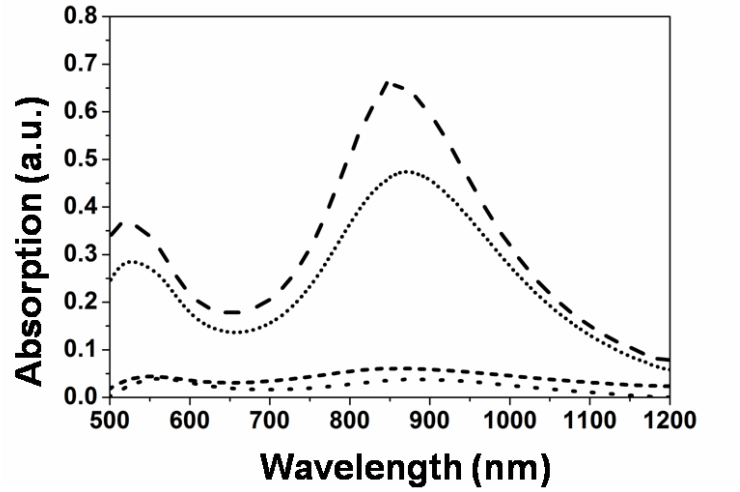

Fig. 3.10. UV-Vis-NIR spectra of PCL-modified AuNRs embedded in 50/50 (black line) and 70/30 (grey line) PCL films with high (solid) and low (dotted) concentrations of nanorods.

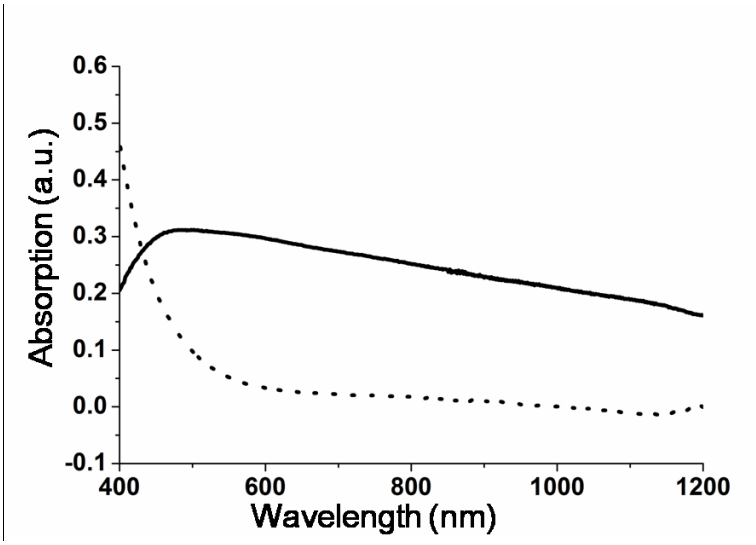

Fig. 3.11. UV-Vis-NIR spectra of 70/30 PCL films with unmodified AuNRs (solid) and without AuNRs (dotted).

Incorporating rigid segments or blending with other components decreases the T_m of PCL, but, incorporation of non-PCL components usually hinders the crystallization and diminished the melting enthalpies (ΔH_m). Therefore, the T_m of PCL by tailoring the nano-architectures of PCL macromonomers is utilized in this study.

Two different films with 50/50 and 70/30 wt% of 2b- and 4b-PCL macromonomers were fabricated through photo- crosslinking of the PCL macromonomers in xylene in the presence of AuNRs. To make AuNRs disperse well in PCL matrix, AuNRs modified through "RI-ROP" reaction was used. The characteristic localized surface plasmon resonance absorption of freshly prepared AuNRs aqueous solution, and PCL modified AuNRs in THF were shown in **Fi. 3.9.** AuNRs has two surface plasmon resonance peaks, one in the visible region (transverse surface plasmon resonance, TSPR), another one in the near infrared region (longitudinal surface plasmon resonance, LSPR). Intensity of LSPR is much larger than that of TSPR. If AuNRs aggregated, intensity of LSPR would decrease much comparing with the peaks of TSPR, which could be used to indicate the dispersity of AuNRs in matrices. In aqueous solution, there are two peaks (524 nm, and 829 nm) (Fig. 3.3a). After modified with PCL, AuNRs was stable in THF, and the blue shift of LSPR peaks resulted from the change of dielectric constant around AuNRs (**Fig. 3.9**).

Fig. 3.10 shows UV-Vis-NIR spectra of PCL modified AuNRs embedded in PCL films. Both 50/50 and 70/30 PCL with higher concentration of nanorods (solid line) show strong peak adsorptions of TSPR and LSPR, although the peak adsorptions were not significant when the concentration of AuNRs was low (dotted line). This behavior indicates that AuNRs were uniformly embedded in the PCL films. When unmodified AuNRs were used, only one peak in the visible region was obtained (solid line in **Fig. 3.11**). These results clearly indicate that surface modification of AuNRs with PCL is significantly important for improving the stability of the particles within the PCL film.

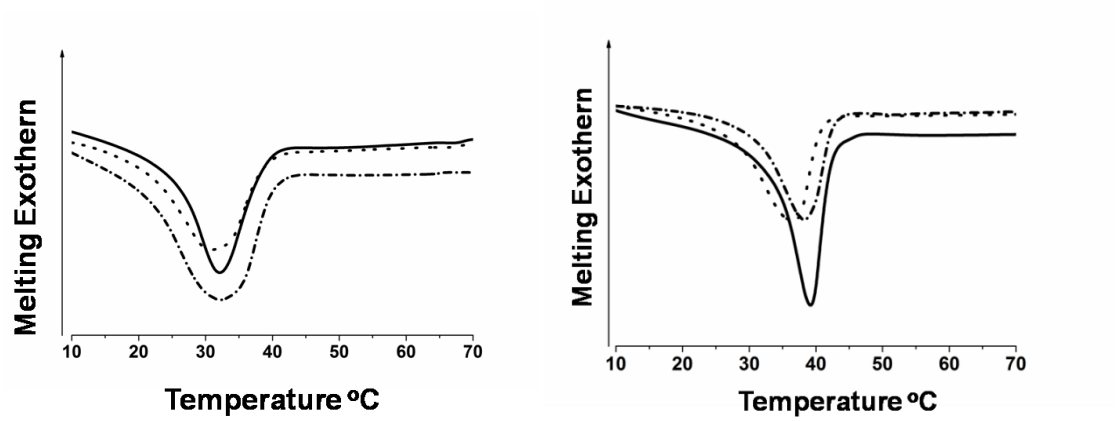

Fig. 3.12. DSC curves for(a)50/50 and (b) 70/30 PCL films without (solid) and with high (solid) or low (dotted) concentrations of nanorods.

The thermal properties of PCL are also important from both fundamental and technological perspective. In this study, we prepared the crosslinked PCL films with two different T_m by optimizing the mixing ratios of 2b- and 4b-PCL macromonomers. According to our previous report, increasing 4b-PCL content leads to a near linear decrease in T_m and endothermic enthalpy change[65]. In **Fig. 3.12 a-b**, the crosslinked PCL films with 2b/4b ratio of 50/50 and 70/30 showed a sharp transition over the T_m around 30-33 and 37-40 ^oC, respectively. The degree of crystallinity of all samples was listed in **Table 3.2**. Importantly, the transition temperature did not change very much by the incorporation of AuNRs. This observation was different from other reports. In general, nanoparticle incorporation results in the loss in crystallinity and reduction in T_m[60]. It is plausible that the surface modification of nanorods with PCL contributed to prevent the loss of crystallization of PCL films.

The strain fixity rate (R_f) and the strain recovery rate (R_r) were approximately 99.9% and 99.5%, respectively[28]. The result was shown in **Table 3.3**. In general, R_f and R_r values become low as T_m decreases because the enthalpy observed around T_m is reduced by hindering crystallization of polymer chains. But, our results indicate that the cross-linked PCL has excellent shape-memory ability.

To examine the heating potential of the films, samples were held within a beam of NIR light (805 nm). **Fig. 3.13** depicts the temperature increase with time for 70/30 PCL film with 0.3 wt% (low concentration) of AuNRs under different excitation laser intensities. Samples showed a sharp increase in temperature during the first 10 s of irradiation before reaching a plateau. Higher intensity irradiation (1.0 Wcm^{-2}) results in a higher final equilibrium temperature (T=39.7 ^oC) as compared to that attained with a lower excitation intensity (0.4 Wcm^{-2}, T=32.0 ^oC). Essentially little change in temperature was observed for samples that did not contain AuNRs (data not shown). These results indicate precise control over the sample heating through changes in light intensity. AuNR concentration also affects the heating profiles. But, we chose the lower concentration (0.3 wt%) of AuNRs for the following shape-memory experiments because this heat dissipation should be capable of producing rapid and complete shape memory transformations in the physiological temperature range.

Table 3.2. Melting enthalpy and degree of crystallinity based on DSC result

Composition	70%-30%	70%-30%-0.3% AuNR	70%-30%-2.5% AuNR	50%-50%	50%-50% 0.4% AuNR	50%-50%-2.4% AuNR
melting enthalpy (J.g-1)	43.4	36.3	36.0	29.2	29.7	29.3
degree of crystallinity (%)	31.1	26.0	25.8	20.9	21.3	21.0

Table 3.3. Shape-memory ability of PCL films

Composition	0% AuNRs	0.4% AuNRs	1.2% AuNRs	2.4% AuNRs
Rf (%)	99.4	99.2	99.4	99.7
Rr (%)	94.8	94.3	93.7	93.7

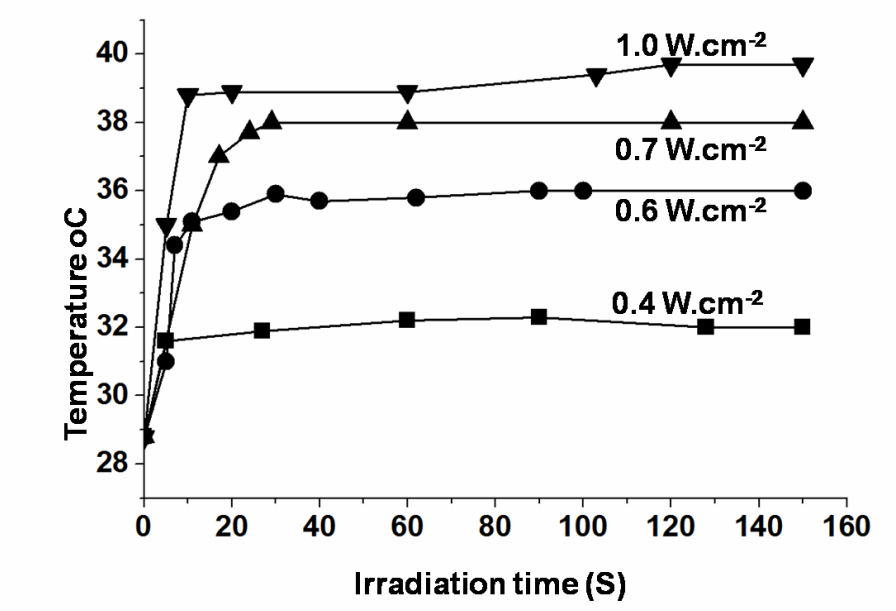

Fig. 3.13. Heating profiles for 70/30 PCL films with 0.3 wt% of AuNRs under different laser intensities of NIR (805 nm); 0.4 (square), 0.6 (circle), 0.7 (triangle), 1.0Wcm^{-2} (inverted triangle).

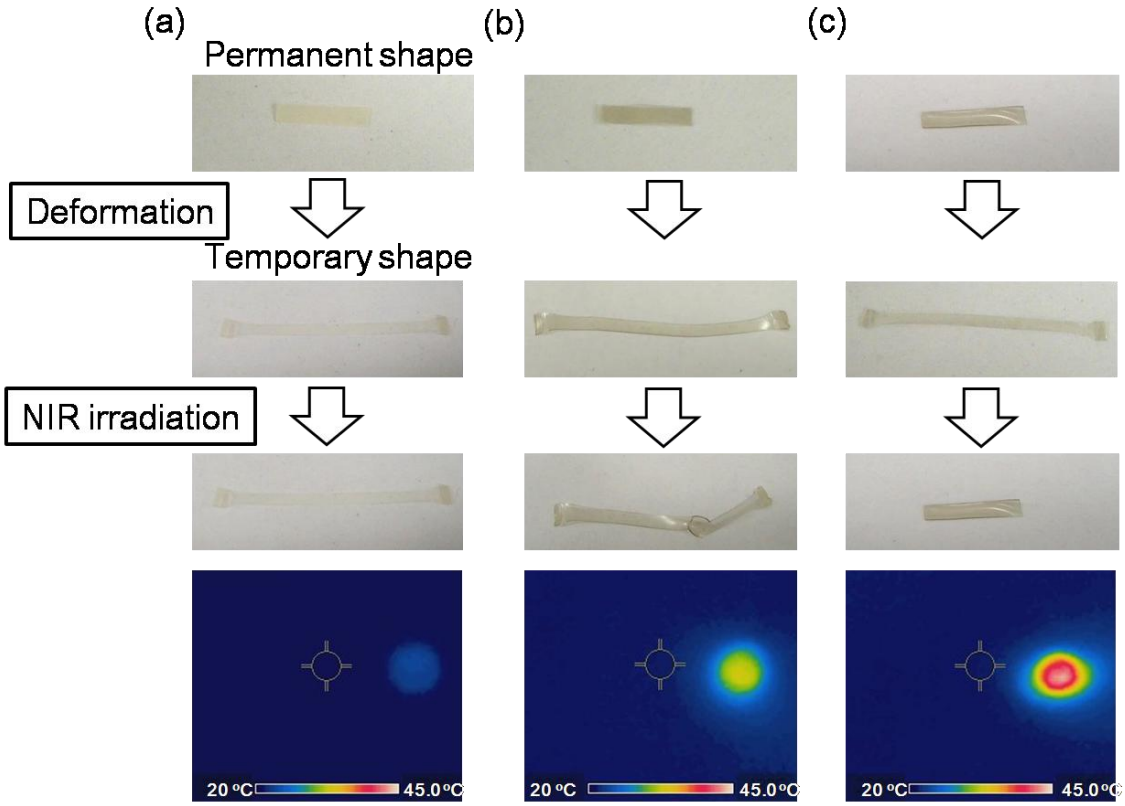

Fig. 3.14. Images of NIR light-induced shape transitions of 70/30 PCL films with 0.3wt% of AuNRs. The films were first heated to 40°C (above T_m) and elongated to the predetermined strain of 100 %. The temperature was then cooled to 4°C (below crystallization temperature T_c) for 10 min to fix applied strain while keeping the tensile strain. The films were irradiated with 805 nm NIR at power densities of 0.4 and 1 Wcm^{-2} for a total of 10 s irradiation time. The IR thermal images of the films after 10 s irradiation of NIR are also shown in the bottom images.

Finally, we examined the NIR light induced shape-memory effect using a 70/30 PCL film with 0.3 wt% of AuNRs. The films were first heated to 40 °C (above T_m) and elongated to the predetermined strain of 100 %. The temperature was then cooled to 4 °C (below crystallization temperature T_c) for 10 min to fix applied strain while keeping the tensile strain. The films were irradiated with 805 nm NIR at power densities of 0.4 and 1 Wcm^{-2} for a total of 10 s irradiation time (**Fig. 3.14**). The bottom images in **Fig. 3.14** show the IR thermal images of the films after 10 s irradiation. PCL film without AuNRs showed negligible recovery since the polymer absorb minimally at the excitation wavelength (**Fig. 3.14a**). When the beam at a power density of 0.4 Wcm^{-2} hit local area of the PCL film with AuNRs, the shape change in the corresponding area was observed (**Fig. 3.14b**). The IR thermal image also shows a temperature increase in the corresponding area. Note that the shape-memory transition was induced even though the observed temperature of the irradiated area was around 32 °C which is lower than the T_m. This is because thermal camera measures IR radiation from objects and estimate the surface temperatures. Therefore, the temperature inside the film can be higher than the T_m. When exposed to 1 Wcm^{-2} of NIR light, the film heated quickly to near 40 °C and changed back to its permanent rectangular shape due to the heat dissipation to the whole film (**Fig. 3.13c**). These results

show the ability of embedded AuNRs to heat a PCL film through its T_m, as well as the spatial control of the shape in physiological temperature range.

It has been reported that it takes hundreds of ps to transfer energy to medium[23]. The responsive time of about 5-10 s is explained by two aspects: First, either in aqueous solution or in solid state, there a one remarkable absorption in near-infrared region. And as shown above, the time from light absorption to heat generation was 100 ps. But because of the high difference between the thermal conductivity of gold and medium, such as water or polymers, it take time to heat the bulk materials.

3.4. Conclusion

In summary, NIR light-responsive shape memory films were successfully prepared through crosslinking of PCL macromonomers in the presence of AuNRs. First, the surface of AuNRs was modified with PCL through SI-ROP. This enabled to incorporate AuNRs into PCL film uniformly without hindering the crystallization of PCL. The shape-switching temperature was also adjusted in physiological temperature range by controlling the melting temperature of PCL. Exposure to NIR light could successfully induce the photothermal heating of embedded AuNRs and consequently, shape-switching transition. Upon NIR irradiation, the film completely recovered its original shape. Local shape-memory transformation was also obtained when the limited area was exposed to the light. These results show the potential ability of the AuNRs embedded PCL film as the remote and spatial controllable shape-memory material that actuates in physiologically relevant temperature ranges. This material is highly attractive for a wide range of applications, including safe and efficient transdermal SMP activation.

Chapter 4 Near-Infrared Light-Induced Remote Activation of Surface Shape-memory to Direct Cell Orientations

4.1. Introduction

Shape-memory polymers (SMPs), which have the ability to remember and recover their original shape upon heating, have drawn much attention from fundamental research to practical applications.[69-71] Especially, development of biodegradable SMP-based devises has increased for pursuing various biomedical applications over the last decade, such as use in minimally invasive surgeries, tissue engineering, or bio-MEMs. Lendlein and Langer, for example, demonstrated the biodegradable SMP sutures for wound closure[25]. An abdominal wound in a rat was loosely sutured using the SMP fiber, and then heated to body temperature to achieve wound closure. Maitland et al. reported SMP-based clot extraction devices to treat ischemic stroke[72]. These devices were designed to be delivered through a catheter and penetrate the clot in a narrow form, and then actuate into a clot-grabbing form for clotextraction. The concept of a drug-eluting SMP vascular stent are also reported by Wache et al[73]. Lantada et al., on the other hand, proposed a resistively heated SMP ring to enhance the annuloplasty procedure for remotely controlled post-operative diameter reduction[74]. The thermally responsive SMP ring would be implanted in a temporary shape corresponding to the shape of the patient's malfunctioning mitral valve, reducing the acute impact of the procedure on the heart. Other potential scenarios in which SMP could be applied include bio-MEMs. We have recently reported SMP-based microfluidic devices that display rewritable properties[75-77]. The effects of dynamic geometric changes of the shape-memory channels on the microfluidic flow were also investigated and shape-memory channel closing was achieved by the application of heat.

Although a thermally induced shape-memory effect can be achieved by an increase in temperature, the shape-memory activation by remote light irradiation could lead to a variety of potential biomedical or other applications. Eisenbach et al., for example, demonstrated the photomechanical and thermal cis-trans isomerization of azochromophores induced in photochromic poly(ethyl acrylate) networks with azo-aromatic crosslinks[78]. Li et al. reported aligned nematicazo side-on elastomers which show fast photochemical contraction by UV light[79]. Lendlein et al. reported that polymers containing cinnamic groups can be deformed and fixed into predetermined shapes by ultraviolet light illumination[80]. When the polymer film is mechanically stretched and illuminated by >260 nm wavelength UV light, the photosensitive groups crosslink and lock the polymer into a new shape. Exposure to UV light at ambient temperatures cleaves the new crosslink bonds, allowing the material to spring back to its original shape. In addition to UV light, near-infrared (NIR) light-induced SMPs have been also reported[59,60,81]. In those cases, the photothermal effect of metal nanoparticles or photochromic dyes embedded in thermally induced SMPs is used to trigger shape-memory transitions[82]. One of the advantages of using NIR light is that NIR wavelengths (650–900 nm) penetrate tissues well due to the limited absorption in most biological tissues, including hemoglobin and water. Gold nanorods (AuNRs) have been widely employed as a NIR-induced heat generating material in numerous biomedical applications, including hyperthermia therapy and biological sensing[83-86]. We have also

reported the AuNR-embedded NIR light-responsive SMPs and demonstrated the local and remote activation of shape memory effects by irradiating with NIR light in physiological temperature range[87].

In this study, the NIR light-induced shape-memory transitions of nanopatterns were demonstrated using AuNR-embedded poly(ε-caprolactone) (PCL) films. We have recently demonstrated PCL cell culture surfaces with shape-memory nanopatterns[28,88]. Here, we extend this surface shape memory phenomenon to the local and remote activation of nanopatternsby spatially limiting the NIR-illuminated region. First, the effects of the concentration of embedded AuNRs, intensity of NIR light, or irradiation time on the shape-memory transition were studied by atomic force microscopy (AFM). The temporary surface patterns were easily programmed on the PCL films and triggered to transition quickly to the permanent surface patterns. The NIR actuated shape memory nanopatterns were also used to control cell morphology remotely and locally. Finally, cell morphologies on the PCL films before and after a topographic transition were investigated by spatially limiting the NIR-illuminated region.

4.2. Experimental

4.2.1 Materials.

To synthesis of AuNRs incorporated PCL films, the same materials were used as the experimental in Chapter 3. Dulbecco's Modified Eagle's Medium (DMEM) and other biological reagents were purchased from Sigma-Aldrich (St. Louis, MO, USA).Without specific description, all of the chemicals were used as received.

4.2.2. AuNRs-PCL nanocomposite films with surface pattern.

First, PCL films with different concentrations of AuNRs were synthesized based on the method introduced in Chapter 3[87]. A silicon wafer with surface pattern was fabricated with electronbeam lithography (EBL) system (ELS-7500EX, Elionix, Hachioji, Japan). A compressive stress of 0.1 MPa was applied to the samples contacted with silicon water at 80 °C and maintained for 5 min. The embossing stress was then released at 4 °C after 10 min of cooling.

4.2.3. NIR- actuated surface shape-memory performance.

Samples with temporary surface patterns was irradiated by NIR light with varying densities (Wavelength of 805 nm NIR). Topography of permanent surface pattern and the temporary pattern was observed by AFM by atomic force microscopy (AFM) (SPM-9500J3, Shimadzu Corporation, Kyoto, Japan) in non-contact mode using a Si3N4 cantilever (spring constant; 42 N/m).

4.2.4. Cell culture.

Before cell cultivation, PCL films were placed in a 37 °C incubator for 1 h to equilibrate with 10 μg mL^{-1} fibronectin. NIH3T3 fibroblasts were seeded at a density of 3.0×10^4 cells cm^{-2} on the films with temporary patterns and cultured in DMEM in the presence of 10% fetal bovine serum (FBS) at 37 °C for 3 hours. After that, the films were then exposed to NIR light (0.8 Wcm^{-1}), causing the surface transition to a flat surface. The cell morphology was continuously monitored and imaged using a phase contrast microscope (Olympus

IX71; Olympus Corporation, Tokyo, Japan). Cells were fixed with paraformaldehyde and treated with Rhodaminephalloidin for F-actin staining and 4,6-diamidino-2-phenylindole (DAPI) for nucleus staining.

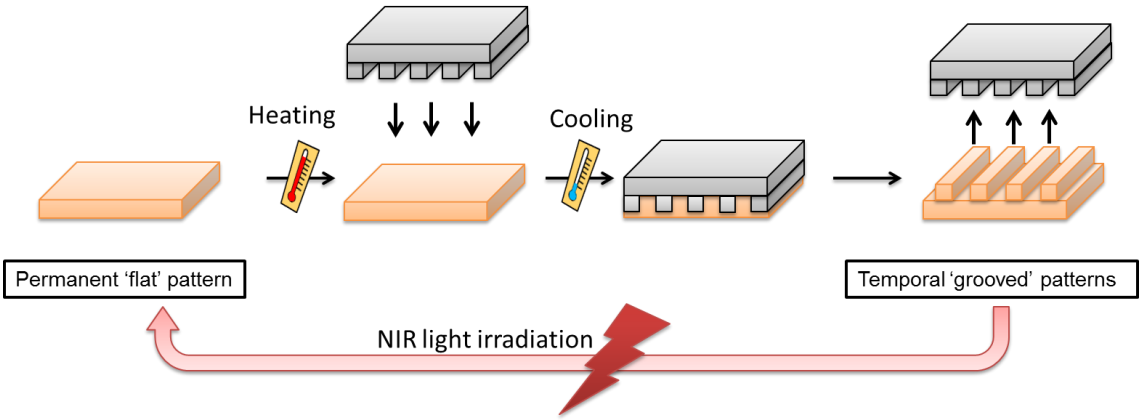

Fig. 4.1. (a) Schematic depiction of the shape fixing and recovery processes. To program "temporal surfacepatterns", flat films are compressed with a nanopatterned silicon mold in a thermo chamber (above the T_m). The embossing stress is then released (below the T_m). NIR irradiation can transition temporary surface patterns to permanent flat surface.

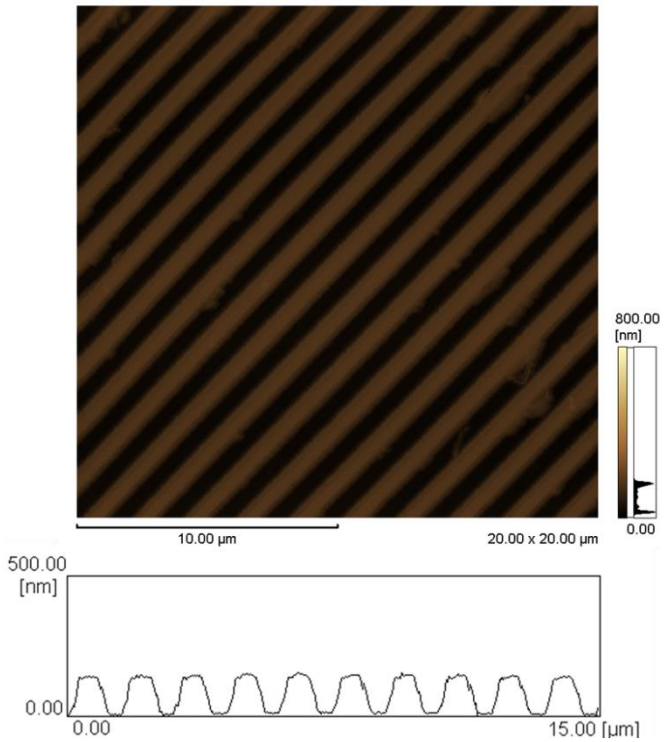

Fig. 4.2. Topographic surface images of the silicon mold observed by AFM.

4.3. Results and discussion

4.3.1. AuNRs-embedded PCL films.

In Chapter 3, we have found that, the deformed film could be recovered by irradiation of NIR light, which depends on the concentration of AuNRs, the intensity of NIR and the irradiation time. Moreover, the transition temperature of all the films is almost the same, regardless of the incorporation of AuNRs[60].

Here, we continued to study of the effect of NIR-light on the shape-recovery performance. **Fig. 4.1** shows the scheme of preparation of film with temporary pattern and NIR-light induced shape memory process. **Fig. 4.2** shows all the PCL films observed over an area of 50 x 50 μm^2. The mixing ratios of two/four- branched films was 70wt/30wt and 50wt/50wt, respectively. Flat surfaces were used for all the permanent-pattern film. The irregular rough structures may result from the crystallization of PCL at 25 °C (left images).

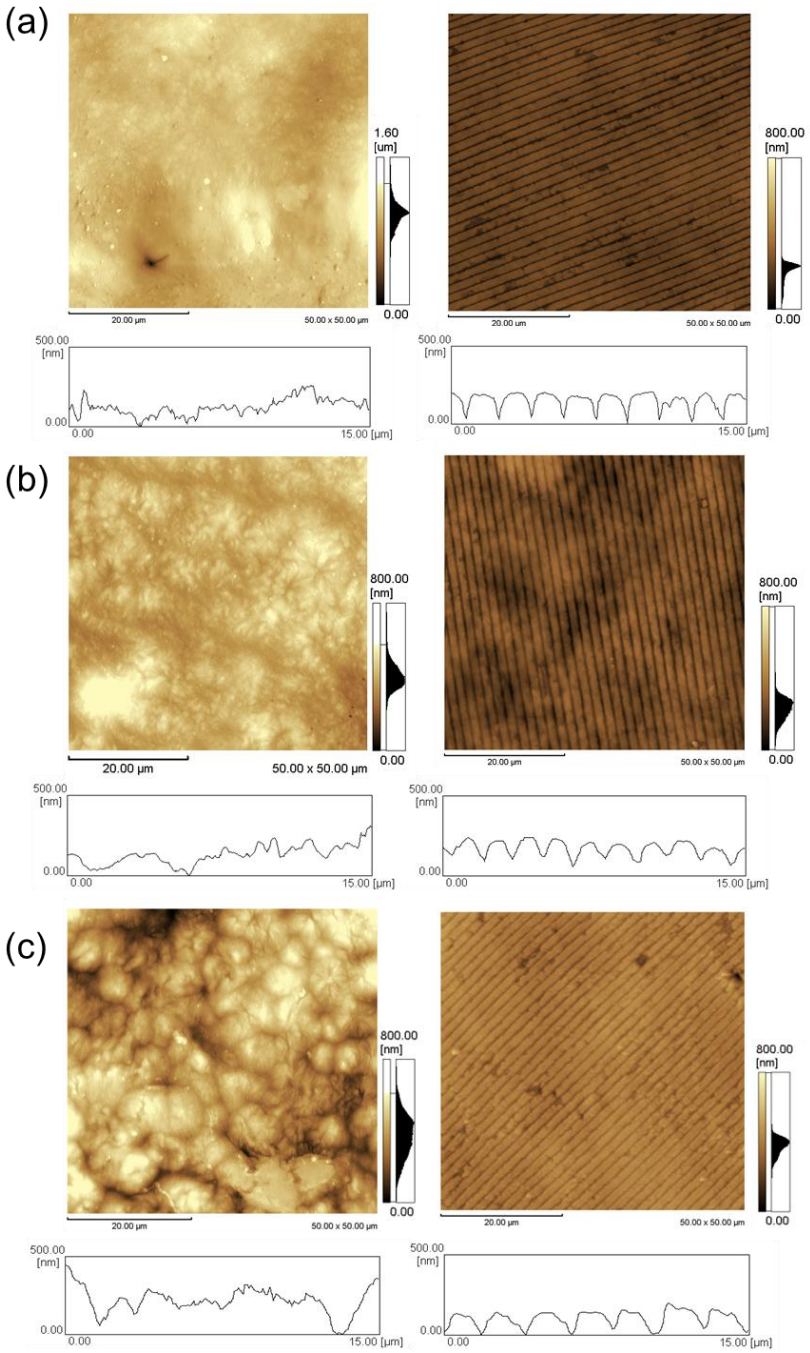

Fig. 4.3. Topography of the permanent shape (left column) and temporary shape (right column) of 70wt/30we PCL film and their height profile. (a) permanent flat shape with 0 (a), 0.4 (b), and 2.4 wt% (c) of AuNRs. All images were obtained in the 50 µm x 50 µm scan range.

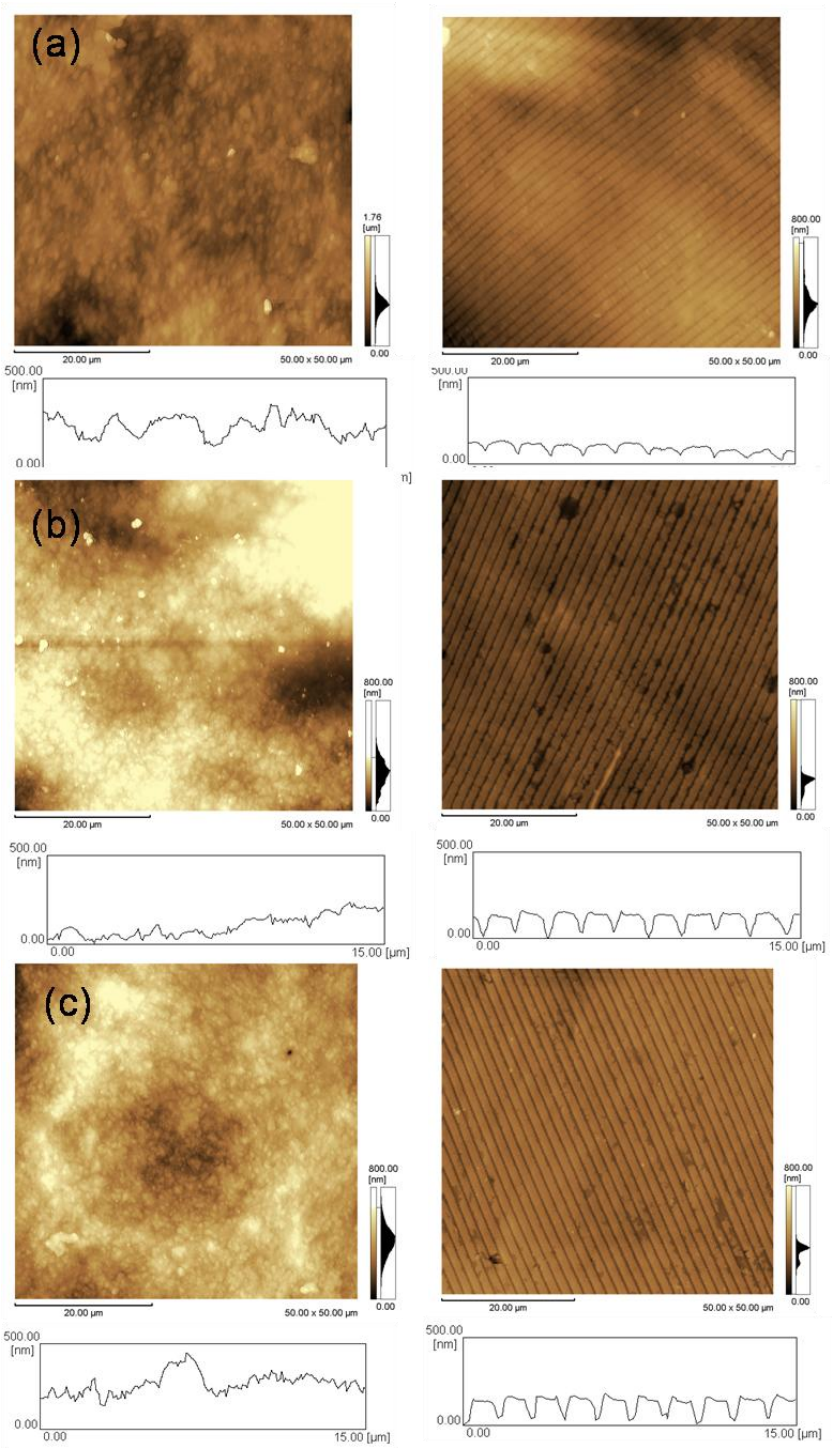

Fig. 4.4. Topography of the permanent shape (left column) and temporary shape (right column) of 50wt/50wt PCL film and their height profile. (a) permanent flat shape with 0 (a), 0.4 (b), and 2.4 wt% (c) of AuNRs. All images were obtained in the 50 µm x 50 µm scan range.

The average pattern depth/groove/ridge of silicon wafer were 130/1000/400 nm, as shown in **Fig 4.2.** The right images in **Fig. 4.3** and **Fig. 4.4** show that the temporal nano grooves were successfully memorized on the PCL films. The large difference was not observed among the samples. These results indicate that temporary surface patterns can be easily programmed into the films, regardless of the AuNR contents.

4.3.2. NIR light-induced shape-memory transition.

In chapter 3, shape memory performance of the elongated temporary has been tested, in which, light intensity and AuNRs concentration influence the heating efficiency and then, the heat recovery ratio. Here, the shape-recovery performance of films with surface pattern was tested. The result of which was shown in **Fig. 4.5.** The films were irradiated with 805 nm NIR at power densities of 0.4, 0.48, 0.52, and 0.8 Wcm^{-2} for a total of 60 s of irradiation time. Lower intensity irradiation showed negligible recovery due to the lower final equilibrium temperature than the T_m. When a beam with a power density of 0.8 Wcm^{-2} impinged on the film with AuNRs, a flat surface was completely recovered (**Fig. 4.5**).

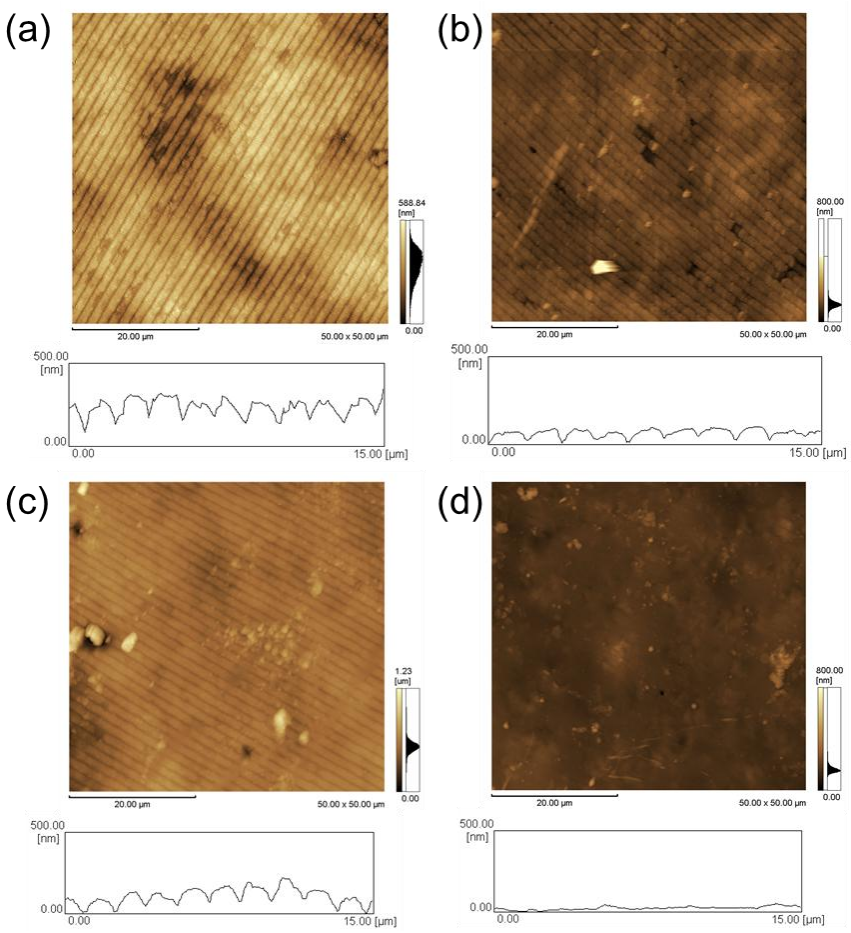

Fig. 4.5. Topographic surface images of the temporal nanopatterned PCL surfaces (70wt/30%) with 0.4 wt% of AuNRs after exposure to NIR at laser intensity of 0.4 (a), 0.48 (b), 0.52 (c), and 0.8 Wcm^{-2} (c). NIR light was irradiated for 60 seconds.

We also investigated the possibility of achieving surface shape-memory transition with spatial control, at a specific surface location. The films were irradiated with NIR light at power densities of 0.48 Wcm^{-2} and 0.8 Wcm^{-2}, and observed with AFM or phase contrast optical microscope. As seen in **Fig. 4.5**, and **Fig. 6**, the surface pattern was erased in the photo illuminated region. Because the light source was not collimated, the resulting pattern did not duplicate well the laser spot and thus the boundary was not clear. This is also possibly due to the diffusion of heat. It has been reported that after light absorption, the gold particle transfers energy to the medium around the particle in a period from 100 ps to 10 ns[89]. But, our results show

the ability of the embedded AuNRs to heat a PCL film above its T_m and the spatial control of the surface nanopatterns.

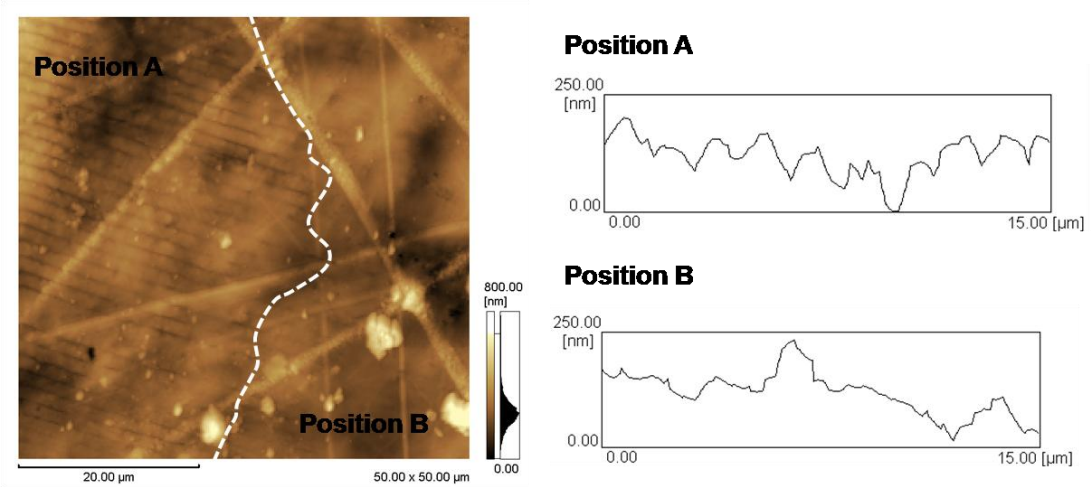

Fig. 4.6. The edge between the areas accepted NIR and without accepted NIR of sample 70wt/wt30 PCL-0.4 wt%. Irradiation inte nsity: 0.48 Wcm^{-2}.

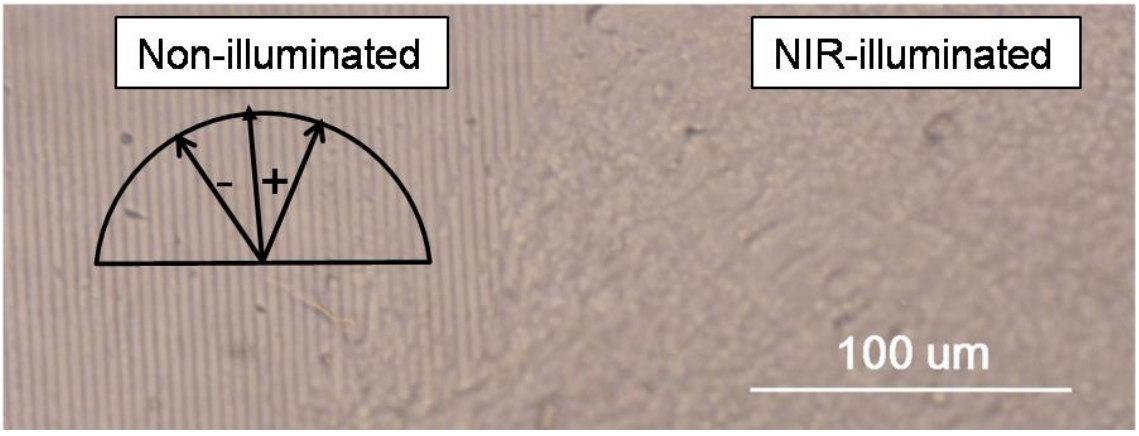

Fig. 4.7. Phase contrast photograph of the boundary between NIR-irradiated and non-irradiated areas of PCL films with 0.4 wt% of AuNRs after exposure to NIR at laser intensity of 0.8 Wcm^{-2} for 60 seconds. NIR light was irradiated in the left half area.

4.3.3. Control of cell morphology by NIR light.

Adherent cells are known to probe and respond to the mechanical properties of the surrounding extracellular matrix (ECM) where they adhere and interact. Anisotropic topographic features, for example, have been shown to induce many cell types to align and migrate along the direction of the anisotropy, a phenomenon called contact guidance[90-92]. Especially, many cell types have been known to reactto dynamic changes in the extracellular environments rather than static effects. Davis et al. reported for the first time a dynamic cell culture system that uses SMP substrates that are programmed to change surface topography during cell culture[93]. From this regard, we have been proposing dynamic cell culture platforms to control cell functions using temperature-responsive

PCL[28,88,94]. We have previously shown how mechanical properties of PCL influence cell behavior using MSCs[95], skeletal myoblasts[96], fibroblasts[94], and neonatal cardiomyocytes[97,98]. We have also fabricated shape-memory substrates from PCL because the crosslinked PCL offers reversible crystallizable regions that can fix a temporary shape and have dual-shape capability, showing a shape memory effect. Typically, the shape-memory changes in those studies have been induced by direct heating of the PCL films[99,100], resulting in difficulties of localized heating. Therefore, light was used to induce the localized photothermal effect of AuNRs within PCL films in this study.

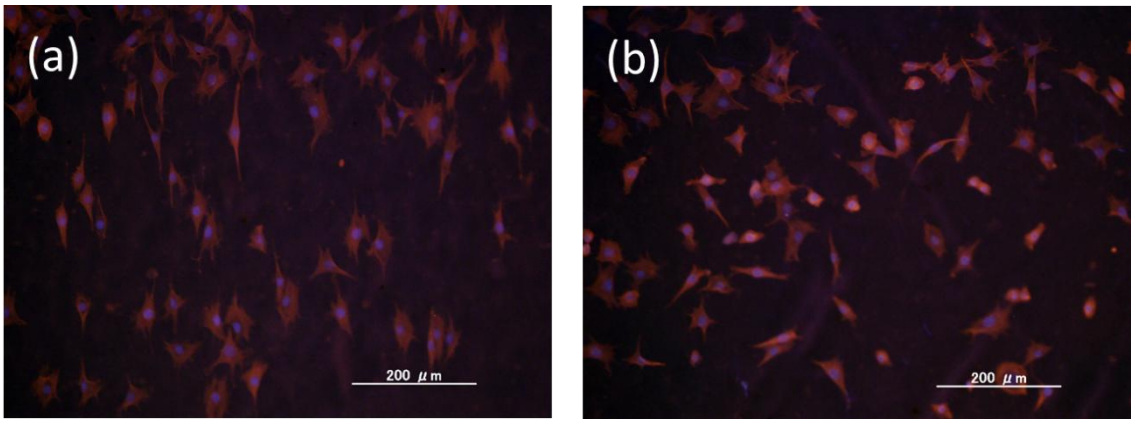

Fig. 4.8. Fluorescent microscope images of NIH 3T3 fibroblasts on temporal patterned PCL filmswith 0.4 wt% of AuNRs.Cells were seeded on the non-illuminated (a) and photo-illuminated (b) regions of the film and cultured at 37°C for 3 hours.

First, we examined the effects of surface patterns on cell morphologies. NIH3T3 fibroblasts were seeded on the photo-illuminated and non-illuminated regions of the film and cultured at 37 °C for 3 hours. In the cell culture experiments, higher intensity and AuNRs concentration were used to induce the photothermal heating efficiently in water. Cells cultured on non-illuminated region were aligned along the direction of the temporal pattern (**Fig. 4.8a**). On the other hand, cells seeded on the photo-illuminated region (flat surface) were randomly orientated (**Fig. 4.8b**).

For the in-situ NIR-induced surface shape-memory experiment, the cells were cultured at 37 °C for 3 hours and then exposed to NIR light (0.8 W cm^{-1}), causing the surface transition to a flat surface. The NIR light was irradiated until the surface transition was completed. Then, cells were cultured for another 3 hours. **Fig. 4.9** shows the phase contrast and fluorescent images of cells seeded on the fibronectin-coated PCL films with the temporal grooved surface. Cell alignment in the photo-irradiated region was lost and random cell migration was ensured, while cells the on non-illuminated region were still aligned along the direction of the temporal pattern. This can be also observed from the histograms of cell-orientation angle against pattern direction (**Fig. 4.10**). As already pointed out in our previous work, the changes in cell alignment are mostly due to respreading of daughter cells[88]. In this study, however, cell alignment was observed 3 h after NIR irradiation.

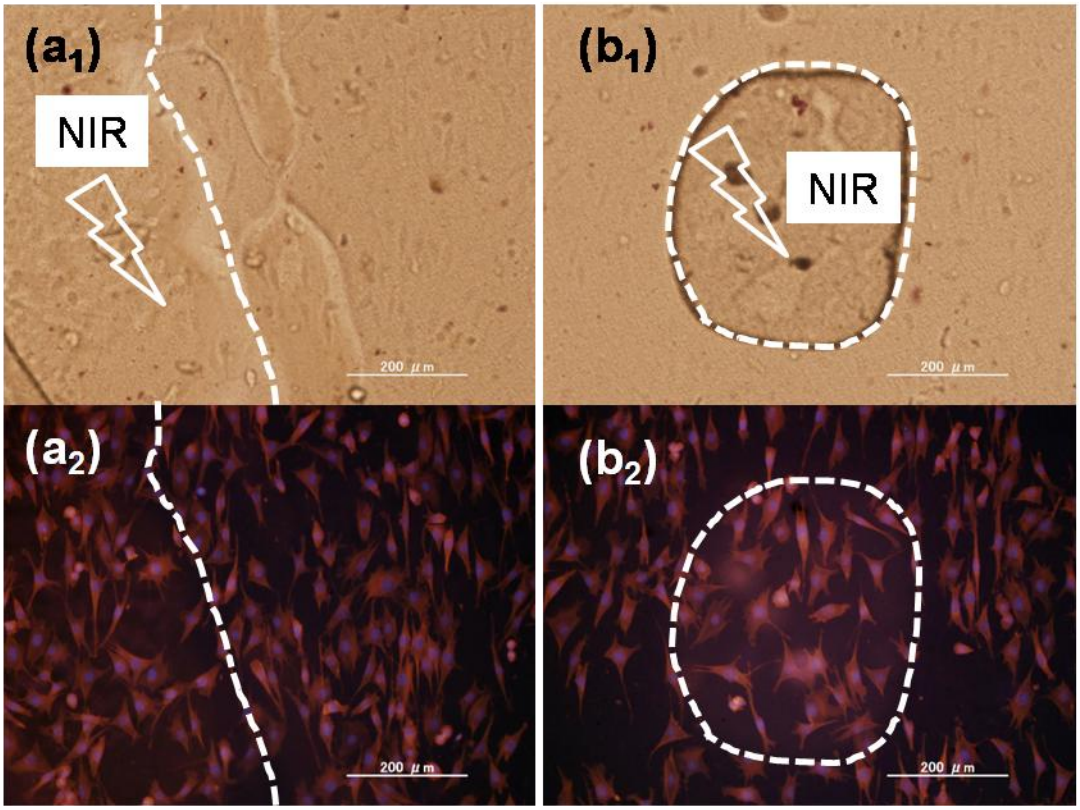

Fig. 4.9. In-situ exposure of NIR to cells on temporal patterned PCL films with 0.4 wt% of AuNRs observed by phase contrast (top) and fluorescent (bottom) microscope. Cells were seeded on the temporal patterned surface and cultured at 37 °C for 3 hours. The NIR light (0.8 Wcm^{-1}) was then irradiated until the surface transition was completed. Cells were cultured for another 3 hours and images were taken.

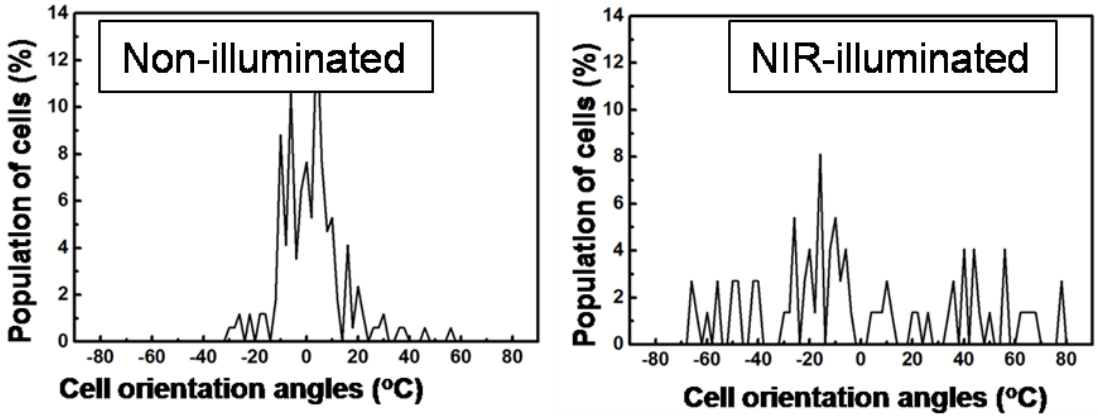

Fig. 4.10. Histograms of cell orientation angle against pattern direction in: a) non-illuminated and b) photo-illuminated regions. Cells were seeded on the temporal patterned surface and cultured at 37 °C for 3 h. The NIR light (0.8 W cm^{-1}) was then irradiated until the surface transition was completed. Cells were cultured for another 3 h and images were taken.

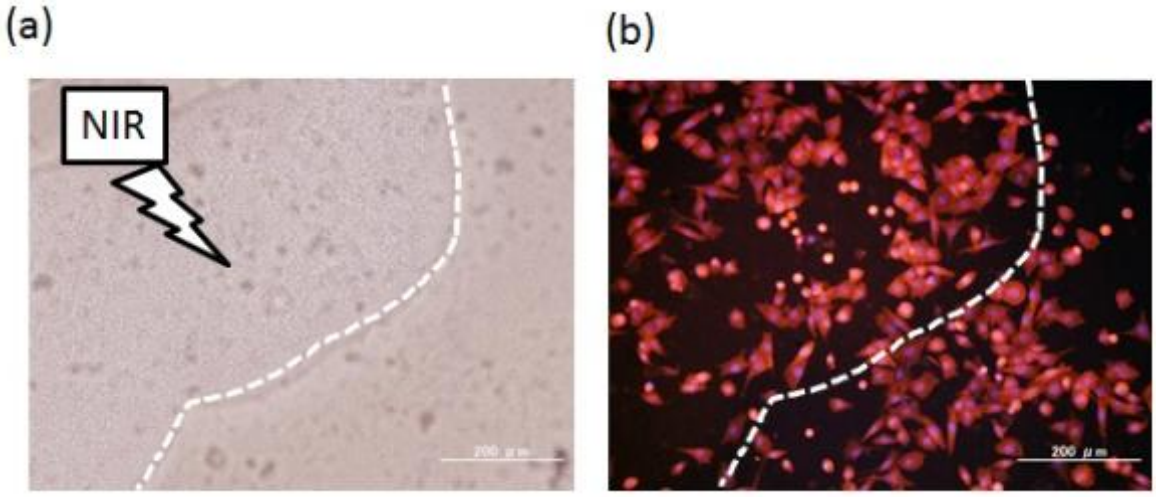

Fig. 4.11. In-situ exposure of NIR to cells on flat PCL films with 2.4 wt% of AuNRs observed by phase contrast (a) and fluorescent (b) microscope. Cells were seeded on the flat surface and cultured at 37 °C for 3 hours. The NIR light (0.8 W cm-1) was then irradiated. Cells were cultured for another 3 hours and images were taken.

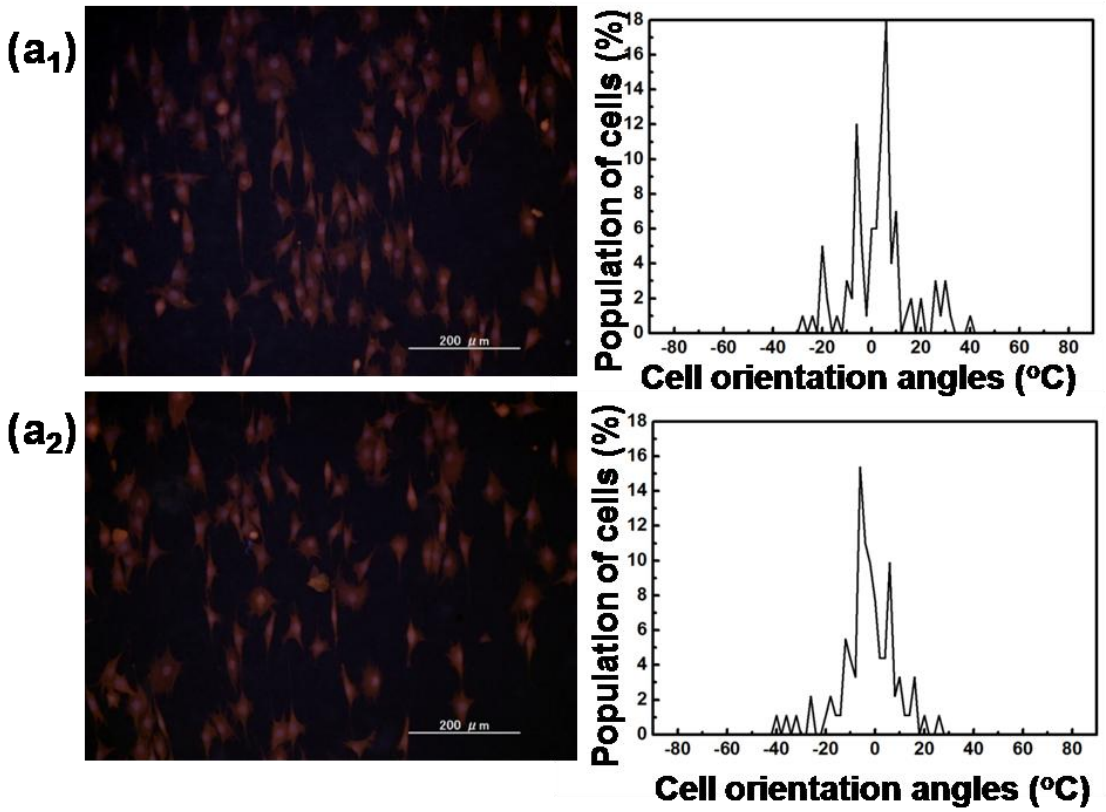

Fig. 4.12. (a) Fluorescent microscope images of NIH 3T3 fibroblasts on temporal patterned PCL films without AuNRs before (left) and after (right) NIR irradiation. Cells were seeded on the temporal patterned surface and cultured at 37°C for 3 hours. The NIR light (0.8 W cm-1) was then irradiated until the surface transition was completed. Cells were cultured for another 3 hours and images were taken. (b) Histograms of cell orientation angle against pattern direction before (left) and after (right) NIR irradiation.

To elucidate the effects of heat and elastic-modulus change on the cell morphology, cells were also cultured on AuNR-incorporated PCL films without patterns at 37 °C for 3 h. The films were then exposed to NIR light. Since the films contain AuNRs, heat was generated and the films became soft. The cell morphologies, however, did not change (**Fig. 4.11**). These results suggest that neither heating nor elastic change affects cell morphology.

We have also cultured cells on PCL films without AuNRs. The cell morphologies did not change on NIR irradiation. This result also suggests that NIR irradiation itself does not affect the cell morphology (**Fig. 4.12**). Therefore, it is plausible that cells remodelled their cytoskeleton in response to dynamic changes in the surface topography. Although the patterning resolution and sizes are not enough to observe single-cell behavior due to the difficulty in precisely controlling the NIR irradiation, utilizing theoretical approach for the photothermal heating may enable further understanding of heat diffusion through PCL films. Alternatively, a photo mask can be used to attain a higher resolution and a smaller size of patterns. It will be also interesting to see in the future how the generated heat would affect the cell viability. We believe that this new remote NIR-light-responsive cell-culture substrate will enable unprecedented observations of time-dependent cell-substrate interactions, without the need for invasive forces against intact adherent cells.

4.4. Conclusion

In summary, NIR light-responsive shape memory films were successfully prepared through the crosslinking of PCL macromonomers in the presence of AuNRs. Temporal surface nanopatterns can be easily programmed into the films, regardless of the AuNR contents. Exposure to NIR light could successfully induce the photothermal heating of embedded AuNRs and, consequently, the shape-switching transition. Upon NIR irradiation, the film completely recovered its original shape. Local shape-memory transformation was also obtained when the limited area was exposed to light. The NIR irradiation was also used to control cell morphology. Cell alignment in the NIR-irradiated region was lost and random cell migration was ensured because it caused the surface transition to a flat surface, while cells on the non-illuminated region were still aligned along the direction of the temporal pattern. This finding is novel in that it is the first study that controls the cell orientation locally and remotely on the shape-memory nanopatterns by NIR light irradiation. Therefore, we believe that NIR-responsive shape-memory system offers significant promise for the creation of topographically tunable substrates because of their remote-capability to undergo large elastic deformations and to rapidly return to their initial undeformed state.

References

(1) Klaine, S. J.; Alvarez, P. J. J.; Batley, G. E.; Fernandes, T. F.; Handy, R. D.; Lyon, D. Y.; Mahendra, S.; McLaughlin, M. J.; Lead, J. R. Nanomaterials in the environment: Behavior, fate, bioavailability, and effects. *Environ. Toxicol. Chem.* **2008**, *27*, 1825-1851.

(2) Lamer, V. K.; Dinegar, R. H. Theory, Production and Mechanism of Formation of Monodispersed Hydrosols. *J. Am. Chem. Soc.* **1950**, *72*, 4847-4854.

(3) Sun, Y. G.; Xia, Y. N. Shape-controlled synthesis of gold and silver nanoparticles. *Science* **2002**, *298*, 2176-2179.

(4) Tao, A. R.; Habas, S.; Yang, P. D. Shape control of colloidal metal nanocrystals. *Small* **2008**, *4*, 310-325.

(5) Turkevich, J.; Stevenson, P. C.; Hillier, J. The Formation of Colloidal Gold. *J. Phys. Chem.* **1953**, *57*, 670-673.

(6) Brust, M.; Walker, M.; Bethell, D.; Schiffrin, D. J.; Whyman, R. Synthesis of Thiol-Derivatized Gold Nanoparticles in a 2-Phase Liquid-Liquid System. *J. Chem. Soc. Chem. Comm.* **1994**, 801-802.

(7) Sperling, R. A.; Parak, W. J. Surface modification, functionalization and bioconjugation of colloidal inorganic nanoparticles. *Philosophical Transactions of the Royal Society a-Mathematical Physical and Engineering Sciences* **2010**, *368*, 1333-1383.

(8) Wilson, R. The use of gold nanoparticles in diagnostics and detection. *Chem Soc Rev* **2008**, *37*, 2028-2045.

(9) Daniel, M. C.; Astruc, D. Gold nanoparticles: Assembly, supramolecular chemistry, quantum-size-related properties, and applications toward biology, catalysis, and nanotechnology. *Chem. Rev.* **2004**, *104*, 293-346.

(10) Lohse, S. E.; Murphy, C. J. The Quest for Shape Control: A History of Gold Nanorod Synthesis. *Chem. Mater.* **2013**, *25*, 1250-1261.

(11) Takenaka, Y.; Kawabata, Y.; Kitahata, H.; Yoshida, M.; Matsuzawa, Y.; Ohzono, T. Effects of surfactant concentration on formation of high-aspect-ratio gold nanorods. *J. Colloid Interface Sci.* **2013**, *407*, 265-272.

(12) Walker, D. A. Directed self-assembly of gold nanorods using surface modification. Graduate Theses and Dissertations, University of South Florida 2008.

(13) Sau, T. K.; Murphy, C. J. Self-assembly patterns formed upon solvent evaporation of aqueous cetyltrimethylammonium bromide-coated gold nanoparticles of various shapes. *Langmuir* **2005**, *21*, 2923-2929.

(14) Gomez-Grana, S.; Hubert, F.; Testard, F.; Guerrero-Martinez, A.; Grillo, I.; Liz-Marzan, L. M.; Spalla, O. Surfactant (Bi)Layers on Gold Nanorods. *Langmuir* **2012**, *28*, 1453-1459.

(15) Niidome, T.; Yamagata, M.; Okamoto, Y.; Akiyama, Y.; Takahashi, H.; Kawano, T.; Katayama, Y.; Niidome, Y. PEG-modified gold nanorods with a stealth character for in vivo applications. *J. Controlled Release* **2006**, *114*, 343-347.

(16) Gole, A.; Murphy, C. J. Polyelectrolyte-coated gold nanorods: Synthesis, characterization and immobilization. *Chem. Mater.* **2005**, *17*, 1325-1330.

References

(17) Thomas, K. G.; Barazzouk, S.; Ipe, B. I.; Joseph, S. T. S.; Kamat, P. V. Uniaxial plasmon coupling through longitudinal self-assembly of gold nanorods. *J. Phys. Chem. B* **2004**, *108*, 13066-13068.

(18) Sun, Z. H.; Ni, W. H.; Yang, Z.; Kou, X. S.; Li, L.; Wang, J. F. pH-controlled reversible assembly and disassembly of gold nanorods. *Small* **2008**, *4*, 1287-1292.

(19) Kinnear, C.; Dietsch, H.; Clift, M. J. D.; Endes, C.; Rothen-Rutishauser, B.; Petri-Fink, A. Gold Nanorods: Controlling Their Surface Chemistry and Complete Detoxification by a Two-Step Place Exchange. *Angew. Chem. Int. Edit.* **2013**, *52*, 1934-1938.

(20) Wei, Q. S.; Ji, J.; Shen, J. C. Synthesis of near-infrared responsive gold nanorod/PNIPAAm core/shell nanohybrids via surface initiated ATRP for smart drug delivery. *Macromol. Rapid Commun.* **2008**, *29*, 645-650.

(21) Khanal, B. P.; Zubarev, E. R. Rings of nanorods. *Angew. Chem. Int. Edit.* **2007**, *46*, 2195-2198.

(22) Orendorff, C. J.; Murphy, C. J. Quantitation of metal content in the silver-assisted growth of gold nanorods. *J. Phys. Chem. B* **2006**, *110*, 3990-3994.

(23) Hashimoto, S.; Werner, D.; Uwada, T. Studies on the interaction of pulsed lasers with plasmonic gold nanoparticles toward light manipulation, heat management, and nanofabrication. *Journal of Photochemistry and Photobiology C-Photochemistry Reviews* **2012**, *13*, 28-54.

(24) Ekici, O.; Harrison, R. K.; Durr, N. J.; Eversole, D. S.; Lee, M.; Ben-Yakar, A. Thermal analysis of gold nanorods heated with femtosecond laser pulses. *J Phys D Appl Phys* **2008**, *41*.

(25) Lendlein, A.; Langer, R. Biodegradable, elastic shape-memory polymers for potential biomedical applications. *Science* **2002**, *296*, 1673-1676.

(26) Lendlein, A.; Kelch, S. Shape-memory polymers. *Angew. Chem. Int. Edit.* **2002**, *41*, 2034-2057.

(27) Small, W.; Singhal, P.; Wilson, T. S.; Maitland, D. J. Biomedical applications of thermally activated shape memory polymers. *J. Mater. Chem.* **2010**, *20*, 3356-3366.

(28) Ebara, M.; Uto, K.; Idota, N.; Hoffman, J. M.; Aoyagi, T. Shape-Memory Surface with Dynamically Tunable Nano-Geometry Activated by Body Heat. *Adv. Mater.* **2012**, *24*, 273-278.

(29) Kweon, H.; Yoo, M. K.; Park, I. K.; Kim, T. H.; Lee, H. C.; Lee, H. S.; Oh, J. S.; Akaike, T.; Cho, C. S. A novel degradable polycaprolactone networks for tissue engineering. *Biomaterials* **2003**, *24*, 801-808.

(30) Lendlein, A.; Schmidt, A. M.; Langer, R. AB-polymer networks based on oligo(epsilon-caprolactone) segments showing shape-memory properties. *Proc. Nat. Acad. Sci. U.S.A.* **2001**, *98*, 842-847.

(31) Rodriguez, E. D.; Luo, X. F.; Mather, P. T. Linear/Network Poly(epsilon-caprolactone) Blends Exhibiting Shape Memory Assisted Self-Healing (SMASH). *ACS Appl. Mat. Interfaces* **2011**, *3*, 152-161.

(32) Neuss, S.; Blomenkamp, I.; Stainforth, R.; Boltersdorf, D.; Jansen, M.; Butz, N.; Perez-Bouza, A.; Knuchel, R. The use of a shape-memory poly(epsilon of-caprolactone)dimethacrylate network as a tissue engineering scaffold. *Biomaterials* **2009**, *30*, 1697-1705.

(33) Ebara, M.; Uto, K.; Idota, N.; Hoffman, J. M.; Aoyagi, T. The Taming of the Cell, Shape-memory nanopatterns direct cell orientation. *Int J Nanomedicine* **2014**, *in press*.

(34) Ebara, M.; Uto, K.; Idota, N.; Hoffman, J. M.; Aoyagi, T. Rewritable and shape-memory soft matter

with dynamically tunable microchannel geometry in a biological temperature range. *Soft Matter* **2013**, *9*, 3074-3080.

(35) Shou, Q. H.; Uto, K.; Iwanaga, M.; Ebara, M.; Aoyagi, T. Near-infrared light-responsive shape-memory poly(epsilon-caprolactone) films that actuate in physiological temperature range. *Polym. J.* **2014**, *46*, 492-498.

(36) Liu, Y. F.; Lee, Y. L. Adsorption characteristics of OH-terminated alkanethiol and arenethiol on Au(111) surfaces. *Nanoscale* **2012**, *4*, 2093-2100.

(37) Vigderman, L.; Khanal, B. P.; Zubarev, E. R. Functional Gold Nanorods: Synthesis, Self-Assembly, and Sensing Applications. *Adv. Mater.* **2012**, *24*, 4811-4841.

(38) Sau, T. K.; Murphy, C. J. Seeded high yield synthesis of short Au nanorods in aqueous solution. *Langmuir* **2004**, *20*, 6414-6420.

(39) Devisser, C.; Heuvelsland, W. J. M.; Dunn, L. A.; Somsen, G. Some Properties of Binary Aqueous Liquid-Mixtures - Apparent Molar Volumes and Heat-Capacities at 298.15 K over Whole Mole Fraction Range. *Journal of the Chemical Society-Faraday Transactions I* **1978**, *74*, 1159-1169.

(40) Peng, G.; Tisch, U.; Adams, O.; Hakim, M.; Shehada, N.; Broza, Y. Y.; Billan, S.; Abdah-Bortnyak, R.; Kuten, A.; Haick, H. Diagnosing lung cancer in exhaled breath using gold nanoparticles. *Nat. Nanotechnol.* **2009**, *4*, 669-673.

(41) Shao, L.; Ruan, Q.; Jiang, R.; Wang, J. Macroscale Colloidal Noble Metal Nanocrystal Arrays and Their Refractive Index-Based Sensing Characteristics. *Small* **2014**, *10*, 802-811.

(42) Grzelczak, M.; Sanchez-Iglesias, A.; Rodriguez-Gonzalez, B.; Alvarez-Puebla, R.; Perez-Juste, J.; Liz-Marzan, L. M. Influence of Iodide Ions on the Growth of Gold Nanorods: Tuning Tip Curvature and Surface Plasmon Resonance. *Adv. Funct. Mater.* **2008**, *18*, 3780-3786.

(43) Cao, J.; Galbraith, E. K.; Sun, T.; Grattan, K. T. V. Effective surface modification of gold nanorods for localized surface plasmon resonance-based biosensors. *Sensor Actuat B-Chem* **2012**, *169*, 360-367.

(44) Nie, Z. H.; Fava, D.; Kumacheva, E.; Zou, S.; Walker, G. C.; Rubinstein, M. Self-assembly of metal-polymer analogues of amphiphilic triblock copolymers. *Nat. Mater.* **2007**, *6*, 609-614.

(45) Kim, D. H.; Wei, A.; Won, Y. Y. Preparation of Super-Stable Gold Nanorods via Encapsulation into Block Copolymer Micelles. *ACS Appl. Mat. Interfaces* **2012**, *4*, 1872-1877.

(46) Mittal, K. L. E.: *Solution Chemistry of Surfactants*; Plenum Press: New York, 1979; Vol. 1.

(47) Feng, L. L.; Xuan, Z. W.; Ma, J. B.; Chen, J.; Cui, D. X.; Su, C. W.; Guo, J. M.; Zhang, Y. J. Preparation of gold nanorods with different aspect ratio and the optical response to solution refractive index. *J. Exp. Nanosci.* **2015**, *10*, 258-267.

(48) Volmer, M.; Stratmann, M.; Viefhaus, H. Electrochemical and Electron Spectroscopic Investigations of Iron Surfaces Modified with Thiols. *Surf. Interface Anal.* **1990**, *16*, 278-282.

(49) Ning, Y. G.; Xie, H.; Xing, H. T.; Deng, W. L.; Yang, D. B. Comparison of self-assembled monolayers of n-alkanethiols and phenylthioureas on the surface of gold. *Surf. Interface Anal.* **1996**, *24*, 667-670.

(50) Thierry, B.; Ng, J.; Krieg, T.; Griesser, H. J. A robust procedure for the functionalization of gold

nanorods and noble metal nanoparticles. *Chem. Commun.* **2009**, 1724-1726.

(51) Nash, M. A.; Waitumbi, J. N.; Hoffman, A. S.; Yager, P.; Stayton, P. S. Multiplexed Enrichment and Detection of Malarial Biomarkers Using a Stimuli-Responsive Iron Oxide and Gold Nanoparticle Reagent System. *Acs Nano* **2012**, *6*, 6776-6785.

(52) Jain, P. K.; Huang, X. H.; El-Sayed, I. H.; El-Sayed, M. A. Noble Metals on the Nanoscale: Optical and Photothermal Properties and Some Applications in Imaging, Sensing, Biology, and Medicine. *Acc. Chem. Res.* **2008**, *41*, 1578-1586.

(53) Duchowicz, R.; Scaffardi, L. B.; Costela, A.; Garcia-Moreno, I.; Sastre, R.; Acuna, A. U. Photothermal analysis of polymeric dye laser materials excited at different pump rates. *Appl. Opt.* **2003**, *42*, 1029-1035.

(54) Loarer, T.; Greffet, J. J.; Huetzaubert, M. Noncontact Surface-Temperature Measurement by Means of a Modulated Photothermal Effect. *Appl. Opt.* **1990**, *29*, 979-987.

(55) Giljohann, D. A.; Seferos, D. S.; Daniel, W. L.; Massich, M. D.; Patel, P. C.; Mirkin, C. A. Gold Nanoparticles for Biology and Medicine. *Angew. Chem. Int. Edit.* **2010**, *49*, 3280-3294.

(56) Huang, X. H.; Jain, P. K.; El-Sayed, I. H.; El-Sayed, M. A. Plasmonic photothermal therapy (PPTT) using gold nanoparticles. *Lasers in Medical Science* **2008**, *23*, 217-228.

(57) Huang, X. H.; El-Sayed, I. H.; Qian, W.; El-Sayed, M. A. Cancer cell imaging and photothermal therapy in the near-infrared region by using gold nanorods. *J. Am. Chem. Soc.* **2006**, *128*, 2115-2120.

(58) Weissleder, R. A clearer vision for in vivo imaging. *Nat. Biotechnol.* **2001**, *19*, 316-317.

(59) Hribar, K. C.; Metter, R. B.; Ifkovits, J. L.; Troxler, T.; Burdick, J. A. Light-Induced Temperature Transitions in Biodegradable Polymer and Nanorod Composites. *Small* **2009**, *5*, 1830-1834.

(60) Le, D. M.; Tycon, M. A.; Fecko, C. J.; Ashby, V. S. Near-infrared activation of semi-crystalline shape memory polymer nanocomposites. *J. Appl. Polym. Sci.* **2013**, *130*, 4551-4557.

(61) Xu, N.; Wang, R.; Du, F. S.; Li, Z. C. Synthesis of thiol-terminated poly (epsilon-caprolactone). *Chem J Chinese U* **2007**, *28*, 1791-1795.

(62) Nikoobakht, B.; El-Sayed, M. A. Preparation and growth mechanism of gold nanorods (NRs) using seed-mediated growth method. *Chem. Mater.* **2003**, *15*, 1957-1962.

(63) Li, Y. N.; Yu, D. S.; Dai, L. M.; Urbas, A.; Li, Q. A. Organo-Soluble Chiral Thiol-Monolayer-Protected Gold Nanorods. *Langmuir* **2011**, *27*, 98-103.

(64) Pitt, C. G.; Jeffcoat, A. R.; Zweidinger, R. A.; Schindler, A. Sustained drug delivery systems. I. The permeability of poly(ϵ-caprolactone), poly(DL-lactic acid), and their copolymers. *Journal of Biomedical Materials Research* **1979**, *13*, 497-507.

(65) Uto, K.; Yamamoto, K.; Hirase, S.; Aoyagi, T. Temperature-responsive cross-linked poly(ε-caprolactone) membrane that functions near body temperature. *J. Controlled Release* **2006**, *110*, 408-413.

(66) Moller, M.; Kange, R.; Hedrick, J. L. Sn(OTf)(2) and Sc(OTf)(3): Efficient and versatile catalysts for the controlled polymerization of lactones. *J. Polym. Sci., Part A: Polym. Chem.* **2000**, *38*, 2067-2074.

(67) Bain, C. D.; Troughton, E. B.; Tao, Y. T.; Evall, J.; Whitesides, G. M.; Nuzzo, R. G. Formation of Monolayer Films by the Spontaneous Assembly of Organic Thiols from Solution onto Gold. *J. Am. Chem.*

Soc. **1989**, *111*, 321-335.

(68) Gascon, J. A.; Pastawski, H. M. Surface effects on the statistics of the local density of states in metallic nanoparticles: Manifestation on the NMR spectra. *Mod. Phys. Lett. B* **2005**, *19*, 1285-1294.

(69) Behl, M.; Razzaq, M. Y.; Lendlein, A. Multifunctional Shape-Memory Polymers. *Adv. Mater.* **2010**, *22*, 3388-3410.

(70) Lendlein, A.; Kelch, S. Shape-memory polymers. *Angew. Chem. Int. Ed.* **2002**, *41*, 2035-2057.

(71) Liu, C.; Qin, H.; Mather, P. T. Review of progress in shape-memory polymers. *J. Mater. Chem.* **2007**, *17*, 1543-1558.

(72) Maitland, D. J.; Metzger, M. F.; Schumann, D.; Lee, A.; Wilson, T. S. Photothermal properties of shape memory polymer micro-actuators for treating stroke. *Lasers Surg. Med.* **2002**, *30*, 1-11.

(73) Wache, H. M.; Tartakowska, D. J.; Hentrich, A.; Wagner, M. H. Development of a polymer stent with shape memory effect as a drug delivery system. *J Mater Sci-Mater M* **2003**, *14*, 109-112.

(74) Lantada, A. D.; Lafont, P.; Rada, I.; Jiménez, A.; Hernández, J. L.; Lorenzo-Yustos, H.; Muñoz-García, J. Active Annuloplasty System for Mitral Valve Insufficiency. *Biomedical Engineering Systems and Technologies* **2009**, *25*, 59-72.

(75) Ebara, M.; Uto, K.; Idota, N.; Hoffman, J. M.; Aoyagi, T. Rewritable and shape-memory soft matter with dynamically tunable microchannel geometry in a biological temperature range. *Soft Matter* **2013**, *9*, 3074-3080.

(76) Takehara, H.; Jiang, C.; Uto, K.; Ebara, M.; Aoyagi, T.; Ichiki, T. Novel Microfluidic Valve Technology Based on Shape Memory Effect of Poly(ϵ-caprolactone). *Applied Physics Express* **2013**, *6*, 037201.

(77) Jiang, C.; Takehara, H.; Uto, K.; Ebara, M.; Aoyagi, T.; Ichiki, T. Evaluation of Microvalves Developed for Point-of-Care Testing Devices Using Shape-Memory Polymers. *J. Photopolym. Sci. Technol.* **2013**, *26*, 581-585.

(78) Eisenbach, C. D. Isomerization of aromatic azo chromophores in poly(ethyl acrylate) networks and photomechanical effect. *Polymer* **1980**, *21*, 1175-1179.

(79) Li, M. H.; Keller, P.; Li, B.; Wang, X. G.; Brunet, M. Light-driven side-on nematic elastomer actuators. *Adv. Mater.* **2003**, *15*, 569-572.

(80) Lendlein, A.; Jiang, H. Y.; Junger, O.; Langer, R. Light-induced shape-memory polymers. *Nature* **2005**, *434*, 879-882.

(81) Maity, S.; Bochinski, J. R.; Clarke, L. I. Metal Nanoparticles Acting as Light-Activated Heating Elements within Composite Materials. *Adv. Funct. Mater.* **2012**, *22*, 5259-5270.

(82) Small, W.; Wilson, T. S.; Benett, W. J.; Loge, J. M.; Maitland, D. J. Laser-activated shape memory polymer intravascular thrombectomy device. *Opt. Express* **2005**, *13*, 8204-8213.

(83) Ma, Z.; Xia, H.; Liu, Y.; Liu, B.; Chen, W.; Zhao, Y. Applications of gold nanorods in biomedical imaging and related fields. *Chin. Sci. Bull.* **2013**, *58*, 2530-2536.

(84) von Maltzahn, G.; Park, J.-H.; Agrawal, A.; Bandaru, N. K.; Das, S. K.; Sailor, M. J.; Bhatia, S. N. Computationally Guided Photothermal Tumor Therapy Using Long-Circulating Gold Nanorod Antennas.

References

Cancer Res. **2009**, *69*, 3892-3900.

(85) Kojima, C.; Watanabe, Y.; Hattori, H.; Iida, T. Design of Photosensitive Gold Nanoparticles for Biomedical Applications Based on Self-Consistent Optical Response Theory. *The Journal of Physical Chemistry C* **2011**, *115*, 19091-19095.

(86) Shimoda, K.; Fujigaya, T.; Nakashima, N.; Niidome, Y. Spontaneous Temperature Control Using Reversible Spectroscopic Responses of PNIPAM-coated Gold Nanorods. *Chem. Lett.* **2013**, *advpub*.

(87) Shou, Q.; Uto, K.; Iwanaga, M.; Ebara, M.; Aoyagi, T. Near-infrared light-responsive shape-memory poly([epsiv]-caprolactone) films that actuate in physiological temperature range. *Polym. J.* **2014**, *in press*.

(88) Ebara, M.; Uto, K.; Idota, N.; Hoffman, J. M.; Aoyagi, T. The Taming of the Cell; Shape-memory nanopatterns direct cell orientation. *Int. J. Nanomed.* **2014**, *9*, 117-126.

(89) Pérez-Juste, J.; Pastoriza-Santos, I.; Liz-Marzán, L. M.; Mulvaney, P. Gold nanorods: Synthesis, characterization and applications. *Coord. Chem. Rev.* **2005**, *249*, 1870-1901.

(90) Teixeira, A. I.; Abrams, G. A.; Bertics, P. J.; Murphy, C. J.; Nealey, P. F. Epithelial contact guidance on well-defined micro- and nanostructured substrates. *J. Cell Sci.* **2003**, *116*, 1881-1892.

(91) Kim, D.-H.; Lipke, E. A.; Kim, P.; Cheong, R.; Thompson, S.; Delannoy, M.; Suh, K.-Y.; Tung, L.; Levchenko, A. Nanoscale cues regulate the structure and function of macroscopic cardiac tissue constructs. *Proc. Natl. Acad. Sci. USA* **2010**, *107*, 565-570.

(92) Kim, D.-H.; Seo, C.-H.; Han, K.; Kwon, K. W.; Levchenko, A.; Suh, K.-Y. Guided Cell Migration on Microtextured Substrates with Variable Local Density and Anisotropy. *Adv. Funct. Mater.* **2009**, *19*, 1579-1586.

(93) Davis, K. A.; Burke, K. A.; Mather, P. T.; Henderson, J. H. Dynamic cell behavior on shape memory polymer substrates. *Biomaterials* **2011**, *32*, 2285-2293.

(94) Uto, K.; Ebara, M.; Aoyagi, T. Temperature-Responsive Poly(ε-caprolactone) Cell Culture Platform with Dynamically Tunable Nano-Roughness and Elasticity for Control of Myoblast Morphology. *Int. J. Mol. Sci.* **2014**, *15*, 1511-1524.

(95) Tam, J. K. V.; Uto, K.; Ebara, M.; Pagliari, S.; Forte, G.; Aoyagi, T. Mesenchymal stem cell adhesion but not plasticity is affected by high substrate stiffness. *Sci. Technol. Adv. Mat.* **2012**, *13*, 064205.

(96) Romanazzo, S.; Forte, G.; Ebara, M.; Uto, K.; Pagliari, S.; Aoyagi, T.; Traversa, E.; Taniguchi, A. Substrate stiffness affects skeletal myoblast differentiation in vitro. *Sci. Technol. Adv. Mat.* **2012**, *13*, 064211.

(97) Forte, G.; Pagliari, S.; Ebara, M.; Uto, K.; Tam, J. K.; Romanazzo, S.; Escobedo-Lucea, C.; Romano, E.; Di Nardo, P.; Traversa, E.; Aoyagi, T. Substrate stiffness modulates gene expression and phenotype in neonatal cardiomyocytes in vitro. *Tissue Eng. Part A* **2012**, *18*, 1837-1848.

(98) Mosqueira, D.; Pagliari, S.; Uto, K.; Ebara, M.; Romanazzo, S.; Escobedo-Lucea, C.; Nakanishi, J.; Taniguchi, A.; Franzese, O.; Di Nardo, P.; Goumans, M. J.; Traversa, E.; Pinto-do-Ó, P.; Aoyagi, T.; Forte, G. Hippo Pathway Effectors Control Cardiac Progenitor Cell Fate by Acting as Dynamic Sensors of Substrate Mechanics and Nanostructure. *Acs Nano* **2014**, *8*, 2033-2047.

(99) Nagahama, K.; Ueda, Y.; Ouchi, T.; Ohya, Y. Biodegradable Shape-Memory Polymers Exhibiting Sharp

References

Thermal Transitions and Controlled Drug Release. *Biomacromolecules* **2009**, *10*, 1789-1794.

(100) Le, D. M.; Kulangara, K.; Adler, A. F.; Leong, K. W.; Ashby, V. S. Dynamic Topographical Control of Mesenchymal Stem Cells by Culture on Responsive Poly(ϵ-caprolactone) Surfaces. *Adv. Mater.* **2011**, *23*, 3278-3283.

(101) Iqbal, M.; Chung, Y. I.; Tae, G. An enhanced synthesis of gold nanorods by the addition of Pluronic (F-127) via a seed mediated growth process. *J. Mater. Chem.* **2007**, *17*, 335-342.

(102) Sakai, T.; Alexandridis, P. Mechanism of gold metal ion reduction, nanoparticle growth and size control in aqueous amphiphilic block copolymer solutions at ambient conditions. *J. Phys. Chem. B* **2005**, *109*, 7766-7777.

Chapter 5. Conclusions and prospection

5.1. Conclusions

1. The detachment mechanism of interdigitated CTAB bilayer structure by the exchange of solvent (water) with DMSO was systematically investigated. The phase diagram of CTAB- modified AuNRs has been drawn based on the concentration of CTAB and volume ratios of DMSO/water. The ligand-exchange reaction with several types of thiols could be done by screening the condition by phase diagram.

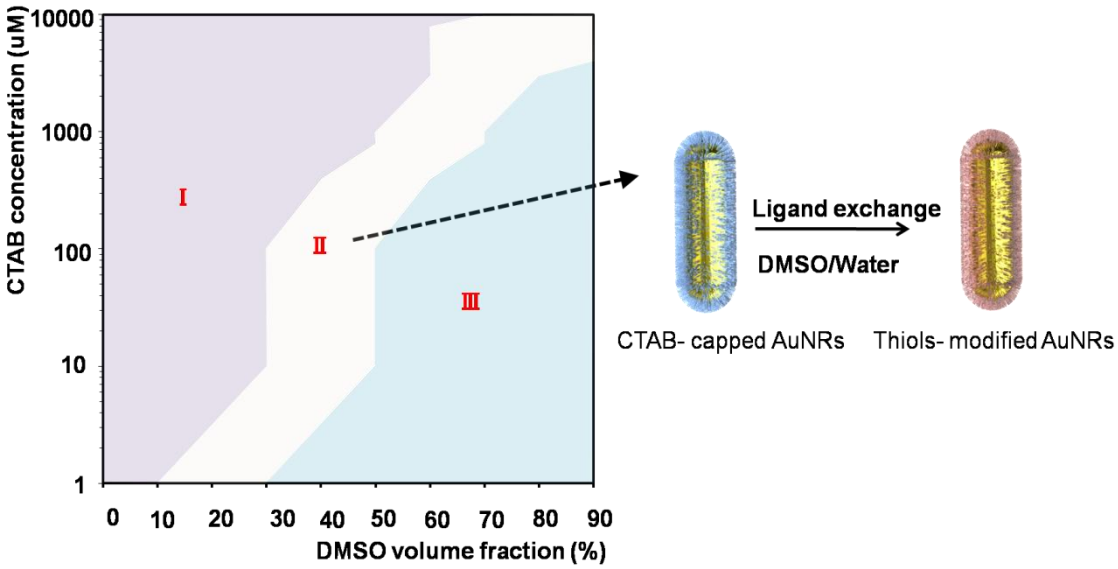

Fig. 5.1. The phase diagram of colloidal stability of AuNRs and its application for ligand exchange with thiols.

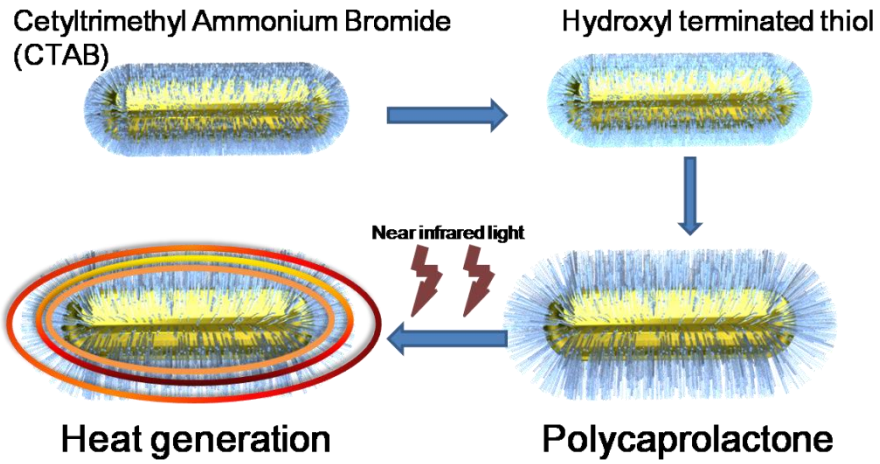

Fig. 5.2. Photothermal effect of PCL- modified AuNRs.

2. NIR light-responsive shape memory films were prepared through crosslinking of PCL macromonomers in the presence of AuNRs. Exposure to NIR light could successfully induce the photothermal heating of embedded AuNRs and consequently, shape-switching transition. Upon NIR irradiation, the film completely recovered its original shape. Local shape-memory transformation was also obtained when the limited area was exposed to the light. These results show the potential ability of the AuNRs embedded PCL film as the

remote and spatial controllable shape-memory material that actuates in physiologically relevant temperature ranges.

3. The NIR actuated shape memory film with surface-nanopatterns were used to control cell morphology remotely and locally. Cells on the illuminated regions changed their morphology as the temporal nanopatterns transitioned to a flat surface.

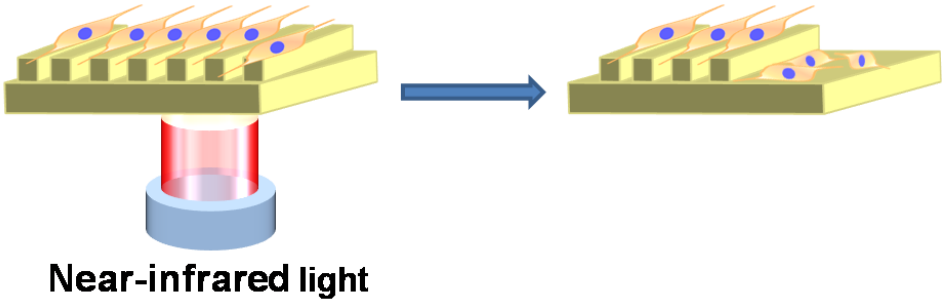

Fig. 5.3. Design of AuNRs-PCL composites film, and its application for controlling cell orientation.

5.2. Prospection

1. Dynamic controlling of absorption/desorption of CTAB from AuNRs surface.

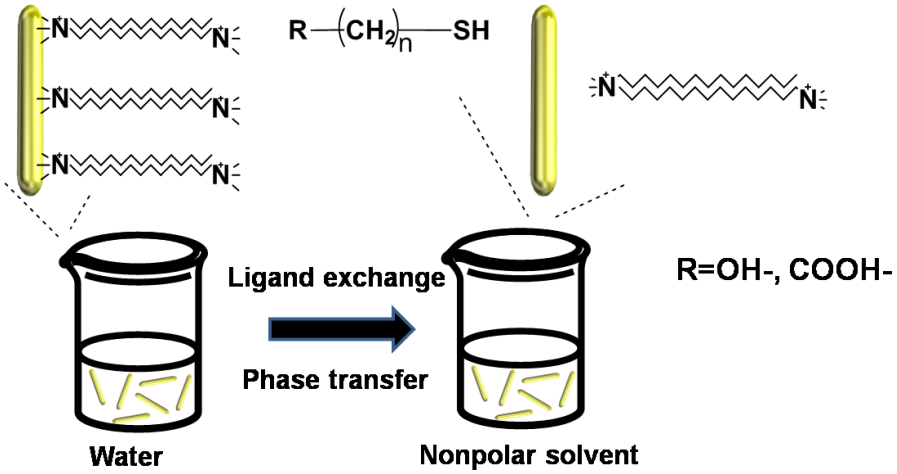

Fig. 5.4. Scheme for ligand exchange reaction performed in the mixture of water/polar organic solvent. Except the efficient removal of surface bound CTAB, the dynamic controlling of adsorption/desorption of thiols is also important for ligand exchange with thiols with various functional group.

By adjusting the concentration of CTAB, the detachment rate could also be controlled. Currently, 11-MUD modified AuNRs also aggregation after three-step modification process. The possible reason is the attachment of thiol to gold is kinetically slow comparing with the detachment of CTAB from AuNRs surface, and aggregation happens. In the mediate ratio of DMSO/Water, the quick color change and disappear of LSPR peak after mixing is one evidence for that.

Therefore, the kinetic control of absorption/detachment of AuNRs needs to be addressed, for example tuning the polarity by changing the solvent. For example, if dropwise addition of a concentrated solution of 4-mercaptophenol in THF directly into an aqueous AuNRs solutions led to CTAB-thiol exchange and a slow precipitation of phenol-functionalized nanorods[21]. Although in that case, about 70% of CTAB was exchange with thiols.

2. Preparing "safe", stable, easy-to-functionalized gold nanoparticles using block-copolymer assisted ligand-exchange.

The issue of aggregation is supposed to be addressed by the following method. That is, introducing the amphiphilic polymers, triblock copolymers, one of them is Poly(ethylene oxide)- poly(propylene oxide)-Poly(ethylene oxide) (PEO-PPO-PEO) (Commeicial name Pluronic). The assistance synthesis of AuNRs with Pluronic F127 (PEO_{100}-PPO_{65}-PEO_{100}) has been reported[101]. Through the different solubility of CTAB and Pluronic, CTAB are expected to detach selectively, and then gold nanorods could be used acts as capping agent through hydrophobic interactions[102]. Such AuNRs are also suitable for further modification.

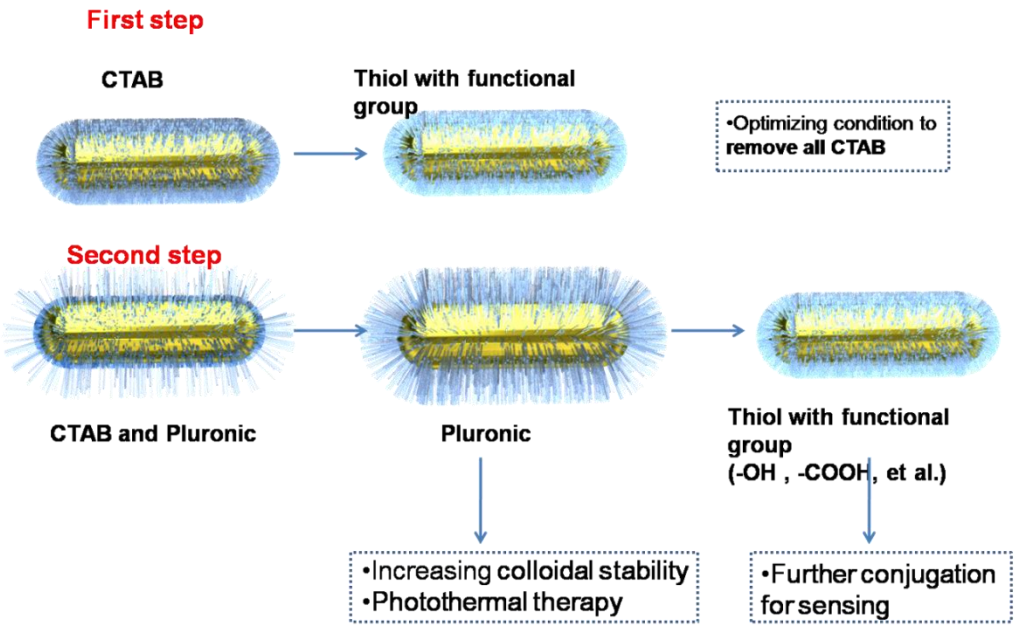

Fig. 5.5. Removal of CTAB as well as sustaining colloidal stability of AuNRs through the assistant of Pluronic F127

3. Application and significance of this work: screening a best condition for ligand-exchange reaction with specific type of thiols.

(a) The solubility of thiol with functional group depending on volume raito of Water/DMSO. (Table 1) For example, the ligand exchange using 11-mercaptoundecanoic acid and 11-mercapto-undecanol could be performed on the condition of C_{CTAB}=4mM, V_{DMSO}=0.7

(b) More importantly, CTAB on AuNRs surface could be fully detached AuNRs with C_{CTAB}<CMC. On this condition, the thiol cannot be solubilized in micelles, therefore the thorough ligand exchange could be performed.

Table 1. Solubility of thiol in mixture solvent Water/DMSO

V_{DMSO} (%)	0	10	20	30	40	50	60	70	80	90
11-mercaptoundecanoic acid (MUA)	X	X	X	X	X	X	Slightly soluble	√	√	√
11-mercapto-undecanol	X	X	X	X	X	X	X	Slightly soluble	√	√

4. Investigation of cell-materials interaction in macro scale.

PCL is one matrix that fibroblast cells can adhere easily. One choice is to selectively grow cells on the specific area.

(a) Photo-cleavable molecules were adhered to whole PCL surface. Through UV-cleavable reaction using photomask, cells are cultured selectively in some areas.

(b) At the same time, by using photomask, NIR was irradiated and temporary-permanent pattern transition can be realized.

(c) By changing the size, shape of photomask, this system is expected to study the cell-materials interaction more precisely.

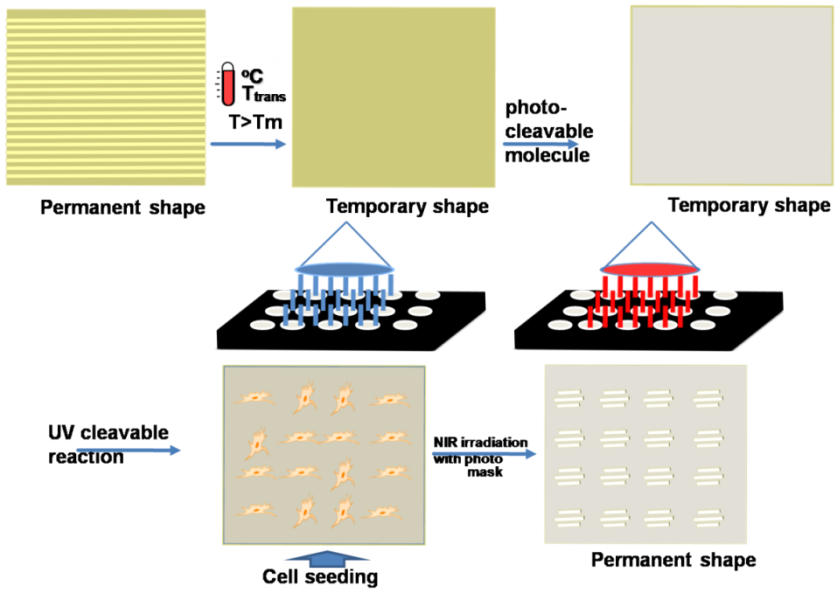

Fig. 5.6. Region-confined controlling of NIR- induced shape-memory process and its application to investigate cell-materials interaction

List of Publications

1. Q. Shou, K. Uto, M. Iwanaga, M. Ebara, T. Aoyagi. Near-infrared light-responsive shape-memory poly(epsilon-caprolactone) films that actuate in physiological temperature range. *Polymer J*. 2014, 46, 492-498.

2. Q. Shou, K. Uto, W. Lin, T. Aoyagi, M. Ebara. Near-Infrared-Irradiation-Induced Remote Activation of Surface Shape-Memory to Direct Cell Orientations. *Macromol. Chem. Phys.* 2014, 215, 2473-2481.

3. Q. Shou, M. Ebara, T. Aoyagi. An Efficient Procedure for the Removal of CTAB Surfactant and Ligand-Exchange with Mercaptoalkanol on the Surface of Gold Nanorods. Colloids Surf., B: Biointerfaces. Under review.

Acknowledgement

First, I want to show my highest gratitude to my supervisor, Prof. Takao Aoyagi. The advice for me in concentrating upon one topic to contribute to science and the encouragement in developing my own interests have been a big motivation to carry out this work, and inspire me to take challenges in future. The wiseness, patience, and kindness of Prof. Aoyagi I felt throughout this study is also a great lesson for me in treating other people.

Thank the committee members, Prof. Guoping Chen, Prof. Tetsushi Taguchi, and Prof. Seiya Tsujimura to review my thesis, and offer many suggestions and comments during my 3 years of study.

I also want to thank Dr. Mitsuhiro Ebara. The suggestions and support throughout the whole research, including experimental design, equipment setup, and manuscript preparation makes this work possible. I also appreciated his sharing of overseas working experience, which is quite helpful for me in getting used to this new environment.

I also feel grateful to Dr. Koichiro Uto. From the very beginning to the end of this work, I got lots of help, including but not limited to instructing me on polymer synthesis and equipment manipulation. I always enjoyed and got inspired from discussions with Dr. Uto on scientific topics.

I would like to thank Dr. Wei-Chih Lin. As he suggested several interdisciplinary ideas and provided the micro-fabricated silicon devices for my experiment. Also, his advice for my future career and sharing of work experiences was greatly appreciated.

I'd like to show my appreciation to all the current members and previous members in Aoyagi-lab: Dr. Kotsuchibashi, Dr. Namekawa, Dr. Sharmy, Dr. Xu, Mr. Okada, Mr. Sato, Mr. Li, Mr. Nakagawa, Ms. Niiyama, Ms. Kasaya, Ms. Saeki, Dr. Forte, Dr. Stefania, Dr. Idota, Dr. Kim, Mr. Yaseta, Mr. Akimoto, Ms. Yoshitake, Ms. Kaneta, Ms. Ebara, Ms. Uto, et al. With their help, I could overcome the difficulty in research and daily life. 3 years of study in the Aoyagi-lab deepens my understanding of teamwork, contribution and the trust across the difference in culture.

Thanks to NIMS and MANA, not only supporting me as a NIMS Junior Researcher, but also providing an excellent facility to do my research. Thanks to the Japanese funding agency for the financial support to carry out this project.

Thanks to all the staff in the Graduate School of Pure and Applied Sciences, International Student Centre in University of Tsukuba, and External Collaboration Division, Academic Collaboration Office in NIMS. All of the support makes my overseas study smooth, fruitful. I really have enjoyed the overseas study.

Thank for the friends in Tsukuba, without their help, it would be very difficult to get used to overseas life. I will always cherish the moments we had in the wonderful parties.

Thank for my parents, younger brother, and the whole family. Their selfless love and everlasting support of me has left time for me to grow up, even at the age that I should have done more for them.